

International Journal of Modern Physics E  
© World Scientific Publishing Company

## HEAVY QUARKS IN THE QUARK-GLUON PLASMA

RALF RAPP

*Cyclotron Institute and Physics Department  
Texas A&M University, College Station, Texas 77843-3366, U.S.A.  
rapp@comp.tamu.edu*

HENDRIK VAN HEES

*Institut für Theoretische Physik, Justus-Liebig-Universität Giessen, D-35392 Giessen, Germany  
Hendrik.vanHees@theo.physik.uni-giessen.de*

Received July 20, 2009  
Revised November 1, 2010

Heavy-flavor particles are believed to provide valuable probes of the medium produced in ultrarelativistic collisions of heavy nuclei. In this article we review recent progress in our understanding of the interactions of charm and bottom quarks in the Quark-Gluon Plasma (QGP). For individual heavy quarks, we focus on elastic interactions for which the large quark mass enables a Brownian motion treatment. This opens a unique access to thermalization mechanisms for heavy quarks at low momentum, and thus to their transport coefficients in the quark-gluon fluid. Different approaches to evaluate heavy-quark diffusion are discussed and compared, including perturbative QCD, effective potential models utilizing input from lattice QCD and string-theoretic estimates in conformal field theories. Applications to heavy-quark observables in heavy-ion collisions are realized via relativistic Langevin simulations, where we illustrate the important role of a realistic medium evolution to quantitatively extract the heavy-quark diffusion constant. In the heavy quarkonium sector, we briefly review the current status in potential-model based interpretations of correlation functions computed in lattice QCD, followed by an evaluation of quarkonium dissociation reactions in the QGP. The discussion of the phenomenology in heavy-ion reactions focuses on thermal model frameworks paralleling the open heavy-flavor sector. We also emphasize connections to the heavy-quark diffusion problem in both potential models and quarkonium regeneration processes.

### Contents

<b>1</b>	<b>Introduction</b>	<b>2</b>
<b>2</b>	<b>Heavy-Quark Interactions in QCD Matter</b>	<b>8</b>
2.1	Heavy-Quark Diffusion in the Quark-Gluon Plasma . . . . .	10
2.2	Perturbative QCD Approaches . . . . .	13
2.2.1	Schematic Leading Order . . . . .	13
2.2.2	Leading Order with Hard Thermal Loop Resummation . . . . .	14
2.2.3	Leading Order with Running Coupling . . . . .	15

2 *Contents*

2.2.4	Next-to-Leading Order . . . . .	17
2.2.5	Three-body elastic scattering . . . . .	18
2.3	Non-Perturbative Interactions . . . . .	19
2.3.1	Effective $Q\bar{q}$ -resonance model . . . . .	20
2.3.2	In-Medium $T$ -matrix with IQCD-based Potentials . . . . .	23
2.3.3	Collisional Dissociation of Heavy Mesons in the QGP . . . . .	28
2.3.4	Estimates of HQ Diffusion in Lattice QCD . . . . .	29
2.4	String Theoretical Evaluations of Heavy-Quark Diffusion . . . . .	30
2.5	Comparison of Elastic Diffusion Approaches . . . . .	32
2.6	Collisional vs. Radiative Energy Loss . . . . .	35
2.7	$D$ Mesons in the Hadronic Phase . . . . .	37
<b>3</b>	<b>Heavy-Quark Observables in Relativistic Heavy-Ion Collisions</b>	<b>40</b>
3.1	Relativistic Langevin Simulations . . . . .	41
3.2	Background Medium in Heavy-Ion Collisions . . . . .	43
3.3	Initial Conditions and Hadronization . . . . .	46
3.4	Model Comparisons of Heavy-Quark Spectra at RHIC . . . . .	49
3.5	Heavy-Meson and Electron Observables . . . . .	56
3.5.1	Energy-Loss Calculations . . . . .	57
3.5.2	Langevin Simulations . . . . .	59
3.6	Viscosity? . . . . .	63
<b>4</b>	<b>Heavy Quarkonia in Medium</b>	<b>65</b>
4.1	Spectral Properties of Quarkonia in the QGP . . . . .	66
4.1.1	Lattice QCD and Potential Models . . . . .	66
4.1.2	Dissociation Widths . . . . .	71
4.2	Quarkonium Production in Heavy-Ion Collisions . . . . .	75
4.2.1	Quarkonium Transport in Heavy-Ion Collisions . . . . .	75
4.2.2	Quarkonium Phenomenology in Heavy-Ion Collisions . . . . .	78
<b>5</b>	<b>Conclusions</b>	<b>87</b>

**1. Introduction**

The investigation of strongly interacting matter constitutes a major challenge in modern nuclear and particle physics. Of particular interest are phase changes between hadronic and quark-gluon matter, similar to the one which is believed to have occurred in the early Universe at a few microseconds after its birth. While the theory of the strong force is by now well established in terms of Quantum Chromodynamics (QCD)<sup>1,2,3</sup>, two of its major manifestations in the world around us - the confinement of quarks and gluons and the generation of hadronic masses - are subject of vigorous contemporary research. Both phenomena occur at energy-momentum scales of  $Q^2 \lesssim 1 \text{ GeV}^2$  where the QCD coupling constant is rather large,  $\alpha_s \gtrsim 0.3$ , and therefore perturbation theory is not reliable and/or applicable. In a

hot and dense medium at sufficiently large temperature ( $T$ ) and/or quark chemical potential ( $\mu_q$ ), one expects the finite-size hadrons to be dissolved into a deconfined Quark-Gluon Plasma (QGP) where the condensates underlying hadronic-mass generation have melted. Numerical simulations of lattice-discretized QCD (lQCD) at finite temperature predict the phase change from hadronic to quark-gluon matter to occur at a “pseudo-critical” temperature of  $T_c \simeq 200 \text{ MeV}$ <sup>4</sup>. This appears to be a rather small scale for a “perturbative QGP” (pQGP) of weakly interacting quarks and gluons to be realized, even though the computed energy density matches that of an ideal (non-interacting and massless) QGP within 20% or so for  $T \gtrsim 1.2 T_c$ .

In the laboratory, one hopes to create a QGP by colliding heavy atomic nuclei at ultrarelativistic energies, with a center-of-mass energy per colliding nucleon pair well above the nucleon rest mass,  $\sqrt{s}/A \gg M_N$ . If the energy deposition in the reaction zone is large enough, and if the interactions of the produced particles are strong enough, the notion of an interacting medium may be justified, despite its transient nature. This notion has been convincingly verified in nuclear collision experiments over the last  $\sim 25$  years at the Super-Proton-Synchrotron (SPS) at the European Organization for Nuclear Research (CERN)<sup>5</sup> and at the Relativistic Heavy-Ion Collider (RHIC) at Brookhaven National Laboratory (BNL)<sup>6</sup>. Transverse-momentum ( $p_T$ ) spectra of different hadron species in the low- $p_T$  regime ( $p_T \lesssim 2\text{-}3 \text{ GeV}$ ) reveal that the produced medium explodes collectively reaching expansion velocities in excess of half the speed of light. In the high- $p_T$  regime ( $p_T \gtrsim 5 \text{ GeV}$ ), which in the heavy-ion environment became available at RHIC for the first time, hadron spectra are suppressed by up to a factor of  $\sim 5$  relative to  $p$ - $p$  collisions, indicative for a strong absorption of high-energy partons traversing the medium<sup>7</sup>. The inclusive production of charm-quark bound states ( $J/\psi$  mesons) is suppressed by a factor of 3-5 at both SPS and RHIC, indicative for their dissolution in the medium (possibly related to deconfinement)<sup>8,9,10</sup>. A large excess of electromagnetic radiation (photons and dileptons) is observed, indicative for medium temperatures around 200 MeV and a “melting” of the  $\rho$ -meson resonance (possibly related to hadronic mass de-generation)<sup>11,12</sup>. A more differential analysis of hadron spectra in non-central Au-Au collisions at RHIC reveals a large elliptic asymmetry of the collective flow (“elliptic flow”): the spatial asymmetry of the initial nuclear overlap zone is converted into an opposite asymmetry in the final hadron  $p_T$  spectra. Within a hydrodynamic modeling of the exploding fireball this observation requires a rapid thermalization and a very small viscosity of the interacting medium<sup>13,14,15,16</sup>. Only then can spatial pressure gradients build up fast enough to facilitate an effective conversion into azimuthal asymmetries in the energy-momentum tensor of the system. The agreement of hydrodynamic predictions with elliptic-flow data at RHIC led to the notion of an “almost perfect liquid”, with a ratio of viscosity to entropy density close to a conjectured lower bound of any quantum mechanical system<sup>17</sup>. The microscopic mechanisms underlying these rather remarkable transport properties are yet to be determined. In this context, heavy quarks (charm and bottom,

## 4 Contents

$Q=c$  and  $b$ ) and their bound states (charmonia and bottomonia) are recognized as particularly suitable probes of the medium produced in ultrarelativistic heavy-ion collisions (URHICs)<sup>18a</sup>. In the present article we will attempt to review the current status of the theory and phenomenology of this promise.

Let us first focus on the sector of individual heavy quarks (open heavy flavor). The fact that their masses are well above the typical temperature of the system,  $m_Q \gg T$ , has at least three important implications:

- (1) The (hard)  $Q\bar{Q}$  production process is essentially restricted to primordial  $N$ - $N$  collisions<sup>20</sup>, i.e., re-interactions in the subsequently evolving medium are not expected to change the number of heavy quarks (reminiscent of the “factorization theorem” of perturbative QCD<sup>21</sup>); this is borne out experimentally by a scaling of  $c\bar{c}$  production,  $N_{c\bar{c}}$ , with the number of binary  $N$ - $N$  collisions,  $N_{\text{coll}}$ , at different collision centralities<sup>22</sup>.
- (2) The thermal relaxation time of heavy quarks ought to be larger than for light quarks, parameterically by a factor  $\sim m_Q/T \approx 5$ -20. With a light-quark and gluon thermalization time of  $\tau_{q,g} \simeq 0.3$ -1 fm/ $c$  (as indirectly inferred from hydrodynamic modeling at RHIC) and an estimated QGP lifetime of  $\tau_{\text{QGP}} \simeq 5$  fm/ $c$  in central Au-Au collisions, one expects  $\tau_c$  ( $\tau_b$ ) to be on the same order as (significantly larger than)  $\tau_{\text{QGP}}$ . Thus, charm (and especially bottom) quarks are not expected to reach thermal equilibrium, but their re-interactions should impart noticeable modifications on the initial momentum spectrum (less pronounced for bottom). The final heavy-quark (HQ) spectra may therefore encode a “memory” of the interaction history throughout the evolving fireball, by operating in between the limits of thermalization and free streaming.
- (3) The theoretical task of describing HQ interactions is amenable to a diffusion treatment, i.e., Brownian motion of a heavy test particle in a bath of a light-particle fluid. Nonrelativistically, the typical thermal momentum of a heavy quark is  $p_{\text{th}}^2 \simeq 3m_Q T \gg T^2$ , and therefore much larger than the typical momentum transfer from the medium,  $Q^2 \sim T^2$ . This allows to expand the Boltzmann equation in momentum transfer to arrive at a Fokker-Planck description of HQ diffusion in the QGP, which directly yields the pertinent transport coefficients as well.

The above three points provide a well-defined framework to construct in-medium HQ interactions in QCD matter and test them against observables in URHICs (quantitative comparisons additionally require to account for effects of hadronization of the quarks, as well as reinteractions in the hadronic medium). The Fokker-

<sup>a</sup>The (weak-decay) lifetime of the top quark of  $\sim 0.1$  fm/ $c$  is too short to render it a viable probe in URHICs; thus, heavy quarks will exclusively refer to charm and bottom in this article. Strange quarks are in between the heavy- and light-quark limit, forming their own complex of valuable observables<sup>19</sup>.

Planck approach is readily implemented for the case of *elastic*  $p + Q \rightarrow p + Q$  scattering off partons in the medium ( $p = q, \bar{q}, g$ )<sup>23,24,25,26,27,28</sup>. In the light-hadron sector, however, the large suppression of high- $p_T$  spectra is believed to be largely caused by *radiative* energy loss of high-energy partons traversing the QGP, i.e., medium-induced gluon radiation of type  $q + g \rightarrow q + g + g$ <sup>7,29,30</sup>. Even in the low- $p_T$  regime, perturbative  $2, 3 \leftrightarrow 3$  scattering processes have been suggested to facilitate the rapid thermalization required by phenomenology (albeit in connection with rather large coupling constants of  $\alpha_s \simeq 0.5$ )<sup>31</sup>. The situation could be quite different in the HQ sector. In the low-momentum limit, gluon-Bremsstrahlung of a heavy quark is suppressed<sup>32</sup> and the dominant momentum-transfer reaction is elastic scattering<sup>26</sup>. As is well known from classical electrodynamics, the radiative energy loss of a muon is suppressed relative to an electron by a mass ratio  $(m_\mu/m_e)^4$ . In perturbative QCD (pQCD) it is currently an open question at what momentum scale radiative energy loss of a heavy quark takes over from the collisional one (which, most likely, will depend on additional parameters such as temperature, path length, etc.). In fact, this may not even be a well-defined question since nonperturbative processes at moderate momentum transfers may supersede perturbative ones before the elastic part of the latter dominates over the radiative one. The relations between perturbative and nonperturbative interactions is one of the key issues to be addressed in this review.

Experimental signatures for the modifications of HQ spectra in URHICs are currently encoded in single-electron ( $e^\pm$ ) spectra associated with the semileptonic decays of charm and bottom hadrons,  $D, B, \Lambda_c, \dots \rightarrow e\nu X$ . These measurements require a careful subtraction of all possible “photonic” sources of electrons, such as photon conversions in the detector material, Dalitz decays of  $\pi$  and  $\eta$ , vector-meson decays, and others. The modifications of the “non-photonic” electron spectra (associated with heavy-flavor decays) in Au-Au collisions are then quantified by the standard nuclear modification factor,  $R_{AA}^e$ , and elliptic flow coefficient,  $v_2^e$ . The available RHIC data in semicentral and central Au-Au collisions at  $\sqrt{s_{NN}} = 200$  GeV exhibit a substantial elliptic flow of up to  $v_2^e \simeq 10\%$  and a large high- $p_T$  suppression down to  $R_{AA}^e \simeq 0.25$ , respectively<sup>33,22,34,35</sup>. Both values are quite comparable to those for light hadrons (the pion  $v_2$  reaches somewhat higher, to about 15%). Radiative energy-loss models<sup>36</sup> based on perturbative QCD cannot explain the  $e^\pm$  data. These data were, in fact, instrumental<sup>37</sup> in reconsidering elastic scattering as a significant source of parton energy loss in the QGP<sup>25,26,27,38</sup>. The combination of pQCD elastic and radiative scattering does not suffice either to reproduce the observed suppression once a realistic bottom component is accounted for in the electron spectra<sup>38</sup>. Elastic scattering based on nonperturbative interactions, as proposed in Refs.<sup>25,28</sup>, simultaneously accounts for the  $e^\pm$  elliptic flow and suppression reasonably well<sup>22</sup>. This has reinforced the hope that HQ observables provide the promised precision tool to characterize transport properties of the “strongly coupled QGP” (sQGP). E.g., if a clear mass hierarchy in thermal relaxation times,  $\tau_Q \propto \frac{m_Q}{T} \tau_q$  (as well as  $\tau_b/\tau_c = m_b/m_c$ ) emerges from a quantitative analysis of URHIC data, it would

6 *Contents*

be suggestive for a universal behavior of light- and heavy-quark transport in the QGP. However, there is still a substantial way to go before such a program can be realized, as discussed below<sup>b</sup>.

It should not be surprising if in-medium properties of open heavy flavor, especially at low momentum, are closely related to medium modifications of heavy quarkonia. The latter have a long history as “probes” of the QGP in heavy-ion collisions, especially as potential indicators of the deconfinement transition, cf. Refs.<sup>8,9,10</sup> for a broad up-to-date coverage of this topic. In particular, progress in finite-temperature lattice QCD<sup>41,42,43</sup> has triggered vigorous reconsideration of the question whether quarkonia, especially their ground states, can survive in the QGP significantly above the critical temperature. These developments include the application of potential models at finite temperature, coupled with the hope that heavy-quark free energies as computed in thermal IQCD can serve as a model-independent input for the low-energy heavy-quark interaction. If charmonium binding indeed remains sufficiently strong in the QGP to support bound states up to rather high temperatures, it is conceivable that the underlying interaction is of a more general relevance and therefore also operative in heavy-light<sup>44</sup> and maybe even light-light<sup>45</sup> systems. Especially in the former case, from the point of view of elastic (on-shell) scattering of a heavy quark in the medium, the conditions for momentum transfer are comparable to the heavy-heavy interaction governing quarkonium properties. Since low-momentum HQ interactions determine their transport properties, one immediately recognizes an intimate relation between HQ transport and in-medium quarkonia. These connections are also being exploited in the analysis of thermal IQCD computations of quarkonium correlation functions<sup>46</sup>. In addition to the binding properties, the inelastic reaction rates of quarkonia with surrounding partons or hadrons are a key ingredient for a quantitative description of their spectral function in QCD matter (also here “quasi-elastic” scattering of thermal partons with a heavy quark inside the quarkonium bound states may play an important role, especially if the binding energy becomes small<sup>47</sup>). A good control over all of these aspects is mandatory to utilize quarkonium properties as diagnostic tool in heavy-ion collisions and eventually deduce more general properties of the medium produced in these reactions. As in the open heavy-flavor sector, this has to be built on a solid knowledge of the space-time history of nuclear collisions, as well as of the initial conditions on quarkonium spectra. The latter aspect could be more involved than for single heavy quarks, since (a) measurements in  $p$ - $A$  collisions show that cold-nuclear-matter (CNM) effects from the incoming nuclei (e.g., the so-called nuclear absorption) affect the primordial charmonium number significantly (e.g., with up to 60% suppression for  $J/\psi$  at SPS energies when extrapolated to central Pb-Pb collisions); (b) the bound-state formation time introduces another rather long time scale (soft energy scale) which is easily of the order of (or longer

<sup>b</sup>A recent review article<sup>39</sup> addresses similar topics but from a more elementary perspective; see also Ref.<sup>40</sup>

than) the thermalization time of the medium (at least for charmonia and excited bottomonia at RHIC energies and higher).

Charmonium suppression beyond the level of CNM effects has been established in semi-/central Pb-Pb and Au-Au collisions at SPS<sup>48</sup> and RHIC<sup>49</sup>, respectively. An intriguing finding is that the observed suppression pattern and magnitude is very comparable at SPS and RHIC, despite the different collision energies which lead to substantial variations in, e.g., light-hadron observables (most notably a factor  $\sim 2$  larger charged particle rapidity density and stronger collective phenomena at RHIC). However, this “degeneracy” was predicted<sup>47</sup> as a consequence of charmonium regeneration mechanisms<sup>50,51,52</sup>: a stronger suppression in the hotter and denser medium at RHIC is compensated by the coalescence of  $c$  and  $\bar{c}$  quarks in the QGP and/or at hadronization (the  $c\bar{c}$  production cross section at RHIC is about a factor of  $\sim 100$  larger than at SPS energies). While an “extra” source of charmonia increases the complexity of pertinent observables in heavy-ion reactions, it also provides another, rather direct, connection between the open and hidden heavy-flavor sectors. Obviously, the secondary yield from  $c\bar{c}$  coalescence necessarily carries imprints of the charm-quark distributions, both in its magnitude (softer  $c$ -quark spectra are expected to result in larger coalescence probabilities) and in its momentum spectra (including elliptic flow). A comprehensive theoretical and phenomenological analysis of open and hidden heavy flavor is thus becoming an increasingly pressing and challenging issue. As a final remark on quarkonia in this introduction, we point out that bottomonium production in heavy-ion reactions is less likely to receive regeneration contributions (at least at RHIC and possibly neither at LHC). In addition, the increase in bottomonium binding energies (compared to charmonia) render them rather sensitive probes of color screening which strongly influences its dissociation rates<sup>53</sup>. Bottomonia thus remain a promising observable to realize the originally envisaged “spectral analysis of strongly interacting matter”<sup>54</sup>.

Our review is organized as follows: In Sec. 2 we outline the theoretical framework of evaluating HQ diffusion in equilibrium QCD matter. We first recall basic steps in setting up the HQ diffusion equation (Sec. 2.1) which determines the time evolution of the HQ distribution function in terms of pertinent transport coefficients based on elastic scattering amplitudes. This is followed by a discussion of several microscopic approaches to calculate the HQ friction and diffusion coefficients in the QGP: perturbative QCD (Sec. 2.2) at leading (2.2.1, 2.2.2, 2.2.3) and next-to-leading order (2.2.4) as well as for three-body scattering (2.2.5); nonperturbative calculations (Sec. 2.3) implementing resonance-like correlations in the QGP using HQ effective theory (Sec. 2.3.1), in-medium  $T$ -matrices with HQ potentials estimated from thermal lattice QCD (Sec. 2.3.2), or collisional-dissociation mechanisms of heavy mesons (Sec. 2.3.3); and string-theoretic evaluations based on the conjectured correspondence to conformal field theories (Sec. 2.4). The variety of the proposed approaches calls for an attempt to reconcile the underlying assumptions

and basic interactions (Sec. 2.5). This is followed by a discussion of inelastic (radiative) energy-loss calculations and their relation to elastic ones (Sec. 2.6). We briefly consider interactions of open heavy-flavor hadrons in hadronic matter (Sec. 2.7). In Sec. 3 we discuss applications of HQ diffusion to URHICs using relativistic Langevin simulations of the Fokker-Planck equation within an expanding finite-size thermal medium (Sec. 3.1). A realistic description of the latter (utilizing hydrodynamics, transport models or suitable parameterizations thereof) is an essential prerequisite to enable a quantitative extraction of transport properties of the QCD medium (Sec. 3.2). Further ingredients are reliable initial conditions (possibly modified by nuclear effects) and the conversion of quarks to hadrons (Sec. 3.3). Implementations of different HQ diffusion coefficients in various space-time models are quantitatively analyzed in terms of the resulting HQ spectra at RHIC, in particular their nuclear modification factor and elliptic flow (Sec. 3.4). Including effects of hadronization (as well as semileptonic electron decays), a quantitative comparison of these calculations to single-electron spectra at RHIC is conducted (Sec. 3.5). We emphasize the importance of a consistent (simultaneous) description of  $p_t$  spectra and elliptic flow. Only then can these observables be converted into a meaningful (albeit preliminary) estimate of charm- and bottom-quark diffusion coefficients in the QGP. We finish the discussion on open heavy flavor with an attempt to utilize these coefficients for a schematic estimate of the ratio of shear viscosity to entropy density in the QGP (Sec. 3.6). In Sec. 4 we elaborate on theoretical and phenomenological analyses of quarkonia in medium and their production in heavy-ion collisions. We first address spectral properties of quarkonia in equilibrium matter (Sec. 4.1); Euclidean correlation functions computed in lattice QCD with good precision have been analyzed in terms of potential models based on screened HQ potentials (Sec. 4.1.1). The interplay of color screening and parton-induced dissociation reactions has important consequences for the evaluation of quarkonium dissociation widths (Sec. 4.1.2). In light of the charmonium equilibrium properties the current status of the phenomenology in heavy-ion collisions is discussed (Sec. 4.2). First, quarkonium transport equations are introduced along with their main ingredients, i.e., dissociation widths and equilibrium numbers using relative chemical equilibrium at fixed HQ number (Sec. 4.2.1); this is followed by model comparisons to  $J/\psi$  data at SPS and RHIC, scrutinizing suppression vs. regeneration mechanisms and their transverse-momentum dependencies (Sec. 4.2.2), and a brief illustration of predictions for  $\Upsilon$  production at RHIC. In Sec. 5 we recollect the main points of this article and conclude.

## 2. Heavy-Quark Interactions in QCD Matter

At an energy scale of the (pseudo-) critical QCD transition temperature, the large charm- and bottom-quark masses imply that the HQ diffusion problem is a non-relativistic one (unless initial conditions bring in an additional large scale). In the weak-coupling regime this further implies that the dominant interactions of the

heavy quark are elastic scattering (gluon radiation is suppressed by an extra power in  $\alpha_s$  and cannot be compensated by a large momentum transfer as could be the case for a fast quark; see, e.g., the discussion in Ref.<sup>26</sup>). It turns out, however, that the perturbative expansion of the charm-quark diffusion coefficient, evaluated using thermal field theory, is not well convergent even for a strong coupling constant as low as  $\alpha_s = 0.1$ <sup>55</sup>. Thus, non-perturbative methods, e.g., resummations of large contributions or interactions beyond perturbation theory, are necessary to improve the estimates of HQ diffusion. This is not surprising since transport coefficients usually involve the zero-momentum limit of correlation functions rendering them susceptible to threshold effects which may increase with the mass of the particles. A simple example of such kind are Coulomb-like bound states (e.g., heavy quarkonia), where the binding energy increases with increasing HQ mass,  $\epsilon_B \propto \alpha_s^2 m_Q$ , to be compared to thermal effects, e.g., at a scale  $\sim gT$  for Debye screening (to leading order in  $g$ ) or at  $\sim T$  for inelastic dissociation reactions with thermal partons. An interesting question in this context is whether potential models are a viable means to evaluate HQ interactions in the QGP. If a suitable formulation of a potential at finite temperature can be established, a promising opportunity arises by extracting these from first principle lattice computations of the HQ free energy. In the heavy-quarkonium sector such a program has been initiated a few years ago<sup>56,57,58,59,60</sup> with fair success, although several open questions remain<sup>61,62,63,58</sup>. If applicable, potential models have the great benefit of allowing for nonperturbative solutions utilizing Schrödinger or Lippmann-Schwinger equations; the calculated scattering amplitudes can then be straightforwardly related to transport coefficients. A key issue in this discussion is the transition to the (ultra-) relativistic regime, which becomes inevitable in applications to experiment toward high momentum. While relativistic kinematics can be readily accounted for, the opening of inelastic (radiative) channels poses major problems. However, here the contact to perturbative calculations may be possible and provide a valuable interface to match the different regimes, at least parametrically (e.g., in the limit of a small coupling constant and/or high temperature). This reiterates the importance of identifying the common grounds of seemingly different calculations for HQ properties in medium.

We start the discussion in this Section by setting up the Brownian Motion framework for heavy quarks in the QGP (Sec. 2.1). The main part of this Section is devoted to the evaluation of the Fokker-Planck transport coefficients. We focus on elastic interactions, classified into (various levels of) perturbative (Sec. 2.2) and nonperturbative approaches (Secs. 2.3 and 2.4). As we will see, there is considerable conceptual overlap in the calculations available in the literature, the main difference being that they are carried out in different approximation schemes (Sec. 2.5). Our presentation also encompasses inelastic reactions with an additional gluon in the final and/or initial state, i.e., radiative energy-loss calculations within perturbative QCD (Sec. 2.6). This raises the issue of their relative magnitude compared to elastic interactions which has recently received considerable re-consideration even for light

quarks and gluons. Finally, we address interactions of hadrons carrying charm or bottom in hadronic matter (Sec. 2.7). Bottom-up extrapolations in temperature (or density) in the hadronic world are useful complements to top-down ones in the QGP, to reveal qualitative trends of, e.g., the HQ diffusion coefficient toward  $T_c$ .

### 2.1. Heavy-Quark Diffusion in the Quark-Gluon Plasma

As emphasized in the Introduction, an attractive feature in analyzing HQ motion in a QGP is the ensuing simplification to a Brownian motion framework<sup>23</sup>. The latter is characterized by a Fokker-Planck equation where HQ interactions are conveniently encoded in transport coefficients. These, in turn, are readily related to underlying (elastic) scattering matrix elements on light partons in the QGP which allow for direct comparisons of microscopic models of the HQ interaction (as elaborated in subsequent sections).

Starting point for the derivation of the Fokker-Planck equation<sup>23</sup> is the Boltzmann equation for the HQ phase-space distribution,  $f_Q$ ,

$$\left[ \frac{\partial}{\partial t} + \frac{\mathbf{p}}{\omega_{\mathbf{p}}} \frac{\partial}{\partial \mathbf{x}} + \mathbf{F} \frac{\partial}{\partial \mathbf{p}} \right] f_Q(t, \mathbf{x}, \mathbf{p}) = C[f_Q], \quad (1)$$

where  $\omega_{\mathbf{p}} = \sqrt{m_Q^2 + \mathbf{p}^2}$  denotes the energy of a heavy quark with three-momentum  $\mathbf{p}$ ,  $\mathbf{F}$  is the mean-field force, and  $C[f_Q]$  summarizes the collision integral which will be analyzed in more detail below. In the following, mean-field effects will be neglected, and by integration over the fireball volume, Eq. (1) simplifies to an equation for the momentum distribution,

$$\frac{\partial}{\partial t} f_Q(t, \mathbf{p}) = C[f_Q], \quad (2)$$

where

$$f_Q(t, \mathbf{p}) = \int d^3\mathbf{x} f_Q(t, \mathbf{x}, \mathbf{p}). \quad (3)$$

The collision integral on the right-hand side of Eq. (2) encodes the transition rate of heavy quarks due to collisions into and out of a small momentum cell  $d^3\mathbf{p}$  around the HQ momentum  $\mathbf{p}$ ,

$$C[f] = \int d^3\mathbf{k} [w(\mathbf{p} + \mathbf{k}, \mathbf{k}) f_Q(\mathbf{p} + \mathbf{k}) - w(\mathbf{p}, \mathbf{k}) f_Q(\mathbf{p})]. \quad (4)$$

Here  $w(\mathbf{p}, \mathbf{k})$  is the transition rate for collisions of a heavy quark with heat-bath particles with momentum transfer  $\mathbf{k}$ , changing the HQ momentum from  $\mathbf{p}$  to  $\mathbf{p} - \mathbf{k}$ . Accordingly the first (gain) term in the integral describes the transition rate for HQ scattering from a state with momentum  $\mathbf{p} + \mathbf{k}$ , into a state with momentum  $\mathbf{p}$ , while the second (loss) term the scattering out of the momentum state  $\mathbf{p}$ .

The transition rate,  $w$ , can be expressed through the cross section of the collision processes in the heat bath. For *elastic* scattering of a heavy quark with momentum

$\mathbf{p}$  on a light quark in the heat bath with momentum  $\mathbf{q}$ , one finds

$$w(\mathbf{p}, \mathbf{k}) = \gamma_{q,g} \int \frac{d^3\mathbf{q}}{(2\pi)^3} f_{q,g}(\mathbf{q}) v_{\text{rel}} \frac{d\sigma}{d\Omega}(\mathbf{p}, \mathbf{q} \rightarrow \mathbf{p} - \mathbf{k}, \mathbf{q} + \mathbf{k}), \quad (5)$$

where  $f_{q,g}$  are the Fermi or Bose distributions for thermal light quarks or gluons, and  $\gamma_q = 6$  or  $\gamma_g = 16$  the respective spin-color degeneracy factors. The relative velocity is defined as

$$v_{\text{rel}} = \frac{\sqrt{(p \cdot q)^2 - (m_Q m_q)^2}}{\omega_Q \omega_q}, \quad (6)$$

where  $p = (\omega_{\mathbf{p}}, \mathbf{p})$  and  $q = (\omega_{\mathbf{q}}, \mathbf{q})$  are the four momenta of the incoming heavy and light quark, respectively. Upon expressing the invariant differential cross section,  $d\sigma/d\Omega$ , in Eq. (5) in terms of the spin-color summed matrix element,  $\sum |\mathcal{M}|^2$ , the collision term, Eq. (4), takes the form

$$C[f_Q] = \frac{1}{2\omega_{\mathbf{p}}} \int \frac{d^3\mathbf{q}}{(2\pi)^3 2\omega_{\mathbf{q}}} \int \frac{d^3\mathbf{p}'}{(2\pi)^3 2\omega_{\mathbf{p}'}} \int \frac{d^3\mathbf{q}'}{(2\pi)^3 2\omega_{\mathbf{q}'}} \frac{1}{\gamma_Q} \sum |\mathcal{M}|^2 \times (2\pi)^4 \delta^{(4)}(p + q - p' - q') [f_Q(\mathbf{p}') f_{q,g}(\mathbf{q}') - f_Q(\mathbf{p}) f_{q,g}(\mathbf{q})] \quad (7)$$

with  $\mathbf{k} = \mathbf{p} - \mathbf{p}' = \mathbf{q}' - \mathbf{q}$ .

The key approximation is now that the relevant momentum transfers to the heavy quark obey  $|\mathbf{k}| \ll |\mathbf{p}|$ . This enables to expand the HQ momentum distribution function,  $f_Q$ , and the first argument of the transition rate,  $w$ , in the collision integral, Eq. (4), with respect to  $\mathbf{k}$  up to second order,<sup>c</sup>

$$w(\mathbf{p} + \mathbf{k}, \mathbf{k}) f_Q(\mathbf{p} + \mathbf{k}, \mathbf{k}) \simeq w(\mathbf{p}, \mathbf{k}) f_Q(\mathbf{p}) + \mathbf{k} \frac{\partial}{\partial \mathbf{p}} [w(\mathbf{p}, \mathbf{k}) f_Q(\mathbf{p})] + \frac{1}{2} k_i k_j \frac{\partial^2}{\partial p_i \partial p_j} [w(\mathbf{p}, \mathbf{k}) f_Q(\mathbf{p})] \quad (8)$$

( $i, j=1,2,3$  denote the spatial components of the 3-vectors, with standard summation convention for repeated indices). The collision integral then simplifies to

$$C[f_Q] \simeq \int d^3\mathbf{k} \left[ k_i \frac{\partial}{\partial p_i} + \frac{1}{2} k_i k_j \frac{\partial^2}{\partial p_i \partial p_j} \right] [w(\mathbf{p}, \mathbf{k}) f_Q(\mathbf{p})], \quad (9)$$

i.e., the Boltzmann equation (2) is approximated by the Fokker-Planck equation,

$$\frac{\partial}{\partial t} f_Q(t, \mathbf{p}) = \frac{\partial}{\partial p_i} \left\{ A_i(\mathbf{p}) f_Q(t, \mathbf{p}) + \frac{\partial}{\partial p_j} [B_{ij}(\mathbf{p}) f_Q(t, \mathbf{p})] \right\}. \quad (10)$$

The drag and diffusion coefficients are given according to Eq. (9) by

$$A_i(\mathbf{p}) = \int d^3\mathbf{k} w(\mathbf{p}, \mathbf{k}) k_i, \quad (11)$$

$$B_{ij}(\mathbf{p}) = \frac{1}{2} \int d^3\mathbf{k} w(\mathbf{p}, \mathbf{k}) k_i k_j.$$

<sup>c</sup>According to the Pawula theorem<sup>64</sup> any truncation of the collision integral at finite order is only consistent with fundamental properties of Markov processes if the truncation is made at the 2<sup>nd</sup>-order term.

## 12 Contents

For an isotropic background medium, especially in the case of (local) equilibrium (implying that the coefficients are defined in the local rest frame of the heat bath), rotational symmetry enables to simplify the coefficients to

$$\begin{aligned} A_i(\mathbf{p}) &= A(\mathbf{p})p_i, \\ B_{ij}(\mathbf{p}) &= B_0(\mathbf{p})P_{ij}^\perp(\mathbf{p}) + B_1(\mathbf{p})P_{ij}^\parallel(\mathbf{p}), \end{aligned} \quad (12)$$

where the projection operators on the longitudinal and transverse momentum components read

$$P_{ij}^\parallel(\mathbf{p}) = \frac{p_i p_j}{\mathbf{p}^2}, \quad P_{ij}^\perp(\mathbf{p}) = \delta_{ij} - \frac{p_i p_j}{\mathbf{p}^2}. \quad (13)$$

Implementing these simplifications into the collision integral, Eq. (7), the scalar drag and diffusion coefficients in Eq. (12) are given by integrals of the form

$$\begin{aligned} \langle X(\mathbf{p}') \rangle &= \frac{1}{2\omega_{\mathbf{p}}} \int \frac{d^3\mathbf{q}}{(2\pi)^3 2\omega_{\mathbf{q}}} \int \frac{d^3\mathbf{p}'}{(2\pi)^3 2\omega_{\mathbf{p}'}} \int \frac{d^3\mathbf{q}'}{(2\pi)^3 2\omega_{\mathbf{q}'}} \frac{1}{\gamma_Q} \sum_{g,q} |\mathcal{M}|^2 \\ &\times (2\pi)^4 \delta^{(4)}(p + q - p' - q') f_{q,g}(\mathbf{q}) X(\mathbf{p}'). \end{aligned} \quad (14)$$

In this notation, the coefficients can be written as

$$\begin{aligned} A(\mathbf{p}) &= \left\langle 1 - \frac{\mathbf{p}\mathbf{p}'}{\mathbf{p}^2} \right\rangle, \\ B_0(\mathbf{p}) &= \frac{1}{4} \left\langle \mathbf{p}'^2 - \frac{(\mathbf{p}'\mathbf{p})^2}{\mathbf{p}^2} \right\rangle, \\ B_1(\mathbf{p}) &= \frac{1}{2} \left\langle \frac{(\mathbf{p}'\mathbf{p})^2}{\mathbf{p}^2} - 2\mathbf{p}'\mathbf{p} + \mathbf{p}^2 \right\rangle. \end{aligned} \quad (15)$$

Note that Eq. (14) includes the sum over gluons and light quarks ( $u, d, s$ ).

The physical meaning of the coefficients becomes clear in the non-relativistic approximation of constant coefficients,  $\gamma \equiv A(\mathbf{p}) = \text{const}$  and  $D \equiv B_0(\mathbf{p}) = B_1(\mathbf{p}) = \text{const}$ , in which case the Fokker-Planck equation further simplifies to

$$\frac{\partial}{\partial t} f_Q(t, \mathbf{p}) = \gamma \frac{\partial}{\partial p_i} [p_i f_Q(t, \mathbf{p})] + D \Delta_{\mathbf{p}} f_Q(t, \mathbf{p}). \quad (16)$$

E.g., for an initial condition

$$f_Q(t=0, \mathbf{p}) = \delta^{(3)}(\mathbf{p} - \mathbf{p}_0), \quad (17)$$

the solution takes the form of a Gaussian distribution,

$$f_Q(t, \mathbf{p}) = \left\{ \frac{\gamma}{2\pi D} [1 - \exp(-2\gamma t)] \right\}^{-3/2} \exp \left[ -\frac{\gamma}{2D} \frac{[\mathbf{p} - \mathbf{p}_0 \exp(-\gamma t)]^2}{1 - \exp(-2\gamma t)} \right]. \quad (18)$$

From the equation for the mean momentum,

$$\langle \mathbf{p} \rangle = \mathbf{p}_0 \exp(-\gamma t), \quad (19)$$

one sees that  $\gamma$  determines the relaxation rate of the average momentum to its equilibrium value, i.e., it is a drag or friction coefficient. The standard deviation of the momentum evolves according to

$$\langle \mathbf{p}^2 \rangle - \langle \mathbf{p} \rangle^2 = \frac{3D}{\gamma} [1 - \exp(-2\gamma t)] , \quad (20)$$

i.e.,  $D$  is the momentum-diffusion constant, describing the momentum fluctuations.

In the limit  $t \rightarrow \infty$ , Eq. (18) approaches the (non-relativistic) Boltzmann distribution,

$$f_Q(t, \mathbf{p}) = \left( \frac{2\pi D}{\gamma} \right)^{3/2} \exp\left( -\frac{\gamma \mathbf{p}^2}{2D} \right) . \quad (21)$$

Since in thermal equilibrium the heavy quarks have to obey an equilibrium distribution with the temperature,  $T$ , of the heat bath, the drag and diffusion coefficients should satisfy the *Einstein dissipation-fluctuation relation*,

$$D = m_Q \gamma T . \quad (22)$$

The relativistic Fokker-Planck equation will be discussed in Sec. 3.1 in connection with its formulation in terms of stochastic Langevin equations.

We note that the spatial diffusion coefficient,  $D_s$ , which describes the broadening of the spatial distribution with time,

$$\langle \mathbf{x}^2(t) \rangle - \langle \mathbf{x}(t) \rangle^2 \simeq 6D_s t , \quad (23)$$

is related to the drag and momentum-diffusion coefficient through

$$D_s = \frac{T}{m_Q \gamma} = \frac{T^2}{D} . \quad (24)$$

## 2.2. Perturbative QCD Approaches

In a first step to evaluate HQ diffusion in a QGP perturbation theory has been applied, thereby approximating the medium as a weakly interacting system of quark and gluon quasiparticles. Such a treatment is expected to be reliable if the temperature is large enough for the typical momentum transfers,  $Q^2 \sim T^2$ , to be in the perturbative regime,  $Q^2 \geq 2 \text{ GeV}^2$  or so. This is most likely not satisfied for matter conditions realized at SPS and RHIC. For more realistic applications to experiment several amendments of the perturbative approach have been suggested which are discussed subsequently (focusing again on elastic HQ scattering on light partons).

### 2.2.1. Schematic Leading Order

The initial estimates of equilibration times and energy loss of heavy quarks in the QGP<sup>23</sup> have started from the leading-order (LO) perturbative diagrams involving the minimum of two strong-interaction vertices, as displayed in Fig. 1. Pertinent matrix elements<sup>65</sup> figuring into Eq. (14) in the vacuum have been computed in

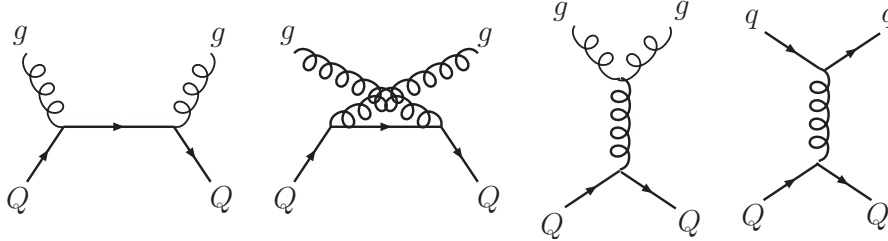


Fig. 1. Feynman diagrams for leading-order perturbative HQ scattering off light partons.

Ref.<sup>65</sup>. The dominant contribution arises from gluon  $t$ -channel exchange, i.e., the 3<sup>rd</sup> and 4<sup>th</sup> diagram in Fig. 1. For forward scattering, the gluon propagator develops the well-known infrared singularity which has been regularized by introducing a Debye-screening mass,

$$G(t) = \frac{1}{t} \rightarrow \frac{1}{t - \mu_D} , \quad \mu_D = gT , \quad (25)$$

where  $g = \sqrt{4\pi\alpha_s}$  denotes the strong coupling constant. Even for a value as large as  $\alpha_s = 0.4$ , and at a temperature of  $T = 300$  MeV (typical for the early stages in heavy-ion collisions at RHIC), the thermal relaxation time,  $\tau_{\text{eq}} = 1/\gamma$ , for charm (bottom) quarks turns out around  $\sim 15(40)$  fm/ $c$  (and therefore much larger than a typical QGP lifetime of  $\sim 5$  fm/ $c$  at RHIC), see, e.g., right panel of Fig. 7 (in Ref.<sup>24</sup> the corrections due to quantum-equilibrium distributions (Bose/Fermi) have been investigated and found to be small). Note that with the above gluon propagator, the pertinent total HQ-parton cross section is parametrically given by  $\sigma_{Qp} \propto \alpha_s^2/\mu_D^2$ , i.e., it essentially increases only linearly in  $\alpha_s$  ( $p = q, \bar{q}, g$ ).

### 2.2.2. Leading Order with Hard Thermal Loop Resummation

In Ref.<sup>26</sup>, the schematic introduction of the Debye mass into the  $t$ -channel gluon-exchange propagator has been extended by a LO hard-thermal loop (HTL) calculation of the charm-quark drag and diffusion coefficients in the QGP. In this approach, the screening of the gluon propagator in the  $t$ -channel diagrams (Fig. 1) is realized by inserting the HTL gluon propagator for the region of small momentum exchange. In Coulomb gauge, with  $q = |\mathbf{q}|$ , this propagator is given by

$$G_{\mu\nu}(\omega, q) = -\frac{\delta_{\mu 0}\delta_{\nu 0}}{q^2 + \Pi_{00}} + \frac{\delta_{ij} - q_i q_j/q^2}{q^2 - \omega^2 + \Pi_T} , \quad (26)$$

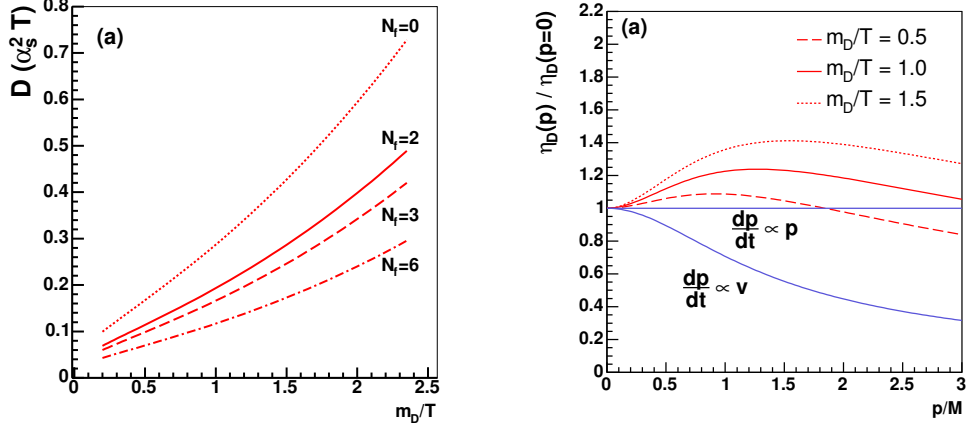


Fig. 2. (Color online) HQ transport coefficients in HTL improved perturbation theory<sup>26</sup>. Left panel: spatial diffusion coefficient at  $p = 0$  as a function of an independently varied Debye mass,  $m_D \equiv \mu_D$ , figuring into the  $t$ -channel gluon exchange propagator, for different quark-flavor content of the (Q)GP. Right panel: momentum dependence of the drag coefficient,  $\eta_D(p) \equiv A(p)$ , for three values of  $\mu_D$  in  $t$ -channel gluon exchange; the lower curve, with  $dp/dt \propto v$ , resembles a calculation in the non-relativistic limit ( $M \equiv m_c = 1.4$  GeV in the  $x$ -axis label denotes the charm-quark mass).

where the  $i, j \in \{1, 2, 3\}$  denote the spatial components of  $\mu, \nu \in \{0, 1, 2, 3\}$ . The HTL self-energies read

$$\begin{aligned} \Pi_T(\omega, \mathbf{q}) &= \mu_D^2 \left\{ \frac{\omega^2}{2q^2} + \frac{\omega(\mathbf{q}^2 - \omega^2)}{4q^3} \left[ \ln \left( \frac{q + \omega}{q - \omega} \right) - i\pi \right] \right\}, \\ \Pi_{00}(\omega, \mathbf{q}) &= \mu_D^2 \left\{ 1 - \frac{\omega}{2q} \left[ \ln \left( \frac{q + \omega}{q - \omega} \right) - i\pi \right] \right\}. \end{aligned} \quad (27)$$

For small energy transfers,  $\omega$ , and a slowly moving heavy quark,  $v \ll 1$ , only the time component of the propagator contributes to the squared matrix elements which in this limit reduces to the Debye-screened Coulomb-like propagator, Eq. (25). Fig. 2 shows the spatial diffusion coefficient and the momentum dependence of the drag coefficient resulting from this calculation. Compared to the screening description with a constant Debye mass, the drag coefficient shows a slight increase for an intermediate range of momenta (cf., e.g., the pQCD curves in Fig. 12).

### 2.2.3. Leading Order with Running Coupling

As indicated in the Introduction, the current data situation at RHIC does not allow for an understanding of the electron data in terms of LO pQCD with reasonably small coupling constant (say,  $\alpha_s \leq 0.4$ ). This was a motivation for more recent studies<sup>66,67</sup>, augmenting the LO pQCD framework in search for stronger effects. Two basic amendments have been introduced. First, the idea of Ref.<sup>26</sup> of introducing a reduced screening mass in the gluon propagator was made more quantitative.

Starting from an ansatz for the screened gluon propagator,

$$G_r(t) \propto \frac{1}{t - r\mu_D^2} . \quad (28)$$

the objective is to obtain an estimate for the constant  $r$  (it was denoted  $\kappa$  in Refs.<sup>66,67</sup>; we changed the notation to avoid conflicts in what follows below). This has been done in analogy to a corresponding QED calculation<sup>68,69</sup>, by requiring that the energy loss of a high-energy quark obtained in a LO-pQCD calculation with the screened propagator, Eq. (28), matches a calculation where for low momentum transfers,  $|t| < |t^*|$ , the HTL propagator, Eq. (26), and for  $|t| > |t^*|$  the perturbative gluon propagator, Eq. (25), is used;  $|t^*|$  is a momentum-transfer scale between  $g^2T^2$  and  $T^2$ . The QED calculation<sup>68,69</sup> yields an energy loss which is independent of the matching scale  $|t^*|$ , while this is not the case in QCD. This problem is treated by introducing an infrared-regulator mass into the hard part of the energy-loss integrals involving the  $t$ -channel exchange-matrix elements, chosen such that the dependence on  $|t^*|$  is weak for  $|t^*| < T^2$  (the validity range of the HTL approximation). This translates into effective values for the  $r$  coefficient in Eq. (28) of  $r \simeq 0.15$ - $0.2$ .

Second, a running strong coupling constant is introduced well into the non-perturbative regime but with an infrared-finite limit. The justification for such a procedure<sup>70</sup> is that it can account for (low-energy) physical observables (e.g., in  $e^+e^-$  annihilation<sup>71</sup>) in an effective way. The parameterization adopted in Refs.<sup>66,67</sup> is based on an extrapolation of Ref.<sup>70</sup> into the spacelike regime,

$$\alpha_{\text{eff}}(Q^2) = \frac{4\pi}{\beta_0} \begin{cases} L_-^{-1} & \text{for } Q^2 \leq 0 \\ 1/2 - \pi^{-1} \arctan(L_+/\pi) & \text{for } Q^2 > 0, \end{cases} \quad (29)$$

where  $\beta_0 = 11 - 2N_f/3$ ,  $N_f = 3$ , and  $L_{\pm} = \ln(\pm Q^2/\Lambda^2)$ . The pertinent substitution in the  $t$ -channel gluon-exchange matrix elements amounts to

$$\frac{\alpha}{t} \rightarrow \frac{\alpha_{\text{eff}}(t)}{t - \tilde{\mu}^2} , \quad (30)$$

where the regulator mass is chosen as  $\tilde{\mu}^2 \in [1/2, 2]\tilde{\mu}_D^2$ , while the Debye-screening mass is determined self-consistently from the equation

$$\tilde{\mu}_D^2 = \left( \frac{N_c}{3} + \frac{N_f}{6} \right) 4\pi\alpha(-\tilde{\mu}_D^2)T^2 . \quad (31)$$

To find the optimal value for the regulator mass a similar strategy of matching the energy loss with a Born approximation has been employed, using the substitution, Eq. (30), in the  $t$ -channel diagrams, with a HTL calculation along the same lines as summarized above for the calculation with non-running  $\alpha_s$ . The results for the drag coefficients for charm quarks under the various model assumptions described above are depicted in Fig. 3. Changing the screening mass from the standard Debye mass,  $\mu_D$ , to that reproducing the HTL energy loss, with  $r = 0.15$  in Eq. (28), increases the drag coefficient by a factor of 2. In view of the large reduction in  $r$

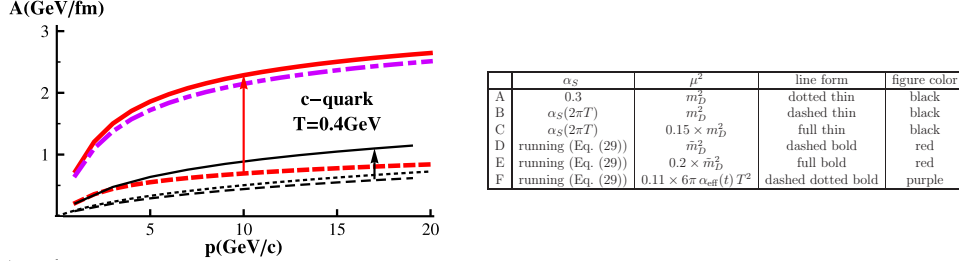


Fig. 3. (Color online) The drag coefficient as a function of HQ three-momentum in the amended pQCD scheme with reduced infrared regulator and running coupling constant (left panel)<sup>66,67</sup>. The corresponding legend (right panel) details the different parameter choices in the calculation.

this appears to be a rather moderate effect. This is simply due to the fact that the change mostly enhances forward scattering which is little effective in thermalizing (isotropizing) a given momentum distribution. Implementing the running-coupling scheme with a small screening mass yields a substantial enhancement by a factor of  $\sim 5$ .

#### 2.2.4. Next-to-Leading Order

The rather large values of the coupling constant employed in the calculations discussed in the previous sections imminently raise questions on the convergence of the perturbative series. This problem has been addressed in a rigorous next-to-leading-order (NLO) calculation for the HQ momentum-diffusion coefficient,  $\kappa = 2D$ , in Refs.<sup>55,72</sup>. This work starts from the definition of  $\kappa$  as the mean squared momentum transfer per unit time, which in gauge theories is given by the time-integrated correlator of color-electric-field operators connected by fundamental Wilson lines:

$$\kappa = \frac{g^2}{3d_H} \int dt \text{Tr}_H \langle W^\dagger(t, 0) E_i^a(t) T_H^a W(t, 0) E_i^b(0) T_H^b \rangle ; \quad (32)$$

$W(t; 0)$  denotes a fundamental Wilson line running from  $t' = 0$  to  $t$  along the static trajectory of the heavy quark,  $T_H^a$  are the generators of the gauge group in the representation of the heavy quark and  $d_H$  its dimension. In leading order this reduces to a Wightman-two-point function of  $A^0$  fields at zero frequency, i.e., in the usual real-time propagator notation,

$$\kappa \simeq \frac{C_H g^2}{3} \int \frac{d^3 \mathbf{p}}{(2\pi)^3} p^2 G^{>00}(\omega = 0, \mathbf{p}), \quad (33)$$

with  $C_H = 4/3$  the Casimir operator of the HQ representation. The integral is IR regulated by HTL corrections, i.e., a Debye mass,  $\mu_D^2 = g^2 T^2 (N_c + N_f/2)/3$ . In the left panel of Fig. 4 the NLO corrections to the LO result, Eq. (33), are depicted in terms of Feynman diagrams. The double line represents the heavy quark, and all propagators and vertices include HTL corrections, leading to a gauge invariant expression as it should be the case for an observable quantity like  $\kappa$ . The

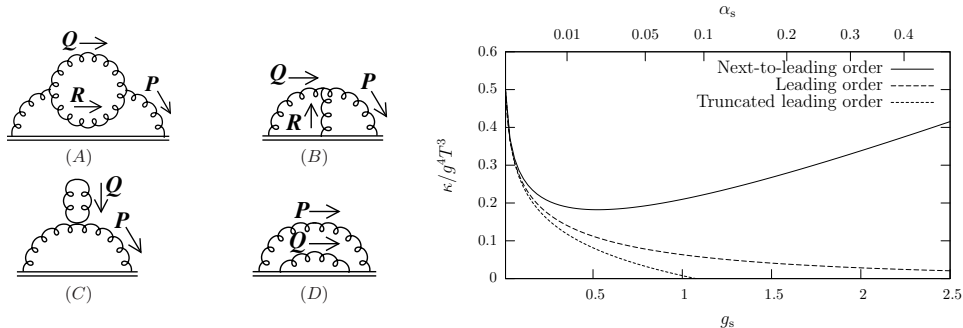


Fig. 4. NLO calculations for HQ diffusion in the QGP<sup>55</sup>. Left panel: NLO diagrams for the momentum-diffusion coefficient,  $\kappa$ ; the double line represents the heavy quark, all propagators are soft and HTL resummed, and all vertices include HTL vertices. Right panel: comparison of LO to NLO result for  $\kappa$  as a function of the strong coupling,  $\alpha_s$ .

diagrams are evaluated in Coulomb gauge within the closed-time path (real-time) Keldysh formalism of thermal quantum-field theory (TQFT). The real part of diagram (A) provides a correction to the Debye mass. Diagrams (C) and (D) take into account real and virtual corrections by additional soft scattering or plasmon emission/absorption of the light or heavy scatterer, respectively. Diagram (B) represents interference between scattering events occurring on the light scatterer's and on the heavy quark's side. Contrary to naive power counting, the NLO calculation provides  $\mathcal{O}(g)$  corrections due to scattering with soft gluons with momentum,  $q \simeq \mu_D$ , and due to overlapping scattering events, dominated by  $t$ -channel Coulombic scatterings involving soft momentum transfers,  $\simeq \mu_D \propto gT$ . The right panel of Fig. 4 shows that the NLO correction to  $\kappa$  is positive, i.e., the momentum-diffusion coefficient becomes larger compared to the LO calculation. The convergence is poor even for rather small coupling constants. A rigorous resummation scheme to cure this behavior is not known to date, especially to establish convergence in the typical range of coupling constants under conditions in relativistic heavy-ion collisions,  $\alpha_s \simeq 0.3-0.4$ . In Ref.<sup>72</sup> the investigation of NLO corrections is extended to the weak-coupling limit of  $\mathcal{N} = 4$  supersymmetric Yang-Mills (SYM) theory. Also in this case the perturbative series turns out to be poorly convergent, even for low couplings.

### 2.2.5. Three-body elastic scattering

Another step in the (would-be) perturbative hierarchy are three-body collisions, which are expected to become increasingly important at high parton density. An attempt to assess the effects of three-body elastic scattering for HQ diffusion has been conducted in Ref.<sup>73</sup>, with pertinent Feynman diagrams as depicted in Fig. 5. Special care has to be taken in regularizing contributions from diagrams with intermediate particles going on-shell; these can lead to divergent real parts in the

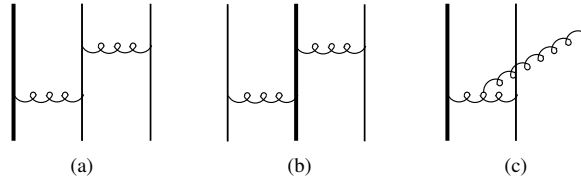


Fig. 5. Different topological classes of diagrams for three-body elastic scattering of a heavy quark (thick lines) off light quarks and antiquarks (thin lines)<sup>73</sup>.

scattering amplitude and represent successive two-body scatterings (rather than genuine three-body scattering). Therefore, in Ref.<sup>73</sup> the intermediate quark lines in diagram (a) and (b) are supplemented with an in-medium collisional width, and only the real part of their propagator is kept in the evaluation of the diagrams. For three-body elastic processes involving one or two gluons, it has been assumed that the dominant contributions arise from diagrams with similar topology as diagram (b) in Fig. 5 for  $Qqq$  scattering; all other contributions are neglected. To compare with two-body gluo-radiative inelastic scattering the LO diagrams have been used to evaluate matrix elements for  $Qq \rightarrow Qqg$ ,  $Q\bar{q} \rightarrow Q\bar{q}g$  and  $Qg \rightarrow Qgg$  processes. Within this scheme, at temperatures  $T = 200\text{-}300$  MeV, three-body elastic scattering processes are estimated to contribute to the  $c$ - and  $b$ -quark friction coefficients with a magnitude comparable to two-body elastic scattering. Again, this raises the question of how to control the perturbative series for HQ diffusion. As a by-product, the friction coefficient for radiative scattering,  $Qp \rightarrow Qpg$ , was estimated to exceed the one from elastic two-body scattering for HQ momenta  $p \gtrsim 12$  GeV (for both charm and bottom).

### 2.3. Non-Perturbative Interactions

The evidence for the formation of a strongly coupled QGP (sQGP) at RHIC has motivated vigorous theoretical studies of the possible origin of the interaction strength (see, e.g., Ref.<sup>74</sup> for a recent review). In particular, several lattice QCD computations of hadronic correlation functions at finite temperature have found indications that hadronic resonances (or bound states) survive up to temperatures of twice the critical one or more (for both a gluon plasma (GP) and a QGP)<sup>41,42,75,76</sup>, cf. also Sec. 4.1.1 of this article. Pertinent spectral functions (extracted from Euclidean correlators using probabilistic methods, i.e., the maximum entropy method) exhibit resonance peaks in both  $Q\bar{Q}$  and  $q\bar{q}$  channels. The consequences of hadronic resonances in the QGP for HQ transport have been elaborated in Refs.<sup>25,28,77,44</sup>. The starting point in Refs.<sup>25,28,77</sup> is the postulate that heavy-light quark ( $Q\bar{q}$ ) resonances, i.e., “ $D$ ” and “ $B$ ” mesons, persist in the QGP. In Refs.<sup>25,28</sup> this has been realized within an effective resonance model for  $Q\bar{q}$  scattering (Sec. 2.3.1) while in Ref.<sup>77</sup> HQ fragmentation into mesons and their subsequent momentum broadening was considered (Sec. 2.3.3). The phenomenological success of these models (cf., e.g.,

the right panel of Fig. 26) called for a more microscopic evaluation of the heavy-light quark correlations. This was realized in Ref.<sup>44</sup> where in-medium heavy-light quark  $T$ -matrices were computed with interaction potentials estimated from HQ free energies in lattice QCD (cf. Sec. 2.3.2). This approach is the direct analog to the potential models used in the heavy quarkonium context (cf. Sec. 4.1.1). We finish this section with a brief discussion of a recent suggestion to extract information on HQ diffusion more directly from thermal lattice QCD (Sec. 2.3.4), which would constitute a valuable benchmark for both perturbative and non-perturbative calculations.

### 2.3.1. Effective $Q\bar{q}$ -resonance model

The heavy-light quark resonance model<sup>25</sup> has been set up by combining HQ effective theory (HQET) with chiral symmetry in the light-quark sector,  $q = (u, d)$ , based on the Lagrangian,

$$\begin{aligned} \mathcal{L}_{Dcq} = & \mathcal{L}_D^0 + \mathcal{L}_{c,q}^0 - iG_S \left( \bar{q}\Phi_0^* \frac{1+\not{v}}{2} c - \bar{q}\gamma^5 \Phi \frac{1+\not{v}}{2} c + h.c. \right) \\ & - G_V \left( \bar{q}\gamma^\mu \Phi_\mu^* \frac{1+\not{v}}{2} c - \bar{q}\gamma^5 \gamma^\mu \Phi_{1\mu} \frac{1+\not{v}}{2} c + h.c. \right), \end{aligned} \quad (34)$$

written in the charm sector (an equivalent one in the bottom sector follows via the replacements  $c \rightarrow b$  and  $D \rightarrow B$  for the HQ and resonance fields, respectively;  $v$ : HQ four-velocity). The pertinent free Lagrangians read

$$\begin{aligned} \mathcal{L}_{c,q}^0 = & \bar{c}(i\not{\partial} - m_c)c + \bar{q}i\not{\partial}q, \\ \mathcal{L}_D^0 = & (\partial_\mu \Phi^\dagger)(\partial^\mu \Phi) + (\partial_\mu \Phi_0^{*\dagger})(\partial^\mu \Phi_0^*) - m_S^2(\Phi^\dagger \Phi + \Phi_0^{*\dagger} \Phi_0^*) \\ & - \frac{1}{2}(\Phi_{\mu\nu}^{*\dagger} \Phi^{*\mu\nu} + \Phi_{1\mu\nu}^\dagger \Phi_1^{\mu\nu}) + m_V^2(\Phi_\mu^{*\dagger} \Phi^{*\mu} + \Phi_{1\mu}^\dagger \Phi_1^\mu). \end{aligned} \quad (35)$$

$\Phi$  and  $\Phi_0^*$  denote the pseudoscalar and scalar meson fields (corresponding to  $D$  and  $D_0^*$  mesons) which are assumed to be degenerate chiral partners (mass  $m_S$ ) as a consequence of chiral restoration in the QGP. The same reasoning applies to the vector and axialvector states (mass  $m_V$ ),  $\Phi_\mu^*$  and  $\Phi_{1\mu}$  (corresponding to  $D^*$  and  $D_1^*$ ). HQ spin symmetry furthermore asserts the degeneracy of spin-0 and -1 states with identical angular momentum, implying  $m_S = m_V$  and the equality of the coupling constants,  $G_S = G_V$ . In the strange-quark sector only the pseudoscalar ( $D_s$ ) and vector ( $D_s^*$ ) resonance states are considered (i.e., chiral symmetry is not imposed).

The boson-resonance propagators are dressed with heavy-light quark self-energies at the one-loop level (cf. left panel of Fig. 6). To leading order in HQET, in accordance with spin symmetry, the self-energies for the vector/axialvector resonances are given by

$$\Pi_{D^*,\mu\nu} = (v_\mu v_\nu - g_{\mu\nu})\Pi_D(s), \quad (36)$$

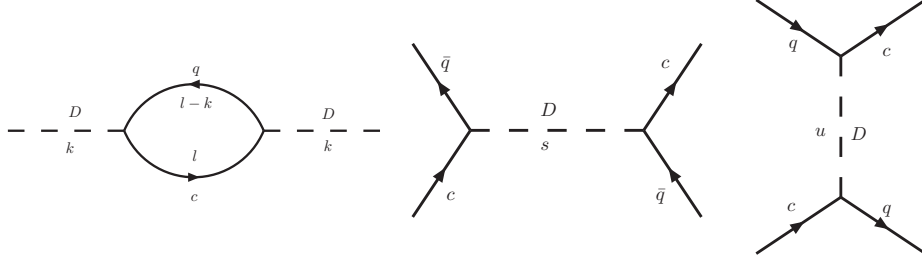


Fig. 6. Left panel: one-loop diagram representing the  $D$ -meson self-energy in the QGP within the effective resonance model<sup>25</sup>. Right and middle panels: elastic  $Q\bar{q}$  and  $Qq$  scattering diagrams for  $s$ - and  $u$ -channel resonance exchange, respectively.

where  $s = p^2$  denotes the meson's four momentum, and  $\Pi_D$  is the self-energy of the pseudoscalar/scalar resonances. Its imaginary part reads

$$\text{Im } \Pi_D(s) = -\frac{3G^2}{8\pi} \frac{(s - m_c^2)^2}{s} \Theta(s - m_c^2), \quad (37)$$

while the real part is calculated from a twice-subtracted dispersion relation with the wave-function and mass counter terms adjusted such that the following renormalization conditions hold,

$$\partial_s \Pi_D^{(\text{ren})}(s)|_{s=0} = 0, \quad \text{Re } \Pi_D^{(\text{ren})}(s)|_{s=m_D^2} = 0. \quad (38)$$

As an alternative regularization scheme, dipole form factors,

$$F(|\mathbf{q}|) = \left( \frac{2\Lambda^2}{2\Lambda^2 + \mathbf{q}^2} \right)^2, \quad (39)$$

have been supplemented to simulate finite-size vertices of the resonance model,

$$\text{Im } \Pi_D^{(\text{ff})}(s) = \text{Im } \Pi_D(s) F^2(|\mathbf{q}|), \quad (40)$$

with  $|\mathbf{q}| = (s - m_c^2)/(2\sqrt{s})$ . In this scheme, the real part is calculated from an unsubtracted dispersion relation, while the bare resonance mass is adjusted to obey the second renormalization condition in Eq. (38).

With charm- and bottom-quark masses of  $m_c = 1.5$  GeV and  $m_b = 4.5$  GeV, the physical resonance masses are adjusted to  $m_D = 2$  GeV and  $m_B = 5$  GeV, respectively. This is in approximate accordance with earlier  $T$ -matrix models of heavy-light quark interactions<sup>78,79</sup>. Likewise, the coupling constant,  $G$ , is adjusted such that the resonance widths vary as  $\Gamma_{D,B} = 0.4 \dots 0.75$  GeV. The resulting heavy-light quark scattering matrix elements (cf. middle and right panels of Fig. 6) have been injected into Eq. (15) to calculate HQ drag and diffusion coefficients. In the left and right panel of Fig. 7 we compare the total HQ elastic scattering cross sections and resulting thermal relaxation times,  $\tau_{\text{eq}} = 1/A(\mathbf{p} = 0)$ , of the resonance model with LO pQCD (cf. the diagrams in Fig. 1). Although the total cross sections are not very different in magnitude, the thermalization times decrease by around

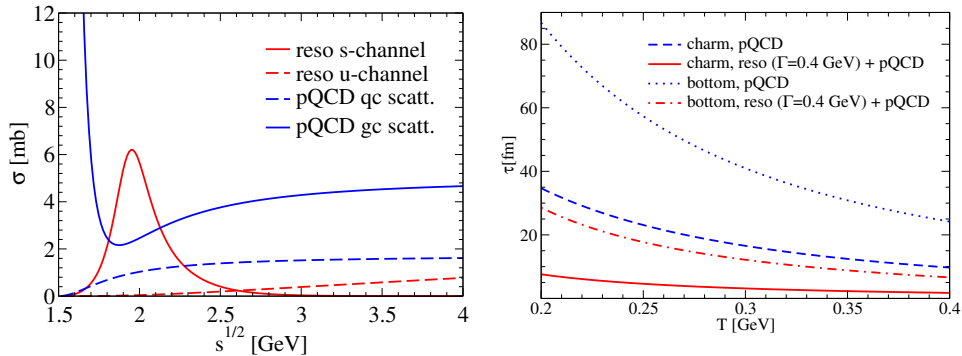


Fig. 7. (Color online) Left panel: total HQ scattering cross sections off light partons in LO pQCD (blue lines) and within the effective resonance model (red lines). Right panel: thermalization times,  $\tau = 1/A(\mathbf{p} = 0)$ , for charm and bottom quarks in LO pQCD with  $\alpha_s = 0.4$  and Debye-screening mass  $\mu_D = gT$ , compared to the results from the resonance+pQCD model, as a function of QGP temperature.

a factor of  $\sim 3$ -4 when adding resonant scattering, for all temperatures  $T = 1$ - $2 T_c$ . The main reason for this behavior is that  $s$ -channel  $Q\bar{q}$  scattering is isotropic in the rest frame of the resonance, while the pQCD cross section is largely forward-peaked ( $t$ -channel gluon exchange), and thus produces a much less efficient transport cross section (which encodes an extra angular weight). The charm-quark equilibration times in the resonance+pQCD model,  $\tau_{\text{eq}}^c = 2$ - $10$  fm/ $c$ , are comparable to the expected QGP lifetime at RHIC of around  $\tau_{\text{QGP}} \simeq 5$  fm/ $c$ . Thus, at least for charm quarks, substantial modifications of their  $p_t$  spectra towards local equilibrium in the flowing medium can be expected.

The consistency of the Fokker-Planck approach can be checked with the dissipation-fluctuation relation, Eq. (77), at  $\mathbf{p} = 0$ , cf. left panel of Fig. 8. For the forward-peaked pQCD-matrix elements, the relation is fulfilled within 3%, while with the isotropic resonance scattering deviations reach up to 11% in the renormalization scheme and up to 26% in the formfactor-cutoff scheme at the highest temperatures considered ( $T = 400$  MeV). Note however, that for a typical thermal evolution at RHIC, average fireball temperatures above  $T = 250$  MeV are only present within the first fm/ $c$ <sup>39</sup>; below this temperature, the deviations are less than 5% for all cases. The right panel of Fig. 8 illustrates that (for identical resonance widths) the formfactor regularization scheme leads to somewhat larger (smaller) friction coefficients at low (high) momentum than the renormalization scheme.

In Fig. 9 the momentum dependence of the drag and transverse diffusion coefficients is depicted using either resonance-scattering or pQCD-matrix elements. Resonance scattering becomes relatively less efficient for higher HQ momenta since the center-of-mass energy in collisions with thermal light antiquarks increasingly exceeds the resonance pole. The variations of the coefficients with the strong coupling constant in the pQCD scattering-matrix elements or the resonance-coupling

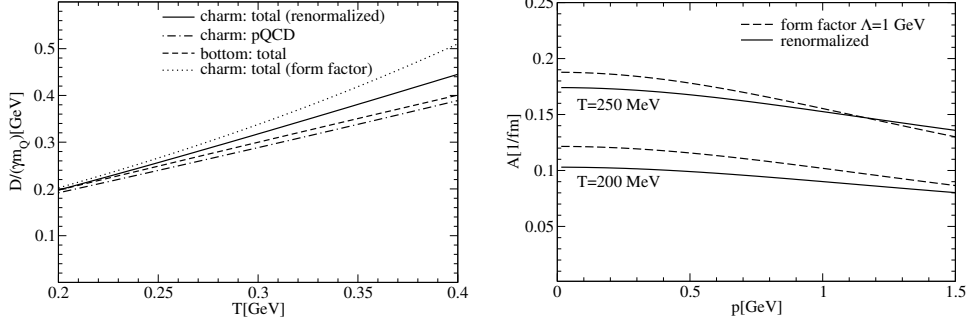


Fig. 8. Left panel: check of the dissipation-fluctuation relation at  $\mathbf{p} = 0$  for  $c$  and  $b$  quarks with and without resonance interactions and in the renormalization and form-factor cutoff schemes. Right panel: momentum dependence of the drag coefficient in the renormalization and the formfactor-cutoff scheme, where the coupling constants have been chosen in both schemes as to obtain a resonance width  $\Gamma = 0.4$  GeV.

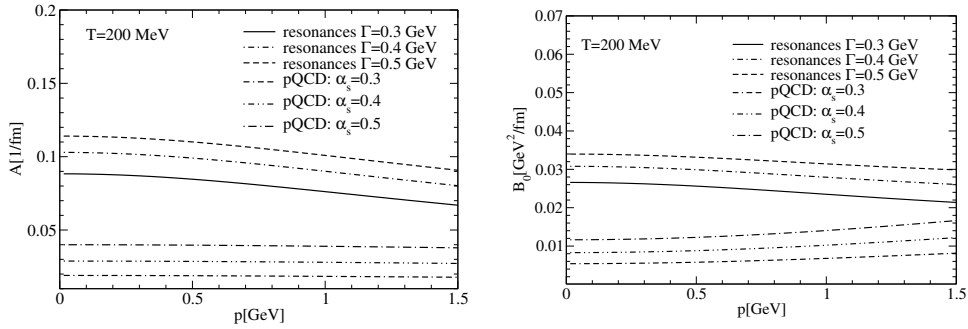


Fig. 9. Drag (left panel) and transverse-diffusion coefficient (right panel) for pQCD and resonance model with varying interactions strengths as a function of the HQ momentum at a temperature of  $T = 200$  MeV.

constant in the effective resonance-scattering model are rather moderate. This is due to compensating effects of an increase of the matrix elements with  $\alpha_s^2$  or  $G^4$ , on the one hand, and the accordingly increased Debye-screening mass for pQCD scattering or the broadening of the resonances widths, on the other hand.

### 2.3.2. In-Medium $T$ -matrix with lQCD-based Potentials

The idea of utilizing HQ free energies computed in lattice QCD to extract a driving kernel for heavy-light quark interactions in the QGP has been carried out in Ref. <sup>44</sup>, with the specific goal of evaluating HQ diffusion. Since the latter is, in principle, determined by low-energy HQ interactions, the potential-model framework appears to be suitable for this task. Moreover, with a potential extracted from lQCD, the calculation could be essentially parameter-free. Currently, however, such an approach

bears significant uncertainty, both from principle and practical points of view, e.g., whether a well-defined potential description can be constructed in medium<sup>80,81,82</sup> and, if so, how to extract this information from, say, the HQ free energy. In the vacuum, both questions have been answered positively<sup>83,84</sup>, thus validating the 30 year-old phenomenological approaches using Cornell potentials for heavy quarkonia, which provide a very successful spectroscopy<sup>85</sup>. The potential approach has been extended to heavy-light mesons in Refs.<sup>86,87</sup>.

A Brueckner-like in-medium  $T$ -matrix approach for heavy-light quark scattering in the QGP has been applied in Ref.<sup>44</sup>, diagrammatically represented in Fig. 10. The underlying (static) two-body potential has been identified with the internal energy

$$U_1(r, T) = F_1(r, T) + TS_1(r, T) = F_1(r, T) - T \frac{\partial F_1(r, T)}{\partial T}, \quad (41)$$

extracted from two lQCD computations of the color-singlet HQ free energy above  $T_c$ , for quenched<sup>88</sup> and two-flavor<sup>89</sup> QCD (pertinent parameterizations are given in Refs.<sup>90</sup> and <sup>45</sup>, hereafter referred to as [Wo] and [SZ], respectively). This choice (rather than, e.g., the free energy) provides an upper limit for the interaction strength<sup>45,90,91,58</sup>. To use Eq. (41) as a potential in a  $T$ -matrix calculation, the internal energy has to be subtracted such that it vanishes for  $r \rightarrow \infty$ ,

$$V_1(r, T) \equiv U_1(r, T) - U_1(r \rightarrow \infty, T), \quad (42)$$

which is dictated by the convergence of the  $T$ -matrix integral in momentum space. It is suggestive to interpret the asymptotic value  $U_1^\infty \equiv U_1(r \rightarrow \infty, T)$  as an in-medium HQ-mass,

$$m_Q(T) = m_Q^0 + \frac{1}{2}U_1^\infty, \quad (43)$$

where  $m_Q^0$  denotes the bare HQ mass (e.g.,  $m_c^0 \simeq 1.25$  GeV<sup>92</sup> for the bare  $c$ -quark mass). However, close to  $T_c$ , the values for  $U_1^\infty(T)$  extracted from lQCD calculations develop a rather pronounced peak structure<sup>93,94</sup>, which renders a mass interpretation problematic. Progress in understanding these properties is closely connected with the proper identification of the potential. First lQCD estimates of the in-medium HQ mass (extracted by relating zero-mode contributions to quarkonium correlators to the HQ susceptibility) indicate a moderate increase when approaching  $T_c$  from above<sup>46</sup>. In Ref.<sup>44</sup> constant (average) in-medium charm- and bottom-quark masses of  $m_c = 1.5$  GeV and  $m_b = 4.5$  GeV, respectively, have been employed.

The  $T$ -matrix approach is readily generalized to color-configurations other than the singlet channel of the  $qQ$  pair. The complete set of color states for  $Q\bar{q}$  (singlet and octet) and  $Qq$  (anti-triplet and sextet) pairs has been taken into account assuming Casimir scaling as in pQCD,

$$V_8 = -\frac{1}{8}V_1, \quad V_{\bar{3}} = \frac{1}{2}V_1, \quad V_6 = -\frac{1}{4}V_1. \quad (44)$$

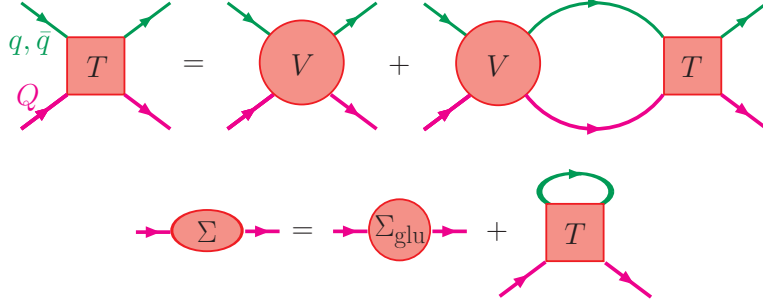


Fig. 10. (Color online) Diagrammatic representation of the Brueckner many-body calculation for the coupled system of the  $T$ -matrix based on the IQCD static internal potential as the interaction kernel and the HQ self-energy.

which is, in fact, supported by finite- $T$  IQCD<sup>95,96</sup>. To augment the static (color-electric) potentials with a minimal relativistic (magnetic) correction for moving quarks<sup>97</sup>, the so-called Breit correction as known from electrodynamics<sup>98</sup> has been implemented via the substitution

$$V_a \rightarrow V_a(1 - \hat{\alpha}_1 \cdot \hat{\alpha}_2), \quad (45)$$

where  $\hat{\alpha}_{1,2}$  are quasiparticle velocity operators.

The above constructed heavy-light potentials can now be resummed in a two-body scattering equation. In accordance with the static nature of the potentials, it is appropriate to use a three-dimensional reduction of the full four-dimensional Bethe-Salpeter equation. This leads to the well-known ladder series which is resummed by the Lippmann-Schwinger (LS) integral equation for the  $T$ -matrix. In the  $q$ - $Q$  center-of-mass (CM) frame it takes the form

$$T_a(E; \mathbf{q}', \mathbf{q}) = V_a(\mathbf{q}', \mathbf{q}) - \int \frac{d^3 \mathbf{k}}{(2\pi)^3} V_a(\mathbf{q}', \mathbf{k}) G_{qQ}(E; k) \times T_a(E; \mathbf{k}, \mathbf{q}) [1 - f_q(\omega_k^q) - f_Q(\omega_k^Q)]. \quad (46)$$

The driving kernel (potential) can now be identified with the Fourier transform of the coordinate-space potential extracted from IQCD,

$$V_a(\mathbf{q}', \mathbf{q}) = \int d^3 \mathbf{r} V_a(r) \exp[i(\mathbf{q} - \mathbf{q}') \cdot \mathbf{r}] \quad (47)$$

in a given color channel,  $a \in \{1, \bar{3}, 6, 8\}$ . The concrete form of the intermediate  $q$ - $Q$  (or  $\bar{q}$ - $Q$ ) propagator,  $G_{qQ}(E, k)$ , depends on the reduction scheme of the underlying Bethe-Salpeter equation. It has been verified<sup>91,44</sup> that, e.g., the Thompson<sup>99</sup> and Blencenbecler-Sugar<sup>100</sup> scheme lead to very similar results in the present context (as was found for nucleon-nucleon scattering). In the former, the two-particle propagator is given by

$$G_{qQ}(E, k) = \frac{1}{E - (\omega_k^q + i\Sigma_I^q) - (\omega_k^Q + i\Sigma_I^Q)}, \quad (48)$$

where  $E$  and  $k$  denote the CM energy and relative momentum of the  $qQ$  pair, respectively. The quasi-particle widths are chosen as  $\Gamma_I^{q,Q} = 2\Sigma_I^{q,Q} = 200$  MeV, and the light quark masses as constant at  $m_q = 0.25$  GeV, with on-shell energies

$$\omega_k^{q,Q} = \sqrt{m_{q,Q}^2 + k^2} . \quad (49)$$

The latter figure into the Pauli blocking factor with Fermi-Dirac distributions,

$$f_{q,Q}(\omega^{q,Q}) = \frac{1}{\exp(\omega^{q,Q}/T) + 1} \quad (50)$$

(at the considered temperatures their impact is negligible). The solution of the  $T$ -matrix Eq. (46) is facilitated by a an expansion into partial waves,  $l$ ,

$$\begin{aligned} V_a(\mathbf{q}', \mathbf{q}) &= 4\pi \sum_l (2l+1) V_{a,l}(q', q) P_l[\cos \angle(\mathbf{q}, \mathbf{q}')] , \\ T_a(E; \mathbf{q}', \mathbf{q}) &= 4\pi \sum_l (2l+1) T_{a,l}(E; q', q) P_l[\cos \angle(\mathbf{q}, \mathbf{q}')] , \end{aligned} \quad (51)$$

which yields a one-dimensional LS equation,

$$\begin{aligned} T_{a,l}(E; q', q) &= V_{a,l}(q', q) + \frac{2}{\pi} \int dk k^2 V_{a,l}(q', k) G_{Qq}(E; k) \\ &\quad \times T_{a,l}(E; k, q) [1 - f_F(\omega_k^Q) - f_F(\omega_k^q)] , \end{aligned} \quad (52)$$

for the partial-wave components,  $T_{a,l}$ , of the  $T$ -matrix. Eq. (52) can be solved numerically by discretization and subsequent matrix-inversion with the algorithm of Haftel and Tabakin<sup>101</sup>. The resulting  $S$ -wave ( $l = 0$ )  $T$ -matrices indeed show resonance structures in a QGP in the channels where the potential is attractive, i.e., in the meson (color-singlet) and diquark (color-antitriplet) channels. The pertinent peaks in the imaginary part of the  $T$ -matrix develop close to the  $Q$ - $q$  threshold, and melt with increasing temperature at around  $1.7T_c$  and  $1.4T_c$ , respectively (cf. left panel of Fig. 11). In the repulsive channels, as well as for  $P$ -waves, the  $T$ -matrices carry much reduced (non-resonant) strength. The increasing strength in the meson and diquark channels (the latter relevant for baryon binding) when approaching  $T_c$  from above is suggestive for “pre-hadronic” correlations toward the hadronization transition.

The next step is to use the  $T$ -matrices to compute the light-quark contribution to HQ self-energies, i.e., the last diagram in the second line of the Brueckner scheme illustrated in Fig. 10. In a given color-channel,  $a$ , the  $T$ -matrix induced self-energy is given by

$$\Sigma_a^Q(\omega, p) = \frac{d_{\text{SI}} d_a}{6} \int \frac{k^2 dk dx}{4\pi^2} [f_F(\omega_k) + f_B(\omega + \omega_k)] T_a(E; \mathbf{p}, \mathbf{k}) , \quad (53)$$

where  $d_{\text{SI}} = 4(2l+1)N_f$  denotes the spin-isospin and angular momentum degeneracy of all  $Qq$  (or  $Q\bar{q}$ ) configurations (assuming spin and light-flavor symmetry) and  $d_a$  the color degeneracy of channel  $a$ ; the factor  $1/6$  averages over the incoming HQ color-spin degrees of freedom. The resulting charm-quark selfenergies (summed

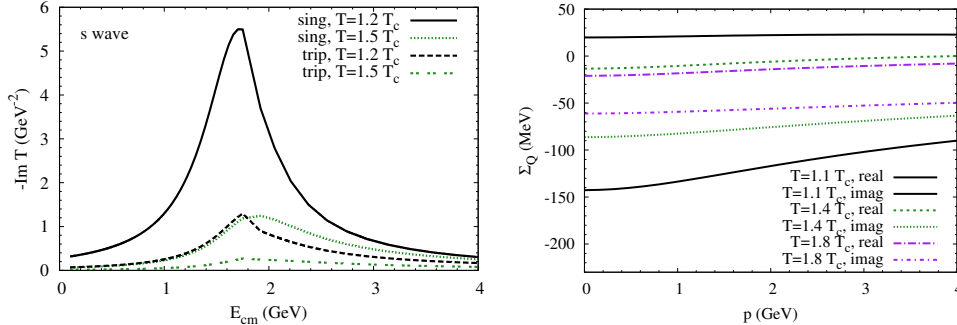


Fig. 11. (Color online) Results of a Brueckner-type approach for  $c$ -quarks in a QGP<sup>44</sup> based on a potential corresponding to the internal energy extracted from quenched lattice QCD<sup>88,90</sup>. Left panel: imaginary part of the in-medium  $T$  matrices for  $S$ -wave  $c$ - $q$  scattering in color-singlet and -triplet channels at two different temperatures; right panel: real and imaginary parts of  $c$ -quark selfenergies based on the  $T$ -matrices in the left panel.

over all light quarks and antiquarks) are displayed in the right panel of Fig. 11. One finds rather small corrections to the HQ mass (presented by the real part of  $\Sigma$ ), but the imaginary parts are substantial,  $\Gamma_c = -2 \text{Im } \Sigma_c \simeq 100\text{-}300$  MeV for temperatures  $T = 1.1\text{-}1.8 T_c$  (with the largest values attained close to  $T_c$ ). These values were the motivation for the choice of input widths in the propagator, Eq. (48), of the  $T$ -matrix equation, thus providing a rough self-consistency. The in-medium mass corrections, on the other hand, are associated with the gluonic contribution to the HQ self-energy (corresponding to the first term in the lower line Fig. 10), which have not been calculated explicitly in Ref. <sup>44</sup>, but represent a rough (average) representation of the asymptotic values of the HQ potential,  $U_\infty^{(1)}$  (as discussed above).

The final step is to implement the  $T$ -matrix elements into a calculation of HQ drag and diffusion coefficients via Eq. (15); one finds

$$\begin{aligned} \sum |\mathcal{M}|^2 &= \frac{64\pi}{s^2} (s - m_q^2 + m_Q^2)^2 (s - m_Q^2 + m_q^2)^2 \\ &\times N_f \sum_a d_a (|T_{a,l=0}(s)|^2 + 3|T_{a,l=1}(s) \cos(\theta_{\text{cm}})|^2). \end{aligned} \quad (54)$$

The resulting friction coefficients are summarized in Fig. 12 as a function of momentum for three temperatures and for two potential extractions from lQCD<sup>45,90</sup>. Generally, the  $Qq$   $T$ -matrix based coefficients are largest at low HQ momentum, as to be expected from the resonance formation close to threshold. The values exceed the LO-pQCD coefficients at small temperatures and for both potentials by a factor of  $\sim 3\text{-}5$ . At higher temperatures the enhancement reduces considerably, to a factor of less than 2 in the [SZ] potential and to essentially equal strength for the [Wo] potential<sup>d</sup>. In fact, the coefficients computed with the [SZ] potential have a slightly

<sup>d</sup>Recall that the LO-pQCD calculations employ a rather large coupling ( $\alpha_s=0.4$ ), and are domi-

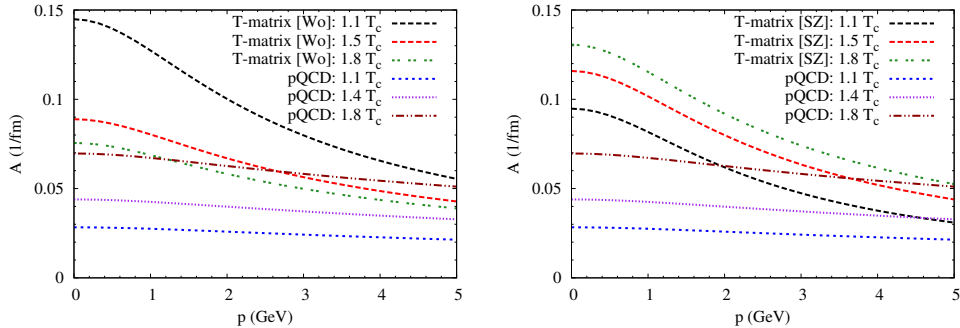


Fig. 12. (Color online) The drag coefficients at different temperatures, using the parameterization of the HQ potential from [Wo] (left panel) and [SZ] (right panel) compared to LO pQCD with  $\alpha_s = 0.4$  and  $\mu_D = gT$ .

(30%) increasing trend with  $T$ , while the [Wo] potential leads to a decreasing trend. This difference needs to be scrutinized by future systematic comparisons of IQCD input potentials. Compared to the resonance model (cf., e.g., left panel of Fig. 9), the  $T$ -matrix calculations yield quantitatively similar results at temperatures not too far above  $T_c$  but become smaller at higher  $T$  due to resonance melting (which is presumably a more realistic feature of a non-perturbative interaction strength).

### 2.3.3. Collisional Dissociation of Heavy Mesons in the QGP

In Ref.<sup>77</sup>, a so-called reaction-operator (GLV) approach has been applied to resum multiple elastic scatterings of a fast  $Q\bar{q}$  pair. The quenching of heavy quarks in a QGP is calculated by solving coupled rate equations for the fragmentation of  $c$  and  $b$  quarks into  $D$  and  $B$  mesons and their dissociation in the QGP. The main mechanisms for HQ energy loss are collisional broadening of the meson's transverse momentum and the distortion of its intrinsic light-cone wave function. The latter is modeled in a Cornell-type potential ansatz<sup>87</sup> (note that this bears some similarity to the  $T$ -matrix approach discussed in Sec. 2.3.2). This in-medium HQ/heavy-meson fragmentation/dissociation mechanism leads to comparable high- $p_t$  suppression for  $B$  and  $D$  mesons, which is quite contrary to perturbative calculations for both collisional and radiative energy loss (where the suppression of  $b$  quarks is significantly less pronounced than for  $c$  quarks). This feature largely results from the much smaller formation times of  $B$ -mesons compared to  $D$ -mesons, leading to a faster fragmentation-dissociation cycle for  $b$  quarks/ $B$  mesons.

nated by scattering off gluons in the heat bath; thus a minimal merging of the gluon sector with the  $T$ -matrix calculations would consist of adding the gluonic part of LO-pQCD; this procedure is adopted below whenever combined results are shown or utilized. In principle, a non-perturbative treatment should also be applied to HQ-gluon scattering.

### 2.3.4. Estimates of HQ Diffusion in Lattice QCD

It has recently been suggested that, unlike in the case of other transport coefficients (e.g., the shear viscosity), the HQ diffusion coefficient might be amenable to a determination within lQCD, based on an analytic continuation of the color-electric-field correlator along a Polyakov loop<sup>102</sup> (see also Ref. <sup>103</sup> for earlier related work). The starting point of these considerations is the spectral function of the HQ current correlator,

$$\rho_V^{\mu\nu}(\omega) = \int dt \exp(i\omega t) \int d^3\mathbf{x} \left\langle \frac{1}{2} \left[ J_Q^\mu(t, \mathbf{x}), J_Q^\nu(0, 0) \right] \right\rangle, \quad (55)$$

where  $J_Q^\mu$  denotes the HQ current operator in the Heisenberg picture. The spatial diffusion coefficient,  $D_s$ , can be extracted from this spectral function by the pole position at  $\omega = -iD_s\mathbf{k}^2$ , where  $\mathbf{k}$  is the HQ momentum. The condition for a pole leads to the Kubo relation

$$D_s = \frac{1}{3\chi^{00}} \lim_{\omega \rightarrow 0} \sum_{i=1}^3 \frac{\rho_V^{ii}(\omega)}{\omega}, \quad (56)$$

where  $\chi_{00}$  is the conserved-charge susceptibility

$$\chi^{00} = \frac{1}{T} \int d^3\mathbf{x} \langle J_Q^0(t, \mathbf{x}) J_Q^0(0, 0) \rangle. \quad (57)$$

For a heavy quark, the spectral function, Eq. (55), is expected to develop a sharp peak around  $\omega = 0$  which can be described by a Lorentzian function close to this point. The width of this function is given by the drag coefficient, which obeys the fluctuation-dissipation relations, discussed in Sec. 2.1. Using HQ effective theory techniques it is shown that in the static limit the momentum-diffusion coefficient,  $\kappa = 2D$ , is given by a correlator involving color-electric fields and  $J_Q^0$  operators whose Euclidean analogue can be mapped to an expectation value involving Wilson lines and color-electric fields, similar to Eq. (32). This purely gluonic correlation function can in principle be evaluated in lQCD.

Another lattice-based approach to assess HQ diffusion has been suggested in Ref.<sup>104</sup> in terms of (discretized) classical gauge theory. The limitation of this approach is set by the thermal (hard) scale  $\sim\pi T$  where quantum theory suppresses excitations. Since the HQ thermalization rate is expected to be governed by the electric screening scale  $\sim gT$ , this limitation may not be severe for small and moderate coupling ( $gT \ll T$ ), and thus allow for valuable insights. First, it has been verified that, in the weak coupling limit, the discretized (nonperturbative) classical computation indeed agrees well with pQCD. Upon increasing the coupling strength, the classical lattice results for the HQ momentum diffusion coefficient increasingly exceed the LO perturbative result, by about an order of magnitude for a moderate coupling strength corresponding to  $\alpha_s \simeq 0.2$ . Next, the NLO term (with slightly increased strength to account for HTL effects), as calculated in Ref.<sup>55</sup>, has been added to the LO calculation which extends the agreement of pQCD with the classical lattice results to larger (but still weak) coupling. For  $\alpha_s \simeq 0.2$  the increase over

LO amounts to a factor  $\sim 2$ , which means that the classical lattice result remains substantially larger (by a factor of  $\sim 5$ ) than the NLO value. Besides reconfirming the poor convergence of pQCD, this also suggests that the perturbative series is not alternating but that higher order terms keep increasing the value of the HQ momentum diffusion coefficient. Semi-quantitatively, such an enhancement is in the ballpark of the factor  $\sim 3-4$  found in the effective resonance model (Sec. 2.3.1) or  $T$ -matrix approach (Sec. 2.3.2).

#### **2.4. String Theoretical Evaluations of Heavy-Quark Diffusion**

The conjectured correspondence between certain classes of string theories, formulated in five-dimensional Anti-de-Sitter space ( $\text{AdS}_5$ ), and gauge theories with conformal invariance (conformal field theory, CFT) has opened interesting possibilities to address nonperturbative aspects of QCD. The so-called AdS/CFT correspondence implies a “duality” of a weakly coupled gravity to a strongly coupled supersymmetric (and conformal) gauge theory, specifically  $\mathcal{N} = 4$   $\text{SU}(N_c)$  super-Yang-Mills (SYM) theory. This connection has been exploited to formulate the problem of HQ diffusion at finite temperature and extract an “exact” nonperturbative result for HQ transport coefficients in the SYM plasma<sup>105,106,107</sup>. The translation to QCD matter is beset with several caveats<sup>108</sup>, e.g., the particle content of the SYM medium is quite different compared to the QGP. While this may be corrected for by a suitable rescaling of the temperature by matching, e.g., the energy densities<sup>e</sup>, a more problematic difference is the absence of a scale (other than temperature) in conformal SYM. Thus, the latter does not possess a breaking of scale invariance, a running coupling constant, confinement nor spontaneous chiral symmetry breaking, and consequently no notion of a critical temperature, either. Thus SYM is quite different from QCD in the zero- and low-temperature regimes. However, at sufficiently high  $T$ , where the QCD medium deconfines its fundamental charges, the resemblance to SYM might be much closer. E.g., the pressure in SYM in the strong coupling limit amounts to about 75% of the Stefan-Boltzmann limit, close to what is found in thermal lattice QCD for a wide range above  $T_c$ . In addition, the finding of an extremely small shear viscosity in strongly coupled SYM,  $\eta/s = 1/4\pi$  (conjectured to be a universal lower bound)<sup>17</sup>, and the apparently low-viscosity QCD medium deduced from the success of hydrodynamic models at RHIC, is another good reason to further pursue exact nonperturbative calculations in SYM for quantities that are relevant for RHIC phenomenology. If nonperturbative effects in the strongly coupled QGP at moderate temperatures,  $T = 1-2 T_c$ , are ultimately connected to the presence of the phase change(s) (and thus inherently to the critical temperature as a relevant scale), the CFT-QCD connection would not be a rigorous one. But even in this case, the nonperturbative computation of transport

<sup>e</sup>This procedure works quite well when comparing quantities in quenched and unquenched lattice QCD computations, e.g. for the critical temperature.

coefficients of a strongly coupled system at a given reference temperature “not too close” to  $T_c$  should provide useful insights.

The first step in computing HQ diffusion for CFT is the introduction of a heavy quark into the conformal field theory. This can be achieved by either introducing a heavy charge via breaking the gauge group from  $N_c + 1$  to  $N_c$  (which, strictly speaking, generates  $(2N_c + 1)$  “Higgsed” “ $W$ ” bosons)<sup>109</sup>, or by adding a finite-mass  $\mathcal{N} = 2$  hypermultiplet with charges in the fundamental representation as a “probe” of the CFT medium. In either case, the pertinent object on the 4-dimensional boundary of the 5-dimensional AdS space represents a fundamental charge. In Refs.<sup>105,106</sup>, the HQ drag has been evaluated by computing its momentum degradation,  $dp/dt = -\gamma p$ , through the force on the trailing string, resulting in a friction (or drag) coefficient,

$$\gamma_{\text{AdS/CFT}} = \frac{\pi\sqrt{\lambda}T_{\text{SYM}}^2}{2m_Q}, \quad (58)$$

where  $\lambda = g_{\text{SYM}}^2 N_c$  denotes the ’t Hooft coupling constant. Alternatively, in Ref.<sup>107</sup> the problem was formulated focusing on the diffusion term. For time scales longer than the thermal relaxation time of the medium, but short compared to the HQ relaxation time, the fluctuation term in the Langevin equation (63) dominates over the drag term. The evaluation of the noise (or force) correlator is then carried out via the fluctuations of the string, resulting in a noise coefficient which is directly related to the diffusion coefficient (cf. Eqs. (65) and (74) below). Furthermore, the latter can be related to the friction coefficient using the Einstein relation, Eq. (22); it turns out that the result is identical to Eq. (58), which also verifies that a Langevin process consistent with the fluctuation-dissipation theorem applies in the SYM theory (see, however, Refs.<sup>110,111</sup>, where the applicability of the Langevin framework in AdS/CFT for high-momentum quarks is discussed). The square-root dependence of  $\gamma_{\text{AdS/CFT}}$  on the coupling constant  $\lambda$  clearly characterizes its nonperturbative nature; in this sense it is parametrically large for comparatively small coupling constants. The temperature dependence is rather “conventional”, as to be expected since there are no additional scales in the problem (the HQ mass in the denominator implies the standard suppression of the HQ relaxation rate by  $\sim T/m_Q$ ).

The next question is how to convert the result into a (semi-) quantitative estimate for the QCD plasma. Naively, one may just insert the values of the strong coupling constant,  $g_s$ , and QGP temperature,  $T$ , for  $g_{\text{SYM}}$  and  $T_{\text{SYM}}$ , respectively. A more suitable identification probably consists of matching physical quantities which leads to somewhat different parameter values. E.g., in Ref.<sup>108</sup>, comparable temperatures were identified by matching the energy densities ( $\varepsilon$ ) of the QGP and SYM-plasma. Since the latter has a factor  $\sim 3$  larger particle content (degeneracy factor), one has a smaller temperature at the same  $\varepsilon$ ,  $T_{\text{SYM}} \simeq T/3^{1/4}$ . For the coupling constant, one can exploit the fact that in AdS/CFT the potential between a heavy charge and anticharge is essentially of Coulomb-type, both at zero<sup>109</sup> and finite temperature<sup>112,113</sup>. In the latter case, the potential goes to zero at some finite

range, characteristic for Debye-screening behavior. This range can be used to identify the length scale in comparison to typical screening radii of heavy-quark free energies as computed in thermal lattice QCD (although some ambiguity remains)<sup>108</sup>. Matching the magnitude of the potentials at the screening radius then allows for a matching of the coupling constants. This leads to significantly smaller values for  $\lambda$  (by a factor of 3-6) than the naive identification with  $\alpha_s = 0.5$ . In connection with the redefined temperature, the improved AdS/CFT-based estimate for the HQ friction coefficient in QCD amounts to  $\gamma \simeq 0.3-0.9 c/\text{fm}$  at  $T = 250 \text{ MeV}$ , which is significantly smaller than the “naive” estimate of  $\sim 2 c/\text{fm}$ .

### 2.5. *Comparison of Elastic Diffusion Approaches*

In view of the recent proliferation of seemingly different approaches to evaluate HQ transport coefficients in the QGP it becomes mandatory to ask to what extent they are related and encode similar microscopic mechanisms<sup>114</sup>. It turns out that all of the approaches discussed above incorporate a color-Coulomb-type interaction. This is rather obvious for the  $T$ -matrix approach, where the input potentials from lattice QCD clearly exhibit the Coulomb part at sufficiently small distance (including effects of color screening). The one-gluon exchange in pQCD (which is the dominant contribution to HQ rescattering, recall the two right diagrams in Fig. 1), also recovers the Coulomb potential in the static limit (color screening enters via the Debye mass in the spacelike gluon-exchange propagator). The collisional dissociation mechanism involves the Cornell potential for the  $D$ - and  $B$ -meson wave functions and thus incorporates a Coulomb interaction as well; the emphasis in this approach is on formation-time effects essentially caused by the different (free) binding energies of  $D$  and  $B$  mesons. In addition, the confining part of the Cornell potential may play a role (as in the  $T$ -matrix approach). Finally, in conformal field theory (AdS/CFT), the absence of any scale promotes the Coulomb potential to the unique form of a potential,  $V(r) \propto 1/r$  (this is the only way of generating a quantity with units of energy). On the other hand, scale-breaking effects are present in the QCD-based approaches in terms of a running coupling constant (pQCD), while the Cornell and lQCD-based potentials additionally feature linear terms  $\propto \sigma r$  where the string tension introduces a further (nonperturbative) scale. In fact, in Ref.<sup>94</sup> it has been argued, based on an analysis of lQCD results for the heavy-quark free (and internal) energy, that “remnants” of the confining force play a prominent role for temperatures not too far above  $T_c$  (e.g., for heavy quarkonium binding).

If one assumes the prevalence of the Coulomb interaction, the obvious first question is with what strength (coupling constant) it figures into the different approaches, which should be fairly straightforward to determine. A more involved issue is to scrutinize the underlying approximation schemes and their applicability. E.g., perturbative approaches with large (running) coupling constants have poor (if any) control over higher-order corrections. As usual in such situations, diagrams with large contributions should be identified and resummed (which is, of course, a

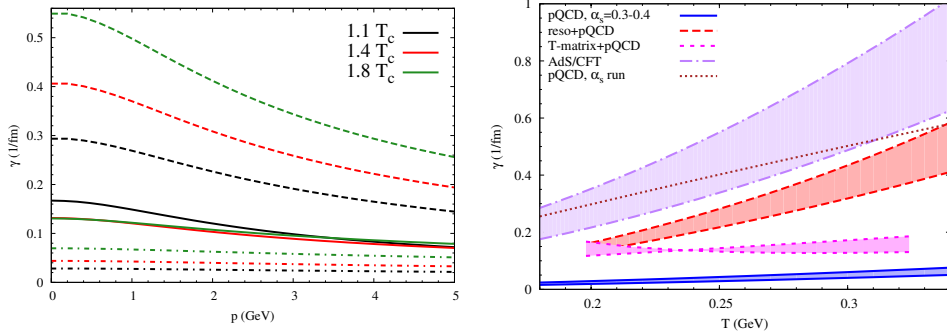


Fig. 13. (Color online) Charm-quark friction coefficients,  $\gamma$ , in the QGP. Left panel: three-momentum dependence at three temperatures (color code) for: LO-pQCD with fixed  $\alpha_s = 0.4$  and  $\mu_D = gT$  (dash-dotted lines), heavy-light quark  $T$ -matrix plus LO-pQCD for gluons (solid lines)<sup>44</sup>, and pQCD with running  $\alpha_s$  and reduced infrared regulator (dashed lines)<sup>66,67</sup>. Right panel: temperature dependence of  $\gamma$  for LO-pQCD,  $T$ -matrix plus LO-pQCD (gluons only), pQCD with running  $\alpha_s$ , and from AdS/CFT correspondence matched to QCD<sup>108</sup> with  $C = 1.5-2.6$ <sup>115</sup>.

non-trivial task, e.g., maintaining gauge invariance); it would be illuminating to extract a static gluon-exchange (Coulomb) potential for a given set of parameters. The  $T$ -matrix approach performs a resummation of the ladder series of a static (color-electric) potential; magnetic interactions are implemented in a simplified manner using the Breit current-current interaction from electrodynamics. It has been verified that for large center-of-mass energies, the  $qQ$   $T$ -matrix recovers the result for perturbative scattering. However, a number of effects are neglected and need to be scrutinized, including the interactions with gluons beyond pQCD, retardation, extra gluon or particle/antiparticle emission (e.g., in a coupled channel treatment) and the validity (and/or accuracy) of a potential approach at finite temperature (this issue will reappear in the context of heavy quarkonia in Sec. 4). In the collisional dissociation approach, it would be interesting to explore medium effects in the employed potential (i.e., on the mesonic wave function). Ideally, by improving on specific assumptions in a given approach, an agreement would emerge establishing a common result. Explicit connections with the AdS/CFT results are more difficult to identify. Maybe it is possible to push the  $T$ -matrix approach into a regime of “large” coupling, or study the existence and properties of ( $D$  and  $B$ ) bound states in the string theory setting. In Fig. 13 we summarize the drag coefficients as function of momentum (for three temperatures, left panel) and temperature (for  $p = 0$ , right panel) resulting from the approaches discussed above, i.e.,

- (i) leading-order pQCD calculations with fixed  $\alpha_s = 0.4$  and Debye-screening mass,  $\mu_D = gT$ , in the  $t$ -channel gluon-exchange contributions to the matrix elements for elastic  $gQ$  and  $qQ$  scattering,
- (ii) in-medium  $T$ -matrix calculations using lQCD-based  $qQ$  potentials, augmented by the leading-order pQCD matrix elements for elastic  $gQ$  scattering<sup>44</sup>,

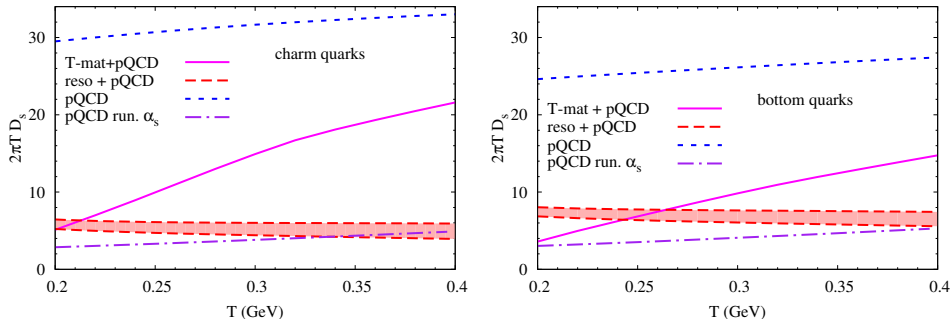


Fig. 14. (Color online) Spatial diffusion coefficient,  $D_s = T/(\gamma m_Q)$ , for  $c$  (left) and  $b$  quarks (right) in a QGP for: LO-pQCD with fixed  $\alpha_s = 0.4$  (dashed lines), effective resonance model + LO-pQCD (bands for  $\Gamma_{D,B} = 0.4-0.75$  GeV)<sup>25</sup>,  $T$ -matrix approach + LO-pQCD (gluons only)<sup>44</sup> and pQCD with running  $\alpha_s$  (dash-dotted line)<sup>66,67</sup>. The AdS/CFT result corresponds to  $2\pi T D_s = 2\pi/C \simeq 1.5 - 4$  (not shown in the plots).

- (iii) pQCD calculations with running  $\alpha_s$  and reduced screening mass<sup>66,67</sup>, and
- (iv) the AdS/CFT correspondence matched to QCD<sup>108</sup> with  $\gamma_{\text{QCD}} = CT^2/m_Q$  for  $C = 1.5-2.6$ <sup>115</sup>.

At all temperatures, the  $T$ -matrix approach, (ii), produces significantly more HQ interaction strength than LO pQCD, (i), while for  $T > 0.2$  GeV the thermalization rate for the  $T$ -matrix is a factor of  $\sim 2-4$  less than for AdS/CFT, (iv), or for LO-pQCD with running coupling and reduced infrared regulator, (iii). Close to  $T_c \simeq 180$  MeV, however, the three approaches (ii), (iii) and (iv) are not much different and share overlap around  $\gamma \simeq 0.2$  c/fm. The spread in the numerical results reiterates the necessity for systematic checks as indicated above.

Finally, one can convert the drag coefficients into estimates of other HQ transport coefficients of the QGP. Within the Fokker-Planck approach the spatial diffusion coefficient,  $D_s$ , is directly related to the drag coefficient,  $\gamma$ , as given by Eq. (24). Fig. 14 shows the dimensionless quantity  $2\pi T D_s$  for charm (left panel) and bottom quarks (right panel) as a function of temperature for LO pQCD, LO pQCD with running coupling and reduced infrared regulator, effective resonance model and  $T$ -matrix approach. The former three are fairly constant as a function of temperature while the  $T$ -matrix approach exhibits a significant increase with temperature, indicating maximal interaction strength close to  $T_c$ . This originates from the increasing potential strength (decrease in color-screening) with decreasing temperature, enhancing resonance correlations at lower temperature. It is tempting to interpret this feature as a precursor phenomenon of hadronization. However, its robustness needs to be checked with a broader range of lattice potentials. We recall that the internal-energy based potentials probably provide an upper estimate for the strength of the interaction. It is interesting to note that for all approaches the results for  $b$  quarks coincide with the ones for  $c$  quarks within  $\sim 20-30\%$ . The largest deviation is seen in the  $T$ -matrix approach, where the (spatial) diffusion coefficient

is smaller for  $b$  quarks than for  $c$  quarks ( $B$ -meson resonances survive until higher temperatures than  $D$  resonances). This is qualitatively similar to what has been found for the collisional dissociation mechanism, where the relative enhancement of the  $b$ -quark energy loss (compared to charm) is due to smaller  $B$ -meson formation times. Since the latter are related to larger  $B$ -meson binding energies, the dynamical origin of the smaller  $D_s$  for  $b$  quarks appears to be of similar origin as in the  $T$ -matrix approach. The relative magnitudes of the various approaches reflect what we discussed before for the drag coefficient.

## 2.6. Collisional vs. Radiative Energy Loss

For slowly moving heavy quarks in the QGP, the parametrically dominant interaction is elastic scattering. However, at high  $p_T$ , radiative scattering is believed to eventually become the prevailing energy-loss mechanism. It is currently not known at which  $p_T$  this transition occurs. Therefore, it is important to assess the relative importance between elastic and inelastic scattering processes in the medium, even at the level of perturbative scattering only. Toward this purpose, we first recollect basic results on the gluon-Bremsstrahlung mechanism for light-parton, and then HQ, energy loss in the QGP, followed by a direct comparison to collisional energy loss for heavy quarks.

A seminal perturbative treatment of gluo-radiative energy loss (E-loss) of high-energy partons in the QGP has been given in Refs.<sup>116,117</sup> (BDMPS). The medium is modeled as static scattering centers which implies that the E-loss is purely radiative. The key finding is that the E-loss due to multiple in-medium scattering of a high-energy parton grows as  $L^2$ , where  $L$  is the path length of the parton traversing the medium. The static scattering centers, at positions  $\mathbf{x}_i$ , are described by screened Coulomb potentials,

$$V_i(\mathbf{q}) = \frac{g}{\mathbf{q}^2 + \mu_D^2} \exp(-i\mathbf{q}\mathbf{x}_i) . \quad (59)$$

The range of the potentials is assumed to be small compared to the mean free path,  $\lambda$ , of the scattered parton, i.e.,  $1/\mu_D \ll \lambda$ . In this case successive scatterings can be considered as independent, thus enabling an eikonal approximation for the elastic scattering on static centers, i.e., a classical propagation of the particle with energy  $E \gg \mu_D$ , undergoing independent kicks, thereby radiating Bremsstrahlung gluons. In analogy to the QED case an important ingredient is the coherent resummation of the multiple-scattering Bremsstrahlung amplitudes (“Landau-Pomeranchuk-Migdal effect”) which can be formulated as a diffusion equation for the effective scattering amplitudes (or pertinent currents). The total radiative E-loss of a high-energy parton traversing a medium of path length  $L$  is then given by

$$\Delta E = \frac{\alpha_s}{2} \hat{q} L^2 , \quad (60)$$

where  $\hat{q}$  is the diffusion coefficient for transverse-momentum broadening in scattering off the static scattering centers,  $\langle q_T^2 \rangle = \hat{q}L$ . Perturbative calculations of the

transport coefficient result in a value of about  $\hat{q} \simeq 1 \text{ GeV}/\text{fm}^2$  at typical energy densities of  $\epsilon \simeq 10 \text{ GeV}/\text{fm}^3$  (translating into  $T \simeq 250 \text{ MeV}$ ) relevant for the QGP at RHIC<sup>118</sup>. It turns out, however, that the description of high-momentum pion suppression at RHIC in the BDMPS formalism requires an approximate ten-fold increase of the perturbative value for  $\hat{q}$ <sup>29</sup>. Recent calculations of perturbative E-loss including both elastic and radiative contributions within a thermal-field-theory framework indicate that collisional E-loss may be significant even for high- $p_T$  light partons<sup>30</sup>. This would imply a reduction of the value required for  $\hat{q}$  from RHIC phenomenology.

An early calculation<sup>119</sup> of radiative charm-quark E-loss,  $-dE/dx$ , in the QGP has found that it dominates over the elastic one down to rather small momenta,  $p \leq 2 \text{ GeV}$ <sup>24</sup>. In Ref.<sup>32</sup> it has been pointed out that the application of radiative E-loss to heavy quarks leads to the appearance of the so-called “dead cone”, i.e., the suppression of forward gluon radiation for  $\Theta < m_Q/E$ , where  $\Theta$  denotes the direction of motion of the gluon with energy  $E$ , relative to the direction of the HQ momentum<sup>32</sup>. It has been predicted that the reduced HQ E-loss leads to a heavy-to-light hadron ratio above one in the high- $p_T$  regime accessible at RHIC. Within the BDMPS model, extended to heavy quarks, it has been argued<sup>120</sup>, however, that medium-induced gluon radiation tends to fill the dead cone. As will be discussed in Sec. 3.5, a similar value for  $\hat{q}$  as in the light-hadron sector is necessary to come near the observed suppression of high- $p_T$  electrons from HQ decays in terms of radiative E-loss alone<sup>36</sup>.

The BDMPS formalism for light partons has been generalized to resum an expansion of gluo-radiative parton E-loss in the GP with opacity,  $\bar{n} = L/\lambda$ , employing a so-called reaction operator approach<sup>121</sup> (GLV). A reaction operator  $\hat{R}_n$  is constructed that relates the  $n^{\text{th}}$  power in a opacity-inclusive radiation probability distribution to classes of diagrams of order  $n - 1$ . This results in a recursion relation for the radiation probability distribution, corresponding to a certain resummation to all orders in opacity, which can be implemented in Monte-Carlo simulations for jet quenching. The GLV reaction-operator method for light-parton radiative E-loss in the QGP has been extended to heavy quarks in Ref.<sup>122</sup> (DGLV), implementing the kinematical suppression of gluon radiation by the HQ mass in the “dead cone”.

A direct study of the relative magnitude of collisional (elastic) and radiative pQCD HQ E-loss in the GP has been undertaken in Ref.<sup>38</sup>. For the elastic E-loss of a parton with color Casimir constant,  $C_R$ , the leading logarithm expression in an ideal QGP with  $N_f$  effective quark flavors at temperature  $T$ ,

$$\frac{dE^{\text{el}}}{dx} = C_R \pi \alpha_s^2 T^2 \left( 1 + \frac{N_f}{6} \right) f(v) \ln(B_c), \quad (61)$$

has been used. In an ultrarelativistic gas of massless partons the jet-velocity function is given by

$$f(v) = \frac{1}{v^2} \left[ v + \frac{1}{2}(v^2 - 1) \ln \left( \frac{1+v}{1-v} \right) \right], \quad (62)$$

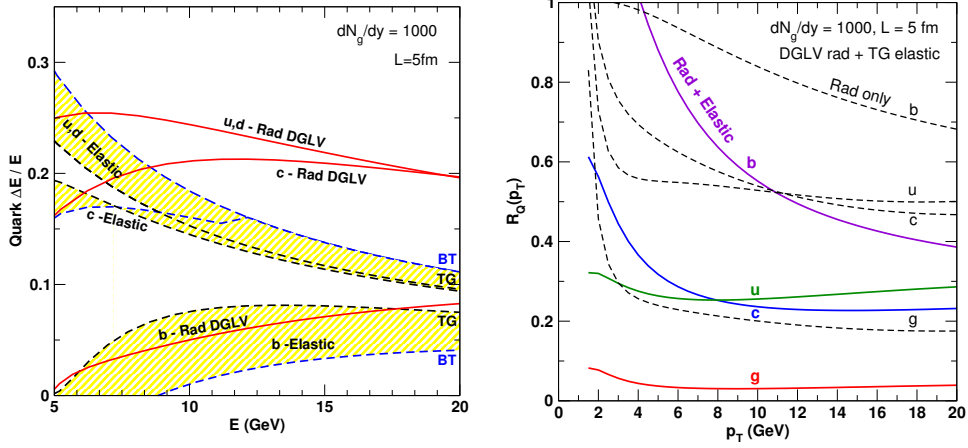


Fig. 15. (Color online) Left panel: average relative E-loss,  $\Delta E/E$ , for  $u$ ,  $c$  and  $b$  quarks as a function of jet energy,  $E$ , in a longitudinally (Bjorken) expanding QGP, with fixed path length  $L = 5 \text{ fm}$ , initial gluon rapidity density  $dN_g/dy = 1000$  and fixed  $\alpha_s = 0.3$ ; the gluon (light-quark) mass is set to  $\mu_D/\sqrt{2}$  ( $\mu_D/2$ ), the  $c(b)$ -quark mass to  $m_c = 1.2(4.75) \text{ GeV}$  (solid lines: radiative E-loss, dashed bands: elastic E-loss in two schemes as discussed in the text). Right panel: parton nuclear modification factor,  $R_{AA} \equiv R_Q$ , for gluons,  $u$ -,  $c$ -, and  $b$ -quarks as a function of  $p_T$  for a fixed path length and  $dN_g/dy = 1000$  (dashed lines: radiative E-loss, solid lines: radiative+elastic E-loss).

while estimates for  $B_c$  are taken from Refs. [Bj]<sup>123</sup>, [TG]<sup>124</sup>, and [BT]<sup>68,69</sup>. The different values for  $B_c$  obtained in these models are considered as reflecting theoretical uncertainties. The radiative E-loss within the DGLV reaction-operator approach is calculated in Ref.<sup>122</sup> based on Refs.<sup>121,125</sup>. The left panel of Fig. 15 compares pQCD radiative and collisional E-loss for various quark flavors (masses) at high  $p_T > 5 \text{ GeV}$  in a gluon plasma (GP) with  $T \simeq 240 \text{ MeV}$ . For light and charm (bottom) quarks the elastic E-loss is comparable to the radiative one up to  $p_T \simeq 10(20) \text{ GeV}$ , and still significant above. The right panel of Fig. 15 reiterates that, within pQCD, collisional E-loss is an essential component in calculating the suppression of light-parton and especially HQ spectra at RHIC. Note that the relative importance of collisional E-loss is expected to increase if non-perturbative effects become relevant (which predominantly figure toward lower  $p_T$ ), or if the GP is replaced by a QGP.

## 2.7. $D$ Mesons in the Hadronic Phase

To complete the discussion of open charm in QCD matter we briefly address medium modifications of charm hadrons in hadronic matter. Pertinent studies may be divided into calculations for cold nuclear matter as well as for hot meson matter.

Early studies of  $D$ -mesons in cold nuclear matter focused on possible mass shifts due to scalar and vector mean fields acting on the light-quark content of the meson<sup>126</sup>. At normal nuclear matter density  $\rho_N \equiv \rho = 0.16 \text{ fm}^{-3}$ , attractive

mass shifts of up to  $-100$  MeV have been reported for  $D^+$  and  $D^0$  mesons (where both mean fields contribute with the same sign) while the mass change of the  $D^-$  and  $\bar{D}^0$  turned out to be small due to a cancellation of the mean fields. Similar findings have been reported in QCD sum rule calculations<sup>127</sup> where the (isospin-averaged)  $D$ -meson mass is reduced by about  $-50$  MeV, mostly as a consequence of the reduction in the light-quark condensate. Rather different results are obtained in microscopic calculations of  $D$ -meson selfenergies (or spectral functions) based on coupled channel  $T$ -matrices for  $DN$  scattering in nuclear matter<sup>128,129</sup>. These calculations incorporate hadronic many-body effects, most notably  $DN$  excitations into charm-baryon resonances not too far from the  $DN$  threshold, e.g.,  $\Lambda_c(2593)$  and  $\Sigma_c(2625)$ , as well as charm exchange into  $\pi\Lambda_c$  and  $\pi\Sigma_c$  channels. In Ref.<sup>128</sup> separable meson-baryon interactions have been employed with parameters constrained to dynamically generate the  $\Lambda_c(2593)$  state. Since the in-medium  $D$ -meson spectral function figures back into the  $T$ -matrix, one is facing a selfconsistency problem (much like for the heavy-light quark  $T$ -matrix discussed in Sec. 2.3.2). Selfconsistent calculations including nucleon Pauli blocking and dressing of intermediate pion and nucleon propagators result in  $D$ -meson spectral functions with a significant broadening of up to  $\Gamma_D \simeq 100$  MeV but a rather small shift of the peak position of about  $-10$  MeV (for  $\varrho_N \equiv \varrho = 0.16 \text{ fm}^{-3}$ ). In Ref.<sup>129</sup>, a somewhat stronger coupling of  $DN$  to the  $\Lambda_c(2593)$  results in a stronger collective  $DN^{-1}\Lambda_c(2593)$  mode (about 250 MeV below the free  $D$ -meson mass) and a pertinent level repulsion which pushes up the “elementary”  $D$ -peak by  $\sim 30$  MeV. Also in this calculation the broadening is significant, by about  $\sim 50$  MeV. The  $D^-$  was found to be rather little affected, neither in mass nor in width. Investigations in the selfconsistent coupled-channel framework have been extended to a nucleon gas at finite temperature<sup>130</sup> with a more complete treatment of  $DN$  scattering, cf. left and middle panels of Fig. 16. The thermal motion of nucleons implies that a larger kinematic regime in the center-of-mass (cm) energies in the scattering amplitude is probed (compared to  $T=0$ ). For the real parts this leads to a further averaging of the positive and negative parts of the amplitude, while the imaginary parts are negative definite (some loss of interaction strength may occur in channels with resonances close to threshold). More quantitatively, at normal nuclear matter density, the resulting mass shifts are 10-20 MeV at  $T = 0$  (attractive for  $D$  and repulsive for  $\bar{D}$ ), decreasing to about half (or less) at  $T = 150$  MeV. On the other hand, the  $D$ -meson width is around 100 MeV at both zero and finite temperature, while the  $\bar{D}$  width is small at  $T = 0$  but increases to about 30 MeV at  $T = 150$  MeV.

Medium modifications of  $D$ -mesons in a hot pion gas have been studied in Ref.<sup>131</sup>. The main idea in this work is to implement the recently discovered scalar  $D_0^*(2310)$  and axialvector  $D_1'(2430)$  states as chiral partners of the pseudoscalar  $D$  and vector  $D^*(2010)$  mesons, respectively. Their large widths of 200-400 MeV are primarily attributed to  $S$ -wave pion decays into  $D$  and  $D^*$ . In a thermal pion gas,  $D_0^*(2310)$  and  $D_1'(2430)$  therefore act as strong resonances in  $D\pi$  and  $D^*\pi$

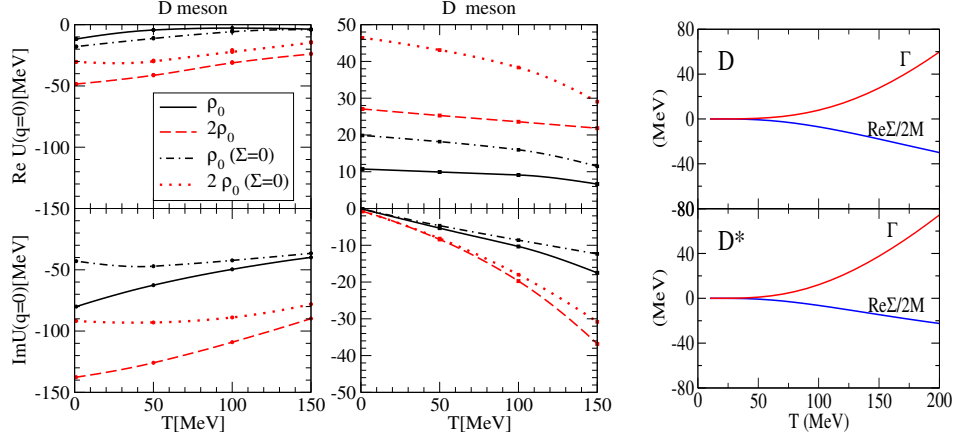


Fig. 16. (Color online) Real and imaginary parts of  $D$ -meson selfenergies in dense and/or hot hadronic matter. Left and middle panels: selfconsistent coupled-channel calculations for in-medium  $D^+$  (left) and  $D^-$  (right) potentials based on  $DN$  scattering in a hot nucleon gas as a function of temperature<sup>130</sup> for two different nuclear densities (and for two different inputs for the  $\bar{D}N$  scattering length); the real (upper panels) and imaginary (lower panels) part of the potentials are defined in terms of the on-shell selfenergy via  $U(q) = \Sigma_D(\omega_D^{qn}(q), q)/2\omega_D^{qn}$  with  $\omega_D^{qn}$  the quasiparticle energy; note that the width is given by  $\Gamma = -2\text{Im}U$ . Right panel: width (upper lines) and mass shift (lower lines) of  $D$  (top) and  $D^*(2010)$  (bottom) mesons in a hot pion gas based on resonant scattering via chiral partners<sup>131</sup>; note that the isospin symmetric pion gas implies equal effects on  $D$ -mesons ( $D^+$ ,  $D^0$ ) and anti- $D$  mesons ( $D^-$ ,  $\bar{D}^0$ ).

scattering, which have been treated in Breit-Wigner approximation. In addition,  $D$ -wave resonances,  $D_1(2420)$  and  $D_2^*(2460)$ , have been accounted for. The resulting collisional widths of  $D$  and  $D^*$  reach up to about  $\sim 40\text{--}60$  MeV for temperatures around  $T = 175$  MeV, while the mass shifts are attractive up to  $-20$  MeV. It can be expected that (e.g., in a selfconsistent calculation) the inclusion of medium effects on the resonances (e.g., chiral partners are expected to approach degeneracy towards chiral restoration) will lead to a reduction in the mass shift (not so much for the widths). Above the critical temperature, it is then natural to switch to a quark-based description, i.e.,  $c + q$  scattering, much like in the effective resonance model discussed in Sec. 2.3.1.

When combining the effects of pion and nucleon scattering on  $D$ -mesons in hot hadronic matter, their total width at temperatures around  $T_c$  adds up to  $\Gamma_D^{\text{tot}}(T = 180 \text{ MeV}) \simeq 150$  MeV. This is only by about a factor of  $\sim 2$  smaller than what was found for  $c$ -quarks at  $T = 1.1 T_c$  in the  $T$ -matrix approach for  $c$ - $q$  scattering, cf. right panel of Fig. 11. Since it can be expected that other excited hadrons contribute to  $D$ -meson rescattering (albeit with less strength),  $D$ -meson transport properties may not be much different from those of  $c$ -quarks in the QGP, at least at temperatures close to  $T_c$ . It is therefore of considerable interest to employ in-medium  $D$ -meson  $T$ -matrices to evaluate heavy-flavor transport coefficients in hadronic matter.

### 3. Heavy-Quark Observables in Relativistic Heavy-Ion Collisions

One of the main motivations for the vigorous theoretical studies of HQ diffusion in the QGP is the possibility of utilizing HQ observables in ultrarelativistic heavy-ion collisions as a quantitative probe of the matter produced in these reactions. If the latter reaches approximate local thermal equilibrium, such applications can be performed by solving the Fokker-Planck equation for a heavy quark diffusing within a collectively expanding background medium with space-time dependent temperature and flow field (applicable for “sufficiently slow” charm and bottom quarks). This is typically realized with a Monte-Carlo simulation using a test-particle ansatz for an equivalent stochastic Langevin equation. In such a formulation, a direct relation between the input in terms of a (temperature-dependent) HQ diffusion coefficient and the modifications of HQ spectra in the evolution can be established. In addition, the Langevin formulation admits an efficient implementation of the dissipation-fluctuation relation for relativistic kinematics.

Alternatively, the modifications of HQ spectra in URHICs have been evaluated by implementing test particles into numerical transport simulations of the background medium<sup>132,133,134</sup>. This, in principle, accounts for non-equilibrium effects in the medium evolution (which could be particularly relevant for high- $p_t$  particles in the bulk), but the connection to the diffusion concept becomes less direct (HQ cross sections need to be evaluated in an equilibrium medium to extract “equivalent” diffusion coefficients). However, when analyzing theoretical predictions of HQ spectra we also compare to results of transport models for the bulk evolution.

We start our presentation in this Section by briefly outlining how the Fokker-Planck equation is implemented into numerical simulations based on a relativistic Langevin process (Sec. 3.1). This is followed by a discussion of different models for the background medium in relativistic heavy-ion collisions, where we focus on thermal models including hydrodynamics and expanding fireballs (Sec. 3.2). The main task here is to provide realistic benchmarks for the conversion of transport coefficients into modifications of HQ spectra. This furthermore requires the definition of controlled initial conditions for the HQ spectra (Sec. 3.3), usually taken from  $p$ - $p$  collisions, possibly augmented by nuclear effects (in particular a “Cronin”  $p_t$ -broadening). Available Langevin simulations combining different inputs are quantitatively compared at the level of the final-state HQ spectra resulting from the QGP and “mixed” phases in central and semicentral Au-Au collisions at RHIC (Sec. 3.4). Even though HQ spectra are not observable, they provide the cleanest theoretical level of comparison, before further processing through hadronization, electron decay and charm/bottom composition occurs. The latter three steps are necessary to enable comparisons to currently available electron data (Sec. 3.5), and thus arrive at an empirical estimate of the HQ diffusion coefficient characterizing the QCD medium produced at RHIC. In a more speculative step, the extracted HQ transport coefficient may be used to schematically estimate the ratio of shear viscosity to entropy density (Sec. 3.6), which has recently received considerable attention in

connection with viscous hydrodynamic simulations at RHIC.

### 3.1. Relativistic Langevin Simulations

The Fokker-Planck equation, introduced in Sec. 2.1, is equivalent to an ordinary stochastic differential equation. Neglecting mean-field effects of the medium, the force acting on the heavy particle is divided into a “deterministic” part, describing its average interactions with the light particles in the medium (friction or drag), and a “stochastic” part, taking into account fluctuations around the average on the level of the standard deviation. Thus the relativistic equations of motion for a heavy quark become a coupled set of stochastic differential equations, which for an isotropic medium can be written in the form

$$\begin{aligned} dx_j &= \frac{p_j}{E} dt, \\ dp_j &= -\Gamma p_j dt + \sqrt{dt} C_{jk} \rho_k, \end{aligned} \quad (63)$$

where  $E = (m_Q^2 + \mathbf{p}^2)^{1/2}$ , and  $\Gamma$  and  $C_{jk}$  are functions of  $(t, \mathbf{x}, \mathbf{p})$  with  $j, k=1,2,3$ ; they are related to the transport coefficients  $A$  and  $B$  (discussed in the previous section) below.  $\Gamma$  and  $C_{jk}$  describe the deterministic friction (drag) force and the stochastic force in terms of independent Gaussian-normal distributed random variables  $\boldsymbol{\rho} = (\rho_1, \rho_2, \rho_3)$ ,

$$P(\boldsymbol{\rho}) = \left(\frac{1}{2\pi}\right)^{3/2} \exp\left(-\frac{\boldsymbol{\rho}^2}{2}\right), \quad (64)$$

In the limit  $dt \rightarrow 0$ , the covariance of the fluctuating force is thus given by

$$\left\langle F_j^{(\text{fl})}(t) F_k^{(\text{fl})}(t') \right\rangle = C_{jl} C_{kl} \delta(t - t'). \quad (65)$$

However, with these specifications the stochastic process is not yet uniquely defined, but depends on the specific choice of the momentum argument of the covariance matrix,  $C_{jk}$ , in Eq. (63)<sup>135</sup>, i.e., the definition of the stochastic integral. Usual schemes are given by the pre-point Ito, the mid-point Stratonovic-Fisk, and the post-point Ito (or Hänggi-Klimontovich<sup>136</sup>) interpretation of the stochastic integral. We can summarize all these realizations of the stochastic process by specifying the actual momentum argument in the covariance matrix by

$$C_{jk} \rightarrow C_{jk}(t, \mathbf{x}, \mathbf{p} + \xi d\mathbf{p}), \quad (66)$$

where  $\xi = 0, 1/2, 1$  corresponds to the pre-point Ito, the mid-point Stratonovic, and the post-point Ito realizations, respectively. The equation for the corresponding phase-space distribution function can be found by calculating the average change of an arbitrary phase-space function,  $g(\mathbf{x}, \mathbf{p})$ , with time. According to Eq. (63), with

the specification Eq. (66) of the stochastic process, we find

$$\begin{aligned} \langle g(\mathbf{x} + d\mathbf{x}, \mathbf{p} + d\mathbf{p}) - g(\mathbf{x}, \mathbf{p}) \rangle = & \left\langle \frac{\partial g}{\partial x_j} \frac{p_j}{E} + \frac{\partial g}{\partial p_j} \left( -\Gamma p_j + \xi \frac{\partial C_{jk}}{\partial p_l} C_{lk} \right) \right. \\ & \left. + \frac{1}{2} \frac{\partial^2 g}{\partial p_j \partial p_k} C_{jl} C_{kl} \right\rangle dt + \mathcal{O}(dt^{3/2}). \end{aligned} \quad (67)$$

Here, the arguments of both,  $\Gamma$  and  $C_{jk}$ , have to be taken at  $(t, \mathbf{x}, \mathbf{p})$  since the corrections are of the neglected order,  $\mathcal{O}(dt^{3/2})$ . In the derivation of this equation the statistical properties of the random variables  $\rho_i$ , implied by Eq. (64),

$$\langle \rho_j \rangle = 0, \quad \langle \rho_j \rho_k \rangle = \delta_{jk}, \quad (68)$$

have been used. It follows that the average of an arbitrary phase-space function is by definition given by the phase-space distribution function for the heavy particle (in our context a heavy quark),  $f_Q(t, \mathbf{x}, \mathbf{p})$ , e.g.,

$$\frac{d}{dt} \langle g(\mathbf{x}, \mathbf{p}) \rangle = \int d^3\mathbf{x} \int d^3\mathbf{p} g(\mathbf{x}, \mathbf{p}) \frac{\partial}{\partial t} f_Q(t, \mathbf{x}, \mathbf{p}). \quad (69)$$

After integrations by parts, and since Eq. (67) holds for any function  $g$ , one finally arrives at the Fokker-Planck equation,

$$\frac{\partial f_Q}{\partial t} + \frac{p_j}{E} \frac{\partial f_Q}{\partial x_j} = \frac{\partial}{\partial p_j} \left[ \left( \Gamma p_j - \xi C_{lk} \frac{\partial C_{jk}}{\partial p_l} \right) f_Q \right] + \frac{1}{2} \frac{\partial^2}{\partial p_j \partial p_k} (C_{jl} C_{kl} f_Q). \quad (70)$$

The drag term, i.e., the first term on the right-hand side of this equation, depends on the definition of the stochastic integral in terms of the parameter  $\xi$ . Comparison with Eq. (10) shows that, independent of the choice of  $\xi$ , the covariance matrix is related to the diffusion matrix by

$$C_{jk} = \sqrt{2B_0} P_{jk}^\perp + \sqrt{2B_1} P_{jk}^\parallel, \quad (71)$$

while the friction force is given by

$$A p_j = \Gamma p_j - \xi C_{lk} \frac{\partial C_{jk}}{\partial p_l}. \quad (72)$$

Numerical investigations have shown that the drag and diffusion coefficients inferred from microscopic models according to Eqs. (15) in general do not warrant a good agreement of the long-time limit of the solution to the Fokker-Planck evolution with the relativistic equilibrium Jüttner-Boltzmann distribution (where the temperature is given by the background medium). The problem is with the longitudinal diffusion coefficient,  $B_1$ , which induces an overestimate of the corresponding fluctuating forces. Thus, one typically *adjusts* the drag coefficient by choosing  $B_1$  in Eq. (70) to satisfy the asymptotic equilibration condition<sup>137,138,26</sup>.

To find the dissipation-fluctuation relation, imposed by the equilibration condition, we first study the heavy quark's motion in a heat bath in thermal equilibrium

in its rest frame. Then the momentum distribution of the heavy quarks should become a Jüttner-Boltzmann distribution,

$$f_Q^{\text{eq}}(\mathbf{p}) \propto \exp(-E/T) \quad (73)$$

with the temperature,  $T$ , imposed by the heat bath. For a Langevin process with  $B_0 = B_1 = D$ , i.e.,

$$C_{jk} = \sqrt{2D(E)}\delta_{jk} , \quad (74)$$

where the diffusion coefficient has been written as a function of the heavy quark's energy,  $E$ , the equilibration condition for a given parameter  $\xi$  in Eq. (66) is obtained by using Eqs. (73) and Eq. (74) in Eq. (70):

$$\Gamma(E)ET - D(E) + T(1 - \xi)D'(E) = 0 . \quad (75)$$

Since the drag and diffusion coefficients are usually given numerically, the most convenient update rule for the Langevin process is achieved by setting  $\Gamma = A$  and  $\xi = 1$ , i.e., using the post-point Ito (Hänggi-Klimontovich) rule for the stochastic integral in Eq. (63) and imposing the simple relativistic dissipation-fluctuation relation,

$$\Gamma = A, \quad D = AET . \quad (76)$$

This guarantees the proper approach of the heavy quark's phase-space distribution to the appropriate equilibrium distribution with the temperature imposed by the heat bath.

For the more general form of the covariance matrix, Eq. (71), the post-point Ito value,  $\xi = 1$ , has been chosen in Ref.<sup>28</sup>, and the longitudinal diffusion coefficient is set to

$$B_1 = AET , \quad (77)$$

while the drag coefficient  $A$  as well as the transverse diffusion coefficient,  $B_0$ , are used as given by Eq. (15) for the various microscopic models for HQ scattering in the QGP. Comparing to Eq. (75), one finds that this is equivalent to the strategy followed in Ref.<sup>26</sup> of using the prepoint-Ito rule,  $\xi = 0$ , but to adjust the drag coefficient according to the dissipation-fluctuation relation Eq. (75).

### 3.2. Background Medium in Heavy-Ion Collisions

For HQ transport coefficients computed in an equilibrium QGP, the natural and consistent framework to describe the evolving medium in heavy-ion collisions are hydrodynamic simulations, formulated in the same (thermodynamic) variables. This choice is further rendered attractive by the success of ideal hydrodynamics in describing bulk observables at RHIC, in particular  $p_T$  spectra and elliptic flow of the most abundant species of hadrons<sup>13,14,15,16</sup>. The agreement with meson and baryon spectra typically extends to  $p_T \simeq 2\text{-}3$  GeV, respectively. At the parton level, this converts into a momentum of  $p_t \simeq 1$  GeV, which approximately coincides with

the “leveling-off” of the experimentally observed  $v_2(p_t)$  (at higher momenta hydrodynamics overestimates the elliptic flow). On the one hand, this appears as a rather small momentum in view of the ambition of describing HQ spectra out to, say,  $p_t \simeq 5$  GeV. However, one should realize that (a) more than 90% of the bulk matter is comprised of light partons with momenta below  $p_t \simeq 1$  GeV, and (b) the velocity of a  $p_t = 5$  GeV charm quark (with  $m_c = 1.5$  GeV) is very similar to a  $p_t = 1$  GeV light quark (with  $m_q = 0.3$  GeV). This suggests that most of the interactions of a  $p_t = 5$  GeV charm quark actually occur with soft light partons (which are well described by a hydrodynamic bulk). This has been verified by explicit calculations<sup>139</sup> and is, after all, a prerequisite for the applicability of the Fokker-Planck approach (i.e., small momentum transfer per collision). On the other hand, one may be concerned that the overestimate of the experimentally observed elliptic flow at intermediate and high  $p_t$  within hydrodynamics may exaggerate the HQ elliptic flow in Langevin simulations. This is, however, not necessarily the case, since the transfer of  $v_2$  from the bulk to the heavy quark critically depends on the light-parton phase space density (the drag coefficient is proportional to it); since the hydrodynamic spectra fall significantly below the experimental ones at higher  $p_T$ , the phase space density of the hydrodynamic component is relatively small. It is therefore not clear whether the (small) fraction of thermalized particles at high  $p_t$  implies an overestimate of the total  $v_2$ ; this may be judged more quantitatively by comparing to transport calculations.

In parallel to hydrodynamic descriptions of the bulk medium, expanding fireball models have been employed. These are simplified (and thus convenient) parameterizations of a full hydrodynamic calculation in terms of an expanding volume and spatial flow-velocity field, but otherwise based on similar principles and variables. E.g., entropy conservation is used to convert a given volume into a temperature via an underlying equation of state (EoS). The reliability of a fireball model crucially hinges on a realistic choice of the parameters, in connection with a proper description of the final state in terms of particle production and collective flow. In principle, a fireball model offers some additional flexibility in varying the evolution, which may provide useful checks of the sensitivity to specific aspects of the expansion.

Several key parameters of thermal medium evolution models employed in HQ Langevin simulations are compiled in Tab. 1. The starting point of both hydro and fireball models are the initial conditions of the thermal medium, characterized by a formation time when the medium is first assumed to be (locally) equilibrated. At RHIC, typical formation times are estimated to be in the range of  $\tau_0 \simeq 0.3$ -1 fm/c. With a total entropy fixed to reproduce the measured rapidity density of hadrons at a given centrality, e.g. at impact parameter  $b \simeq 7$  fm/c, these formation times translate into average initial temperatures of  $T_0 \simeq 250$ -350 MeV. If the entropy density scales as  $s \propto T^3$ , one can roughly compare the initial conditions in different approaches using  $S = s_0 V_0$  and  $V_0 \propto \tau_0$ . E.g., an initial  $T_0^{\max} = 265$  MeV based on

	MT	HGR	AHH	GA
$\tau_0$ [fm/c]	1.0	0.33	0.6	0.6
$T_0$ [MeV]	265 (max)	340 (avg)	250 (avg)	330 (max) 260 (avg)
$T_c$ [MeV]	165	180	170	165
initial spatial	wounded nucleon	isotropic	lin. comb. of $N_{\text{coll}}$ and $N_{\text{part}}$	lin. comb. of $N_{\text{coll}}$ and $N_{\text{part}}$
$b$ [fm]	6.5	7	5.5	7
bulk- $v_2$	5	5.5 %	3%	4.75 %
$\tau_{\text{FB}}$ [fm/c]	$\sim 9$	$\sim 5$	$\sim 9$	$\sim 7$
QGP-EoS	massless ( $N_f = 3$ )	massless ( $N_f = 2.5$ )	massless ( $N_f = 3$ )	massless ( $N_f = 3$ )
HQ Int.	pQCD HTL	pQCD+reso pQCD+T-mat	AdS/CFT	pQCD run. $\alpha_s$
$m_{c,b}$ [GeV]	1.4	1.5, 4.5	1.5, 4.8	1.5, 5.1

Table 1. Survey of parameters figuring into hydrodynamic and fireball evolutions employed in the Langevin simulations of HQ spectra for semicentral Au-Au collisions at RHIC, corresponding to Refs. [MT]<sup>26,140</sup>, [HGR]<sup>28,44,141</sup>, [AHH]<sup>115,142</sup> and [GA]<sup>67,13</sup>.

$\tau_0 = 1 \text{ fm}/c$  increases by a factor of  $3^{1/3}$  upon decreasing  $\tau_0 = 0.33 \text{ fm}/c$ , resulting in  $T_0^{\text{max}} \simeq 382 \text{ MeV}$ ; if the number of light flavors in the EoS is reduced,  $T_0$  increases as well; e.g.,  $T_0^{\text{avg}} = 260 \text{ MeV}$  based on  $\tau_0 = 0.6 \text{ fm}/c$  and  $N_f=3$  (as in Ref. <sup>67</sup>) increases to  $T_0^{\text{avg}} = 260 \text{ MeV} (0.6/0.33)^{1/3} (47.5/42.25)^{1/3} \simeq 330 \text{ MeV}$  for  $\tau_0 = 0.33 \text{ fm}/c$  and  $N_f=2.5$  (reasonably consistent with Ref. <sup>28</sup>, cf. Tab. 1). The QGP-dominated evolution lasts for about 2-4 fm/c, followed by a mixed phase of similar duration at a critical temperature  $T_c \simeq 165\text{-}180 \text{ MeV}$ . The effects of a continuous (cross-over) transition, as well as of the hadronic phase, have received little attention thus far, but are not expected to leave a large imprint on HQ observables. After all, the cross-over transition found in lQCD exhibits a marked change in energy density over a rather narrow temperature interval. A more important aspect is the consistency between the EoS used to extract the temperature of the bulk evolution and the corresponding degrees of freedom figuring into the calculation of the HQ transport coefficients. In hydrodynamical backgrounds used thus far<sup>26,115,67</sup> the evolution is described with a 2+1-dimensional boost-invariant simulation with an ideal massless-gas EoS. The initial state is typically determined by distributing the entropy in the transverse plane according to the wounded nucleon density. Unfortunately, the impact parameters in current Langevin simulations vary somewhat, which is particularly critical for the magnitude of the subsequently developed elliptic flow. The value of the critical temperature has some influence on the QGP lifetime (lower temperatures leading to larger QGP duration), as does the hadron-gas EoS (more hadronic states imply a larger entropy density at  $T_c$  and

thus a reduced duration of the mixed phase). The termination point of the evolution (beginning, middle or end of mixed phase) is rather significant, especially for the HQ  $v_2$  which needs about 5 fm/c to build up most of its magnitude.

In Refs.<sup>28,44</sup> the medium is parameterized, guided by the detailed hydrodynamic calculations of Ref.<sup>141</sup>, as a homogeneous thermal elliptic “fire cylinder” of volume  $V(t)$ . The QGP temperature is determined via the QGP entropy density,  $s$ , under the assumption of isentropic expansion (total  $S = \text{const}$ ),

$$s = \frac{S}{V(t)} = \frac{4\pi^2}{90} T^3 (16 + 10.5N_f) . \quad (78)$$

The thus inferred temperature is used in Eq. (15) to compute the friction coefficients,  $A$ , and transverse diffusion coefficient,  $B_0$ , with the longitudinal diffusion coefficient fixed by the dissipation-fluctuation relation, Eq. (77). In the mixed phase at  $T_c = 180$  MeV the QGP drag and diffusion coefficients are scaled by a factor  $\propto \rho^{2/3}$  to account for the reduction in parton densities (rather than using hadronic calculations). Special care has to be taken in the parameterization of the elliptic flow in noncentral Au-Au collisions: the contours of constant flow velocity are taken as confocal ellipses in the transverse plane with the pertinent transverse flow set consistently in perpendicular direction. The time evolution of the surface velocity of the semi-axes of the elliptic fire cylinder parameterizes the corresponding results of the hydrodynamic calculations in Ref.<sup>141</sup>, in particular the time-dependence of the elliptic-flow parameter,  $v_2$ , for the light quarks. The parameters are adjusted such that the average surface velocity reaches  $v_{\perp}^{(s)} = 0.5c$  and the anisotropy parameter  $v_2 = 5.5\%$  at the end of the mixed phase. Finally, the velocity field is specified by scaling the boundary velocity linearly with distance from the center of the fireball, again in accordance with the hydrodynamic calculation<sup>141</sup>.

### 3.3. Initial Conditions and Hadronization

The Langevin simulations of HQ diffusion in the QGP require initial conditions for charm- and bottom-quark phase-space distributions. For the spatial part of the initial distribution in the transverse plane all calculations adopt binary-collision scaling following from a Glauber model, reflecting a hard process for the primordial production mechanism. Furthermore, all calculations thus far focus on a limited rapidity window around midrapidity, where the longitudinal distribution is assumed to be uniform in space-time rapidity. As for the initial HQ  $p_t$  spectra, Ref.<sup>26</sup> employs a fit to a leading-order parton-model calculation from the CompHEP package<sup>143</sup>,

$$\frac{dN}{dyd\eta d^2p_t} \propto \delta(\eta - y) \frac{1}{(p_t^2 + \Lambda^2)^\alpha}, \quad (79)$$

with  $\alpha = 3.5$  and  $\Lambda = 1.849$  GeV. In Refs.<sup>28,44</sup>, PYTHIA results for  $c$ -quark spectra have been tuned to reproduce available  $D$ -meson spectra in d-Au collisions at RHIC (assuming  $\delta$ -function fragmentation, cf. left panel of Fig. 17). The pertinent semileptonic single-electron decay spectra approximately account for  $p$ - $p$  and d-Au

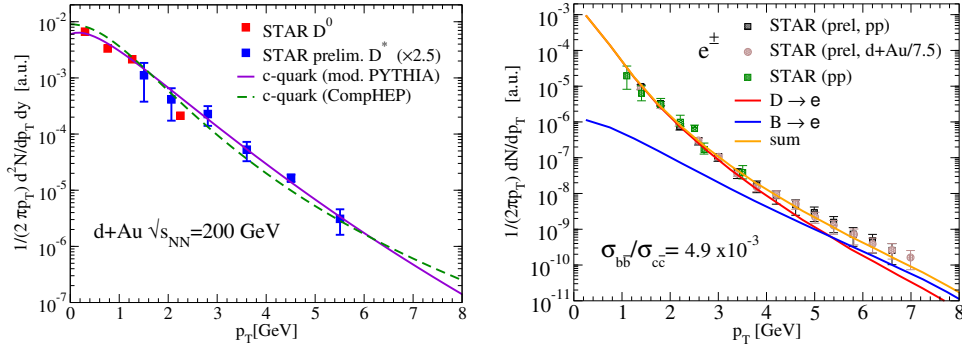


Fig. 17. (Color online) Fits of  $D$ - and  $D^*$ -meson  $p_T$  spectra in 200 AGeV d-Au collisions at RHIC with a modified PYTHIA simulation (left panel) and the corresponding non-photonic single-electron  $p_T$  spectra in  $p$ - $p$  and d-Au collisions<sup>144</sup>. The missing yield of high- $p_T$  electrons is fitted with the analogous  $B$ -meson decay spectra, thus fixing the bottom-charm ratio at  $\sigma_{bb}/\sigma_{cc} \simeq 4.9 \cdot 10^{-3}$ .

spectra up to  $p_T = 4$  GeV; the missing part at higher  $p_T$  is then supplemented by  $B$ -meson contributions. This procedure results in a crossing of the  $D$ - and  $B$ -meson decay electrons at  $p_T \simeq 5$  GeV and a cross-section ratio of  $\sigma_{bb}/\sigma_{cc} \simeq 4.9 \cdot 10^{-3}$  (see right panel of Fig. 17), which is within the range of pQCD predictions<sup>145</sup>.

With initial conditions and bulk medium evolution in place, one can evolve HQ phase-space distributions through the QGP (and mixed phase) of a heavy-ion collision. The final HQ spectra, however, require further processing before comparisons to observables can be made. First, one has to address the hadronization of the HQ spectra into charm and bottom hadrons ( $D$ ,  $D^*$ ,  $\Lambda_c$  etc.). Two basic mechanisms have been widely considered in hadronic collisions, i.e., fragmentation of an individual quark and recombination with an extra quark from the environment. In general, the former is mostly applicable for high-energy partons while the latter requires a sufficient overlap of the mesonic wave function with the phase-space density of surrounding quarks and is therefore more relevant toward lower momentum.

The fragmentation of a quark is implemented by applying the factorization theorem of QCD<sup>21</sup>. At large transverse momenta, the production process of a parton occurs on a short time scale,  $\tau_{\text{prod}} \simeq 1/p_t$ , while hadronization occurs at the considerably larger time scale  $\tau_{\text{had}} \simeq 1/\Lambda_{\text{QCD}}$ . Thus the production cross section for a hadron can be factorized into an elementary parton-production cross section (hard process) and a phenomenological universal transition probability distribution,  $D_{h/i}(z)$ , for a parton  $i$  of momentum  $p_i$  to convert into a hadron with momentum fraction  $z = p_h/p_i \leq 1$ . For light quarks and gluons the fragmentation functions,  $D_{h/i}$ , are rather broad distributions around  $z \simeq 0.5$ , but for heavy quarks they become rather sharply peaked toward  $z = 1$  and are sometimes even approximated by a  $\delta$ -function,  $D(z) = \delta(1 - z)$ .

The mechanism of recombination of a produced quark with other quarks or antiquarks in its environment (e.g., the valence quarks of the colliding hadrons) has

first been introduced in the late 1970's to explain flavor asymmetries in  $\pi$  and  $K$  meson production in hadronic collisions at forward rapidities<sup>146</sup>. In particular, the recombination idea has been rather successful in describing flavor asymmetries in the charm sector<sup>147,148</sup>, even close to midrapidity. In the context of heavy-ion collisions, quark coalescence models, applied at the hadronization transition, provide a simple and intuitive explanation for the observed constituent-quark number scaling (CQNS) of the elliptic flow of light hadrons<sup>149,150</sup> and the (unexpectedly) large baryon-to-meson ratios (e.g.,  $p/\pi \simeq 1$  or  $(\Lambda + \bar{\Lambda})/(4K_S^0) \simeq 1.3$  in central 200 AGeV Au-Au collisions at RHIC) at intermediate transverse momenta ( $2 \text{ GeV} \lesssim p_T \lesssim 5 \text{ GeV}$ )<sup>151,152,153,154</sup>. CQNS refers to a scaling property of the hadronic elliptic flow,  $v_{2,h}(p_T)$ , in terms of a universal function  $v_{2,q}(p_T/n) = v_{2,h}(p_T)/n$ , where  $n$  denotes the number of constituent quarks in a given hadron,  $h$ . CQNS naturally emerges from the recombination of approximately comoving quarks and antiquarks in a collectively flowing medium. Thus, within this picture,  $v_{2,q}(p_t)$  is interpreted as a universal elliptic flow of the quarks with transverse momentum  $p_t$  at the moment of hadronization (typically assumed to be the quark-hadron transition at  $T_c$ ). It can be expected that the phenomenologically very successful coalescence concept also applies in the HQ sector of heavy-ion collisions<sup>155,156</sup>. Note that, unlike quark fragmentation, quark recombination adds momentum and elliptic flow to the produced hadron (through the quark picked up from the environment).

At this point it might be instructive to reiterate a conceptual connection between the quark coalescence model and the idea of resonance correlations in the QGP. The latter were found to be an efficient mechanism for arriving at a small HQ diffusion constant, both within the effective resonance model (Sec. 2.3.1) and within the  $T$ -matrix approach (Sec. 2.3.2). Especially in the  $T$ -matrix approach, the resonance correlations were found to strengthen toward the expected hadronization transition, and thus provide a natural emergence of heavy-light quark coalescence at  $T_c$ . These ideas have recently been implemented in a resonance-based description of the coalescence process in kinetic theory based on a Boltzmann equation<sup>157</sup>. This approach improves instantaneous coalescence formulations in that it respects energy conservation and establishes a well-defined equilibrium limit in the coalescence process (i.e., the thermal distribution for the formed meson). Subsequently, resonance-recombination has been combined with “realistic” quark phase-space distributions, as generated in relativistic Langevin simulations<sup>158</sup>. In particular, it was found that CQNS could be recovered under the inclusion of space-momentum correlations in the quark phase-space distributions.

In Refs.<sup>28,44</sup> HQ spectra at RHIC have been hadronized in a combined coalescence plus fragmentation scheme. For the hadronization of, e.g., charm quarks into  $D$  mesons one obtains the  $D$ -meson spectra as

$$\frac{dN_D^{\text{tot}}}{dy d^2p_T} = \frac{dN_D^{\text{coal}}}{dy d^2p_T} + \frac{dN_c^{\text{frag}}}{dy d^2p_T} . \quad (80)$$

For the first term on the right-hand side, the quark-coalescence model of Ref.<sup>155</sup>

has been employed, where the  $p_T$  spectrum of a  $D$  meson follows from a convolution of light anti-quark and charm-quark phase-space distributions,  $f_{\bar{q},c}$ , as

$$\frac{dN_D^{\text{coal}}}{dyd^2p_T} = g_D \int \frac{p \cdot d\sigma}{(2\pi)^3} \int d^3q f_D(\mathbf{q}, \mathbf{x}) f_{\bar{q}}(\mathbf{p}_{\bar{q}}, \mathbf{r}_{\bar{q}}) f_c(\mathbf{p}_c, \mathbf{r}_c). \quad (81)$$

Here,  $\mathbf{p} = \mathbf{p}_{\bar{q}} + \mathbf{p}_c$  is the  $D$ -meson momentum and  $g_D$  a combinatorial factor accounting for color-neutrality and spin averaging. The  $D$ -meson Wigner function,  $f_D(q, x)$ , is assumed as a double Gaussian in relative momentum  $\mathbf{p}_c - \mathbf{p}_{\bar{q}}$  and size,  $\mathbf{r}_c - \mathbf{r}_{\bar{q}}$ , and  $d\sigma$  is the hyper-surface element 4-vector of the hadronization volume. The charm-quark distribution corresponds to the Langevin output at the end of the mixed phase of the fireball model, while the light-quark distributions are taken from previous applications of the coalescence model to light-hadron observables at RHIC<sup>152</sup>. This represents a parameter-free conversion of HQ distributions into heavy-meson spectra (note that the final state of the expanding fireball model<sup>28</sup> has been matched to the parameterization of collective velocity and elliptic flow for the light-quark distributions in the coalescence model<sup>152</sup>). The coalescence mechanism does not exhaust all heavy quarks in the hadronization process, especially toward higher  $p_t$  (where the light-quark phase-space density becomes small). Therefore, the remaining heavy quarks are hadronized using fragmentation, which for simplicity is treated in  $\delta$ -function approximation (as has been done in connection with the initial conditions). The formation of baryons containing heavy quarks (e.g.,  $\Lambda_c$ ) has been neglected since it has been found to give only small contributions, i.e.,  $\Lambda_c/D \ll 1$ . Quantitative refinements should, however, include these processes, see, e.g., Refs.<sup>159,160</sup>.

Finally, the comparison to electron spectra requires to compute semileptonic decays of heavy-flavor hadrons. Thus far, these have been approximated in three-body kinematics, e.g.,  $D \rightarrow e\nu K$ . An important finding in this context is that the resulting electron  $v_2(p_T)$  traces the one of the parent meson rather accurately<sup>155,161</sup>, implying that electron spectra essentially carry the full information on the heavy-meson  $v_2$ . In the  $p_T$  spectra, the decay electrons appear at roughly half of the momentum of the parent meson. It has also been pointed out<sup>159,160</sup> that  $\Lambda_c$  baryons have a significantly smaller branching fraction into electrons (about 4-5%) than  $D$  mesons (7% and 17% for neutral and charged  $D$ 's, respectively). Thus, in case of a large  $\Lambda_c/D$  enhancement, a net electron ‘‘loss’’ could mimic a stronger suppression than actually present at the HQ level. In fact, even variations in the neutral to charged chemistry from  $p$ - $p$  to  $A$ - $A$  collisions<sup>148</sup> could be quantitatively relevant.

### 3.4. Model Comparisons of Heavy-Quark Spectra at RHIC

We are now in position to conduct quantitative comparisons of diffusion calculations using transport simulations for HQ spectra in 200 AGeV Au-Au collisions at RHIC. We focus on Langevin simulations but also allude to Boltzmann transport models. The modifications of the initial spectra are routinely quantified in terms of the

nuclear modification factor,  $R_{AA}$ , and elliptic-flow parameter,  $v_2$ , defined by

$$\begin{aligned}
 R_{AA}(p_t; b) &= \frac{dN_Q^{AA}(b)/dp_t}{N_{\text{coll}}(b) dN_Q^{pp}/dp_t}, \\
 v_2(p_t; b) &= \frac{\int d\phi \frac{dN_Q^{AA}(b)}{dp_t dy d\phi} \cos(2\phi)}{\int d\phi \frac{dN_Q^{AA}(b)}{dp_t dy d\phi}},
 \end{aligned} \tag{82}$$

respectively;  $dN_Q^{AA}(b)/dp_t$  denotes the HQ  $p_t$  spectrum in an  $A$ - $A$  collision at impact parameter,  $b$ , which is scaled by the spectrum  $dN_Q^{pp}/dp_t$  from  $p$ - $p$  collisions times the number of binary nucleon-nucleon collisions,  $N_{\text{coll}}(b)$  (to account for the same number of heavy quarks). Thus, any deviation of  $R_{AA}$  from one indicates nuclear effects (from the QGP but possibly also in the nuclear initial conditions or from the pre-equilibrium stages). The elliptic-flow parameter,  $v_2(p_t)$ , is the second Fourier coefficient in the expansion of the (final) momentum distributions in the azimuthal angle,  $\phi$ , relative to the reaction plane ( $x$ - $z$  plane) of the nuclear collision. At midrapidity, where the “directed” flow ( $v_1$ ) is expected to vanish, the  $v_2$  coefficient is the leading source of azimuthal asymmetries. A non-zero  $v_2$  is only expected to occur in noncentral  $A$ - $A$  collisions due to an “almond”-shaped nuclear overlap zone (with a long (short) axis in  $y$  ( $x$ ) direction). Typical sources for a non-zero elliptic flow are a path-length difference for absorption of particles traversing the reaction zone or an asymmetry in the collective (hydrodynamic) flow due to stronger pressure gradients across the short axis. Both effects convert the initial spatial anisotropy,  $v_2$ , in a positive momentum anisotropy in the particle  $p_t$ -spectra. While the former mechanism is usually associated with high- $p_t$  particles (typical leading to a  $v_2 < 5\%$ ), the latter is driven by collective expansion due to thermal pressure mostly applicable to low- $p_t$  particles (with significantly larger  $v_2$  values, in excess of 5%). Since in the Langevin simulations heavy quarks are assumed to be exclusively produced in primordial  $N$ - $N$  collisions (i.e., their number is conserved subsequently), the HQ  $R_{AA}$  can be simply calculated as the ratio of the HQ  $p_t$  distribution function at the moment of hadronization to the initial distribution (taken from  $p$ - $p$  collisions),

$$\begin{aligned}
 R_{AA} &= \frac{f_Q(t_{\text{had}}, p_t)}{f_Q(t_0, p_t)}, \\
 v_2(p_t) &= \frac{\int d\phi f_Q(t_{\text{had}}, p_t, \phi) \cos(2\phi)}{f_Q(t_{\text{had}}, p_t)},
 \end{aligned} \tag{83}$$

while the  $v_2$  is computed using its definition given above.

The next five figures (18-22) encompass calculations of  $R_{AA}$  and  $v_2$  in semicentral Au-Au collisions at RHIC for the following approaches:

- (i) Fig. 18 [MT]<sup>26</sup> displays Langevin simulations for  $c$  quarks (with the pre-point Ito realization of the stochastic integral) using a hydrodynamic evolution for  $b = 6.5$  fm; the HQ drag and diffusion coefficients are based on LO hard-thermal

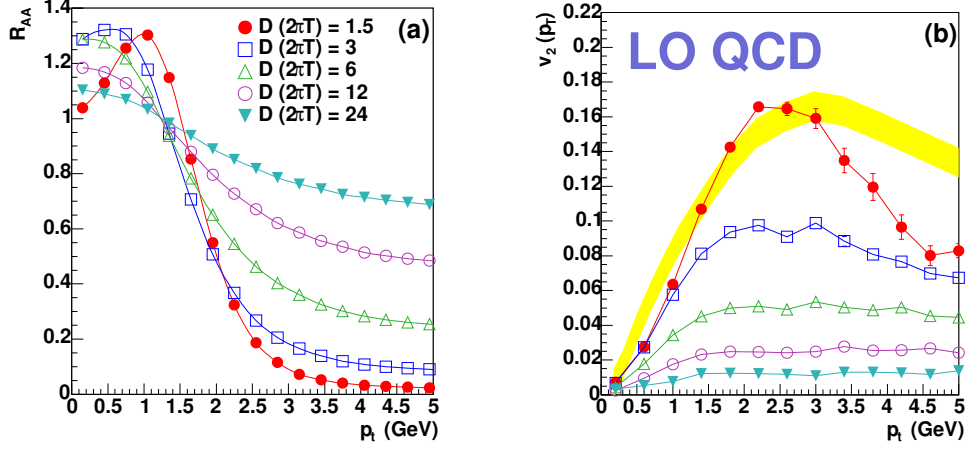


Fig. 18. (Color online) Nuclear modification factor (left panel) and elliptic flow (right panel) of charm quarks as a function of transverse momentum in semicentral ( $b = 6.5$  fm) Au-Au collisions using a hydrodynamic evolution of the bulk medium at RHIC<sup>26</sup>. The calculations are performed for HTL-improved LO-pQCD scattering with variable strong coupling and fixed Debye-screening mass in  $t$ -channel gluon-exchange scattering ( $\mu_D = 1.5T$ ). The relation of the spatial diffusion coefficient,  $D_s$  (denoted  $D$  in the figure legend), to the strong coupling constant,  $\alpha_s$ , is given by the approximate relation  $2\pi TD_s \approx 6(0.5/\alpha_s)^2$ .

loop scattering matrix elements with variable  $\alpha_s$  but fixed Debye screening mass.

- (ii) Fig. 19 [HGR]<sup>28</sup> displays Langevin simulations for  $c$  and  $b$  quarks (with the post-point Ito (Hänggi-Klimontovich) realization) using a thermal fireball expansion for  $b = 7$  fm; the HQ drag and diffusion coefficients are based on the effective resonance+pQCD model<sup>25</sup> for variable resonance width (coupling strength) and  $\alpha_s = 0.4$  in the pQCD part.
- (iii) Fig. 20 [AHH]<sup>115</sup> displays Langevin simulations for  $c$  quarks (with the pre-point Ito realization) using a hydrodynamic expansion for  $b = 5.5$  fm; the HQ drag and diffusion coefficients are based on the strong-coupling limit with AdS/CFT correspondence with a variable coupling strength estimated from matching to QCD<sup>108</sup>.
- (iv) Fig. 21 [HMGR]<sup>44</sup> displays Langevin simulations as under (ii) but with HQ transport coefficients based on the  $T$ -matrix+pQCD approach for two lQCD-based input potentials.
- (v) Fig. 22 [Mol]<sup>134</sup> displays Boltzmann transport simulations using a covariant transport model for  $b = 8$  fm; the HQ interactions are modeled by schematic LO pQCD cross sections, including upscaling by “ $K$  factors”.

Before going into details, let us try to extract generic features of the calculations. In all cases there is a definite correlation between a reduction in  $R_{AA}(p_t > 3 \text{ GeV})$  and an increase in  $v_2(p_t)$ , i.e., both features are coupled to an increase in interaction

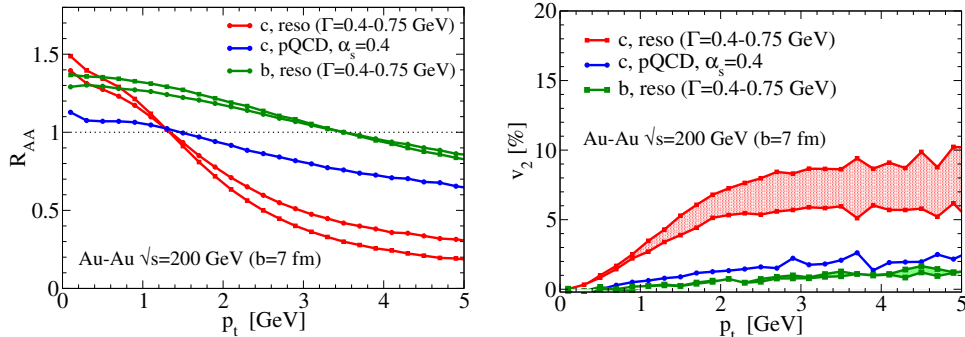


Fig. 19. (Color online) The HQ  $R_{AA}$  (left panel) and  $v_2$  (right panel) for semicentral ( $b = 7$  fm) Au-Au collisions at RHIC within the effective resonance + pQCD model compared to results from LO pQCD elastic scattering only with  $\alpha_s = 0.4$  and corresponding Debye-screening mass  $\mu_D = \sqrt{4\pi\alpha_s T}$ .

strength (decrease in the spatial HQ diffusion coefficient). Furthermore, the  $v_2(p_t)$  shows a typical, essentially linear, increase reminiscent of a quasi-thermal regime followed by a saturation characteristic for the transition to a kinetic regime. In all Langevin calculations the saturation for charm quarks occurs at about  $p_t = 2$ -3 GeV. For the largest interaction strength considered ( $D_s \simeq 1/(2\pi T)$ ), the left panels of Figs. 18 and 20 even suggest a turnover of  $v_2$  (at this point one should recall that all calculations displayed in this section utilize elastic scattering only which is expected to receive appreciable corrections at high  $p_t$  due to radiative processes). On the other hand, for  $p_t = 2$ -3 GeV the nuclear modification factor is still significantly falling, leveling off only at larger  $p_t \simeq 5$ -6 GeV. As expected, bottom quarks exhibit much reduced effects for comparable diffusion constants due to their factor  $\sim 3$  larger mass (see Fig. 19 and lower panels in Fig. 21).

Next, we attempt more quantitative comparisons. Some representative numbers for the resulting  $R_{AA}$  and  $v_2$  values are compiled in Tab. 2<sup>114</sup>. First we compare the LO-pQCD calculations for HQ diffusion in the hydrodynamic and fireball backgrounds corresponding to Figs. 18 and 19, respectively; for a comparable spatial diffusion coefficient,  $D_s \simeq 24$ -30/( $2\pi T$ ), both calculations show a maximal  $v_2$  of about 2% and a  $R_{AA}(p_t=5 \text{ GeV}) \simeq 0.7$  (recall the smaller  $b = 6.5$  fm in [MT] vs. 7 fm in [HGR] which may lead to somewhat smaller  $v_2$ , and the smaller  $T_0 = 265$  MeV [MT] vs. 340 MeV in [HGR] which entails somewhat less suppression). For the [AHH] hydro calculation with an AdS/CFT-motivated ansatz for the HQ friction constant,

$$\gamma = C \frac{T^2}{m_Q}, \quad (84)$$

a diffusion constant of  $D_s = 21/(2\pi T)$  leads to similar results (note that Tab. 2 contains results for  $b = 7.1 \text{ fm}$ <sup>162</sup> while Fig. 20 is calculated for  $b = 5.5$  fm). Let us now turn to stronger coupling, still focusing on the three Langevin simulations in Figs. 18, 19 and 20 which all utilize friction coefficients with a similar temper-

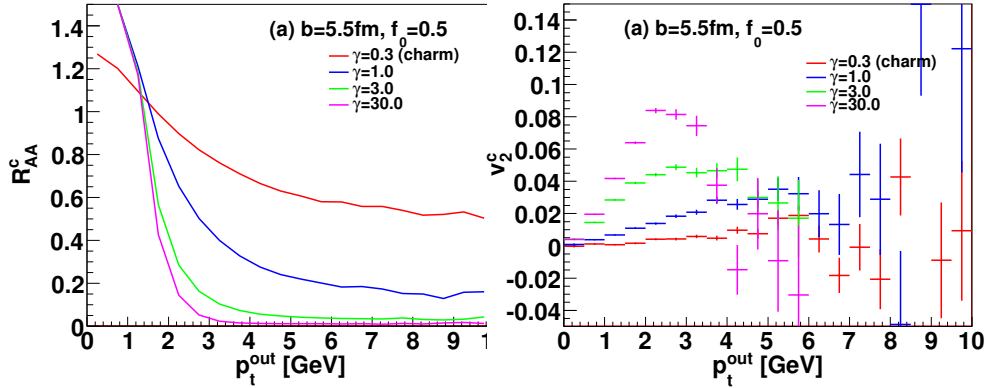


Fig. 20. (Color online)  $R_{AA}$  (left) and  $v_2$  (right) of charm quarks resulting from hydrodynamic simulations of  $b = 5.5$  fm Au-Au ( $\sqrt{s_{NN}} = 200$  GeV) collisions using AdS/CFT-motivated charm-quark diffusion constants with variable strength parameter,  $\gamma$ <sup>115</sup>, which corresponds to the constant  $C$  in Eq. (84).

ature dependence, essentially  $\gamma \propto T^2$  (recall right panel of Fig. 13), corresponding to an approximately constant spatial diffusion constant times temperature,  $D_s(2\pi T) \simeq \text{const}$  (recall left panel of Fig. 14). For  $D_s = 6/(2\pi T)$ , all calculations are again in semi-/quantitative agreement, with a maximum  $v_2$  of 4-6% and  $R_{AA}(p_t=5 \text{ GeV}) \simeq 0.25$ -0.3. The 4% value for Ref.<sup>115</sup> [AHH] will increase somewhat if the hydro evolution is run to the end of the mixed phase rather than terminated in the middle of the mixed phase (this is supported by the discussion in Sec. 3.5.2). We also note that in the fireball model of Ref.<sup>28</sup> [HGR] the inclusive ( $p_t$ -integrated)  $v_2$  at the end of the mixed phase was adjusted to the experimentally observed

Model [Ref.]	$D_s(2\pi T)$	$b$ [fm]	$v_2^{\text{max}}$	$R_{AA}(p_t=5 \text{ GeV})$
hydro + LO-pQCD <sup>26</sup>	24	6.5	1.5%	0.7
hydro + LO-pQCD <sup>26</sup>	6	6.5	5%	0.25
fireball + LO-pQCD <sup>28</sup>	$\sim 30$	7	2%	0.65
fireball + reso+LO-pQCD <sup>28</sup>	$\sim 6$	7	6%	0.3
hydro + “AdS/CFT” (84) <sup>115</sup>	21	7.1	1.5-2%	$\sim 0.7$
hydro + “AdS/CFT” (84) <sup>115</sup>	$2\pi$	7.1	4%	$\sim 0.3$
transport + LO pQCD <sup>134</sup>	$\sim 30$	8	$\sim 2\%$	$\sim 0.65$
transport + LO pQCD <sup>134</sup>	$\sim 7$	8	10%	$\sim 0.4$

Table 2. Overview of model approaches (1<sup>st</sup> column) and input parameters (2<sup>nd</sup> column: spatial charm-quark diffusion coefficient, 3<sup>rd</sup> column: nuclear impact parameter) for Langevin simulations of charm-quark spectra in Au-Au collisions at RHIC; selected values for the resulting elliptic flow ( $v_2^{\text{max}} \simeq v_2(p_t = 5 \text{ GeV})$ ) and nuclear modification factor are quoted in columns 4 and 5. The last two rows represent charm-quark transport calculations in a transport model for the bulk.

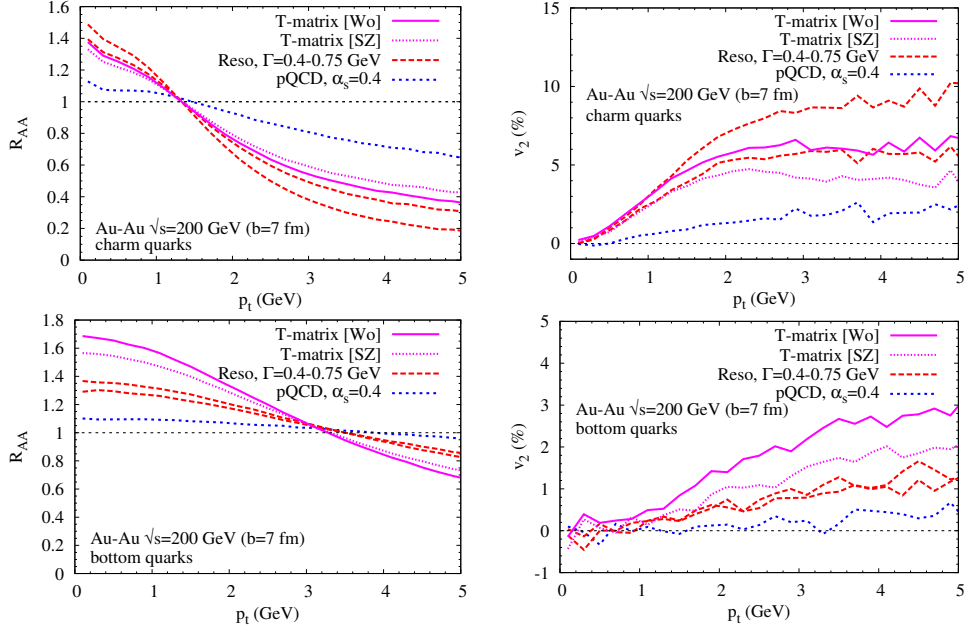


Fig. 21. (Color online) Charm- (top row) and bottom-quark (bottom row) spectra in Au-Au ( $\sqrt{s_{NN}} = 200$  GeV) collisions at RHIC using Langevin simulations for HQ diffusion in an expanding fireball model. The results using HQ diffusion based on LO-pQCD and resonance+pQCD approaches (see also Fig. 19) are compared to the  $T$ -matrix+pQCD calculations<sup>44</sup> (the pertinent uncertainty band reflects different input potentials based on parameterizations of IQCD HQ free energies as given in Refs.<sup>90,45</sup>). The left (right) panels show the  $R_{AA}$  ( $v_2$ ) for central (semicentral) collisions.

light-particle  $v_2 \simeq 5.5$ -6% at an impact parameter of  $b = 7$  fm, i.e., it presumably includes an extra 20% of bulk- $v_2$  compared to the hydrodynamic calculations<sup>f</sup>. Such an amount is typically built up in the subsequent hadronic phase of hydrodynamic evolutions and thus not present in pertinent HQ simulations within a QGP (+ mixed) phase.

We now make some comments specific to individual calculations. The Langevin calculations using HQ  $T$ -matrix interactions (supplemented with pQCD scattering off gluons) shown in Fig. 21 are rather close to the effective resonance model, even though they do not involve tunable parameters. However, they are still beset with substantial uncertainty, as indicated by the use of two different input potentials (in addition, the use of the free energy,  $F_1$ , instead of the internal energy,  $U_1$ , as potential significantly reduces the effects). One also notices that the  $v_2$  at low  $p_t$  is very similar to the resonance model while the suppression at high  $p_t$  is somewhat less pronounced. This is so since the  $T$ -matrix transport coefficients (a) fall off stronger with three-momentum (the resonant correlations are close to the  $Q$ - $q$

<sup>f</sup>This adjustment ensures compatibility of the fireball freezeout with the coalescence model<sup>152</sup>.

threshold), and (b) decrease with increasing temperature (resonance melting). The latter combines with the facts that the suppression is primarily built up in the very early stages (where the  $T$ -matrix is less strong) while the bulk  $v_2$  takes a few fm/ $c$  to build up (at which point the  $T$ -matrix has become stronger). Furthermore, the  $T$ -matrix calculations lead to stronger medium effects on  $b$  quarks than the effective resonance model; this reflects the stronger binding due to the mass effect in the  $T$ -matrix calculation.

A principal limitation of the Langevin approach is the treatment of fluctuations which are by definition implemented in Gaussian approximation. The latter arises due to enforcing the dissipation-fluctuation relation (mandatory to ensure the HQ distributions to approach equilibrium) which tends to underestimate the momentum fluctuations especially at high momentum, compared to a full transport calculation. This leads to an overestimate of the quenching effect at high  $p_t$  even for the same *average* energy loss. One may assess these limitations more quantitatively by comparing to Boltzmann simulations including partonic phases<sup>133,134</sup>, an example of which is displayed in Fig. 22 for charm quarks in  $b = 8$  fm Au-Au collisions at RHIC. The baseline LO-pQCD calculations indicated by the crosses in Fig. 22, labeled by “1.33 mb”, may be compared to the fireball-Langevin simulations represented by the blue lines in Fig. 19. In both calculations the underlying elastic parton-HQ cross sections correspond to a strong coupling constant of  $\alpha_s \simeq 0.4$ . The quenching and elliptic flow come out quite similar in both calculations at least up to  $p_t \simeq 5$  GeV, especially when accounting for the slightly different centrality. E.g., in the Boltzmann treatment, the  $R_{AA}$  for  $p_t = 5$  GeV charm quarks is about 0.6-0.7 with a  $v_2$  of a few percent. For a four-fold increase of the cross section (which would roughly correspond to a reduction of  $D_s(2\pi T)$  from  $\sim 30$  to  $\sim 7$ ), one finds  $R_{AA}(p_t = 5 \text{ GeV}) \simeq 0.4$  and a maximum  $v_2$  of close to 10%. While the latter value is somewhat larger than the Langevin predictions, the agreement is not too bad.

Finally, Fig. 23 shows results from an exploratory calculation in the Langevin approach where HQ drag and diffusion coefficients from elastic scattering in the effective resonance model (cf. Sec. 2.3.1) are combined with induced gluon radiation in the DGLV E-loss formalism (cf. Sec. 2.6)<sup>163</sup>. One of the uncertainties in this calculation is the extrapolation of the radiative E-loss into the low-momentum regime, where it still contributes rather substantially; e.g., the elliptic flow of charm quarks is increased over elastic pQCD+resonance model by ca. 40%, and even more (ca. 100%) relative to pQCD elastic scattering only. Another limitation is the above mentioned caveat in Langevin theory of underestimating the (E-loss) fluctuations implying an overestimate of the quenching at high  $p_t$ . This can also be seen when comparing to the pQCD radiative E-loss calculations<sup>7,164,38</sup>, where the gluon radiation is treated microscopically within an opacity expansion. A consistent merging of radiative and elastic processes in HQ transport thus remains a challenging task.



Fig. 22. (Color online)  $R_{AA}$  (left) and  $v_2$  (right) of charm quarks resulting from covariant transport simulations of  $b = 8$  fm Au-Au ( $\sqrt{s_{NN}} = 200$  GeV) collisions<sup>134</sup>.

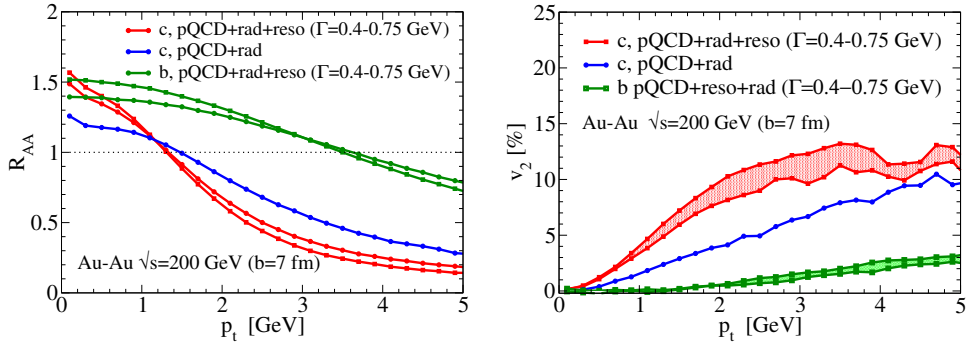


Fig. 23. (Color online) The nuclear modification factor,  $R_{AA}$  (left panel), and elliptic flow,  $v_2$  (right panel), for heavy quarks from collisional<sup>28</sup> and radiative E-loss<sup>121</sup>, cf. Ref.<sup>163</sup>.

### 3.5. Heavy-Meson and Electron Observables

To compare to observables, the HQ spectra discussed in the preceding section need to be converted into spectra of color-neutral final-state particles. At the minimal level, this requires hadronization into charm and bottom mesons and baryons. Thus, a measurement of identified HQ hadrons constitutes the most direct way to make contact with theoretical predictions. Currently, the richest source of information on HQ spectra in Au-Au collisions at RHIC are single-electron ( $e^\pm$ ) spectra, which,

after the subtraction of sources coupling to a photon (“photonic sources”), are associated with semileptonic decays of HQ hadrons. As discussed in Sec. 3.3, the decay electrons largely preserve the modifications of the parent hadron spectra, albeit shifted in  $p_t$  (by roughly a factor of  $\sim 2$ ). The more severe complication is the composition of the  $e^\pm$  spectra, most notably the partition into charm and bottom parents<sup>165</sup>. Since the heavier bottom quarks are, in general, less affected by the medium, their contribution significantly influences the resulting  $e^\pm$  spectra. Unless otherwise stated, the calculations discussed below include a “realistic” input for the charm/bottom partition, i.e., either in terms of pQCD predictions for  $p$ - $p$  spectra or via empirical estimates from  $D$ -meson and electron spectra in  $p$ - $p$  and  $d$ -Au. Within the current theoretical and experimental uncertainties, both procedures agree, with an expected crossing of charm and bottom electrons at  $p_t \simeq 3$ -6 GeV in  $p$ - $p$  collisions at RHIC energy.

Almost all of the approaches for computing HQ diffusion and/or energy loss introduced in Sec. 2 have been applied to  $e^\pm$  data at RHIC. We organize the following discussion into (mainly perturbative) E-loss calculations (usually applied within a static geometry of the nuclear reaction zone) as well as perturbative and nonperturbative diffusion calculations using Langevin simulations for an expanding medium.

### 3.5.1. Energy-Loss Calculations

Radiative energy loss (E-loss) of high-energy partons in the QGP is believed to be the prevalent mechanism in the suppression of light hadrons with high  $p_T \geq 6$  GeV. It turns out that the application of this picture to the HQ sector (Sec. 2.6) cannot account for the observed suppression in the non-photonic  $e^\pm$  spectra.

In the DGLV formalism, the high- $p_T$   $e^\pm$  suppression due to radiative E-loss of  $c$  and  $b$  quarks falls short of the data by about a factor of 3, cf. left panel of Fig. 24<sup>38</sup>. This led the authors to consider elastic E-loss (see also Refs.<sup>27,167</sup>) which was found to be comparable to the radiative one out to the highest electron  $p_T$  measured thus far ( $\sim 10$  GeV). Their combined effect still underestimates the measured suppression by about a factor of  $\sim 2$  for  $p_t > 4$  GeV. Similar findings were reported within the BDMPS approach: for a transport coefficient of  $\hat{q} = 14$  GeV<sup>2</sup>/fm<sup>8</sup>, the  $e^\pm$  spectra cannot be reproduced either, unless an unrealistic assumption of neglecting the bottom contribution is made, cf. middle panel of Fig. 24<sup>36</sup>.

Both E-loss calculations<sup>38,36</sup> are performed for a static (time-averaged) medium of gluons, with fragmentation as the sole mechanism for hadronization. This is expected to be a good approximation at high  $p_T$ . Processes leading to an energy gain in the spectra, e.g., due to drag effects or coalescence with a light quark, are not included. Such processes lead to an increase in the  $p_T$  of the final-state hadron

<sup>8</sup>This value is a factor 5-10 larger than predicted by pQCD, and at the upper limit of being compatible with light hadron suppression<sup>29</sup>.

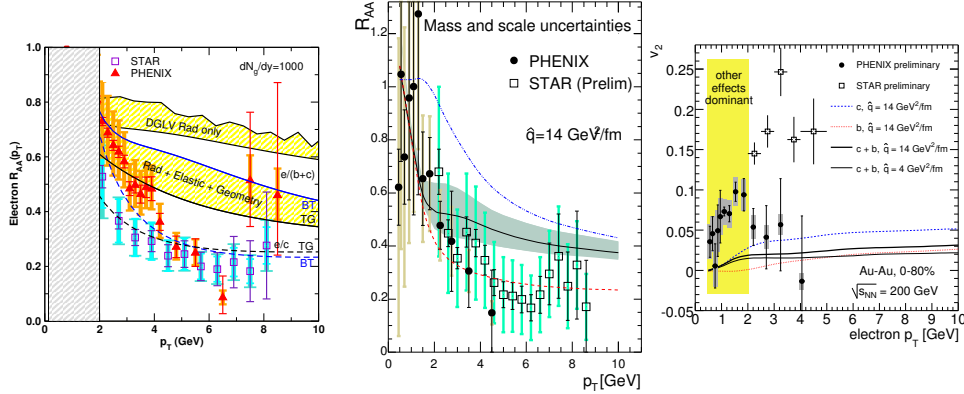


Fig. 24. (Color online) PQCD E-loss calculations for heavy quarks compared to single-electron observables in Au-Au collisions at RHIC<sup>33,166,34</sup> Left panel:  $e^\pm$  nuclear modification factor,  $R_{AA}^e$ , in central collisions in the DGLV approach<sup>38</sup> (upper band: radiative E-loss only; lower band: radiative plus elastic E-loss) for a gluon plasma with rapidity density  $dN^g/dy=1000$ ; the bands represent the uncertainty in the leading-logarithm approximation of the elastic part (as described in Sec. 2.6). Middle and right panel:  $R_{AA}^e$  in central and  $v_2$  in 0-80% central collisions within the BDMPS approach using a transport coefficient of  $\hat{q}=14 \text{ GeV}^2/\text{fm}$ <sup>36</sup>; dashed and dash-dotted curves represent the results for  $c$ - and  $b$ -quark contributions separately, while the solid curve is the combined result with a band indicating the pQCD uncertainty in the charm/bottom partition<sup>145</sup>.

and thus to an increase in the electron  $R_{AA}$ , which would augment the discrepancy with data. The neglect of the diffusive term becomes particularly apparent in the elliptic flow. In the E-loss treatment the only source of an azimuthal asymmetry in the  $p_T$  spectra in non-central Au-Au collisions is the spatial geometry of the overlap zone: particles traveling along the short axis are less likely to be absorbed than those moving along the long axis of the approximately elliptic reaction zone. The positive  $v_2$  generated by this mechanism amounts to up to a few percent and significantly falls short of the observed electron  $v_2$ , see right panel in Fig. 24.

As an alternative mechanism, the collisional dissociation of  $D$  and  $B$  mesons from HQ fragmentation in the QGP (Sec. 2.3.3) has been implemented into an E-loss calculation<sup>77h</sup>. A rather striking prediction of this calculation is that the shorter formation time of  $B$  mesons leads to stronger suppression than for  $D$  mesons above hadron momenta of  $p_t \simeq 15 \text{ GeV}$  at RHIC, cf. left panels in Fig. 25. This turns out to be an important ingredient in the successful reproduction of the  $e^\pm$  suppression data as shown in the right panel of Fig. 25.

<sup>h</sup>The compatibility with the radiative picture of high- $p_t$  light-hadron suppression is presumably little affected since the Lorentz-dilated formation times of light quarks largely result in hadronization beyond the QGP lifetime.

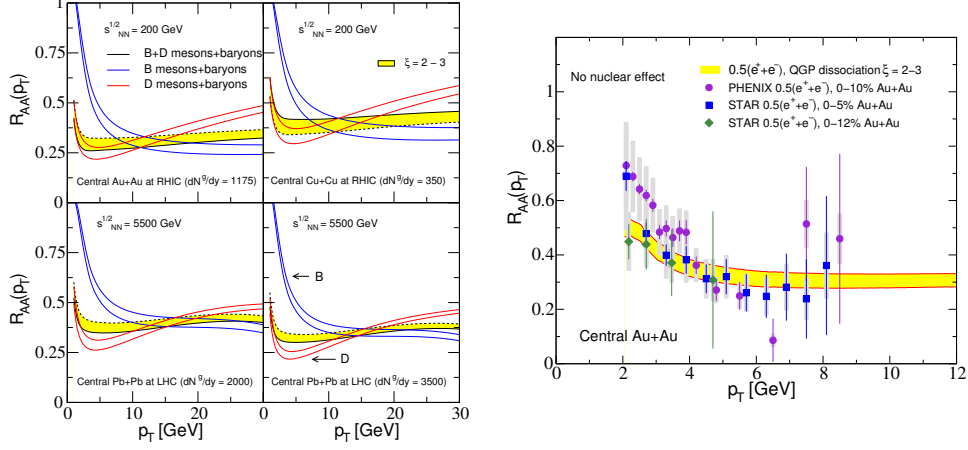


Fig. 25. (Color online) Energy-loss calculations employing the collisional dissociation mechanism for HQ fragmentation into heavy mesons in the QGP<sup>77</sup>. Left panels: nuclear modification factor for  $D$  and  $B$  mesons in central 200 AGeV Au-Au and Cu-Cu at RHIC (upper panels) for gluon-rapidity densities of  $dN^g/dy = 1175$  and  $350$ , respectively, and in central 5.5 ATeV Pb-Pb collisions at LHC for  $dN^g/dy = 2000$  and  $3500$  (lower panels). Right panel:  $R_{AA}$  for  $e^\pm$  in central 200 AGeV Au-Au collisions at RHIC compared to PHENIX and STAR data<sup>22,34</sup>; the yellow bands reflect theoretical uncertainties due to an impact parameter expansion of the heavy-light quark interaction.

### 3.5.2. Langevin Simulations

The importance of elastic scattering for HQ diffusion *and* E-loss has been emphasized, prior to quantitative measurements of  $e^\pm$  spectra, in Refs.<sup>25,26</sup>, albeit within rather different realizations of the underlying HQ interaction (recall Secs. 2.3.1 and 2.2.2, respectively).

The HQ spectra of the effective resonance + LO-pQCD model<sup>25</sup> (using Langevin simulations within an expanding fireball, recall Fig. 19) have been converted into  $e^\pm$  spectra utilizing a combined coalescence/fragmentation scheme at  $T_c$  followed by heavy-meson three-body decays<sup>28,168</sup>. The predicted  $e^\pm$  spectra and elliptic flow show approximate agreement with 2005 PHENIX<sup>33,166</sup> and STAR<sup>169</sup> data, see upper left and right panel of Fig. 26, respectively. Compared to the results for LO pQCD interactions only (blue lines), the resonance interactions (red bands) turn out to be instrumental in generating the required suppression and elliptic flow (see upper panels of Fig. 26). LO-pQCD scattering alone, even with a strong coupling of  $\alpha_s=0.4$ , does not produce sufficient coupling to the bulk medium to suppress the primordial quark spectra, nor to drag the heavy quarks along with the collective flow of the expanding fireball. The effect of heavy-light quark coalescence is illustrated by a calculation where only fragmentation is used as a hadronization mechanism (lower panels in Fig. 26). In this case, the shape of the  $e^\pm$   $R_{AA}$  and the magnitude of the  $v_2$  are not well reproduced. Coalescence processes add both momentum and  $v_2$  to the meson (and thus to the  $e^\pm$ ) spectra, i.e., the suppression becomes smaller.

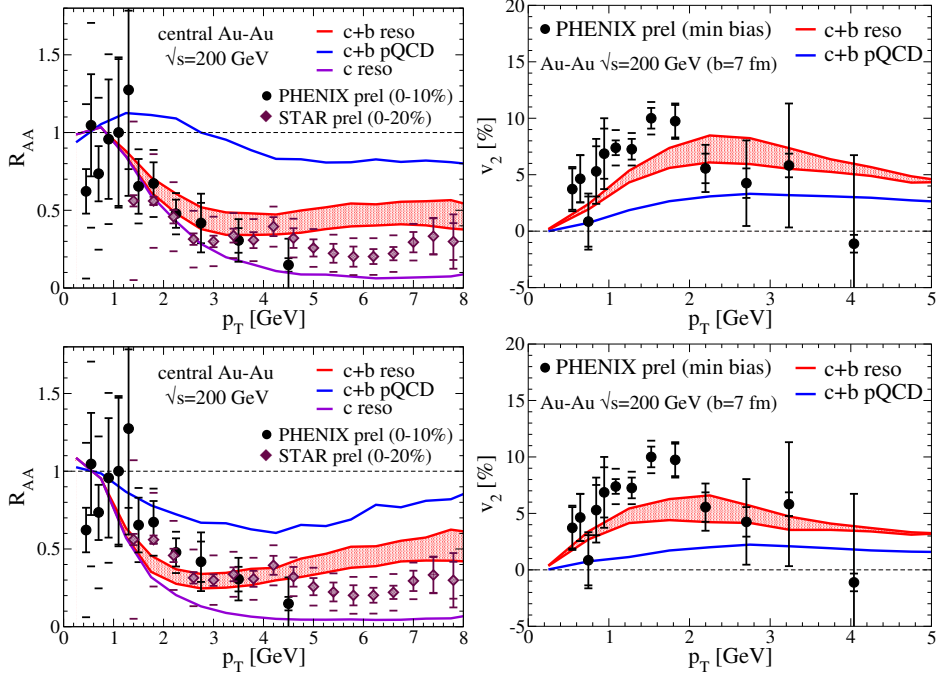


Fig. 26. (Color online) Nuclear modification factor (left panels) and elliptic flow (right panels) of  $e^\pm$  spectra from heavy-flavor decays in Au-Au collisions at RHIC, as computed within HQ Langevin simulations in a thermal fireball employing the resonance+pQCD model for HQ transport in the QGP<sup>28,168</sup>. The upper panels include effects from heavy-light quark coalescence while the latter are switched off in the lower panels. The bands represent the full results for  $D$ - and  $B$ -meson resonance widths of  $\Gamma = 0.4\text{-}0.75$  GeV; the blue lines are obtained for LO-pQCD interactions only, while the purple lines neglect bottom contributions. The data are from Refs.<sup>33,166,169</sup>.

It is furthermore instructive to compare the LO-pQCD results with fragmentation only (lower left panel in Fig. 26) to the pQCD E-loss calculations, especially to the elastic DGLV results where  $\alpha_s=0.3$  has been used (left panel of Fig. 24). The suppression level in the pertinent electron  $R_{AA}$  is quite comparable for a rather large range in  $p_T$ . The increasing trend in the Langevin calculations for  $p_T \gtrsim 5$  GeV is presumably due to the dominant  $b$ -quark contribution (which is barely suppressed even in the resonance model up to  $p_T \gtrsim 5$  GeV, see left of Fig. 19). Let us also estimate the impact of radiative contributions on the resonance model. Within DGLV the electron suppression due to radiative E-loss alone amounts to about 0.6-0.8 for  $p_T \simeq 4\text{-}10$  GeV. Upon multiplying the  $R_{AA}$  for the resonance+pQCD model in the upper left panel of Fig. 26 with this factor, the result would be compatible with current RHIC data.

The PHENIX collaboration has conducted a comprehensive comparison of their 2006  $e^\pm$  data<sup>22</sup> to theoretical calculations predicting *both*  $R_{AA}$  and  $v_2$ <sup>28,36,171</sup>, cf. left panel of Fig. 27. The interpretation reiterates some of the main points made above:

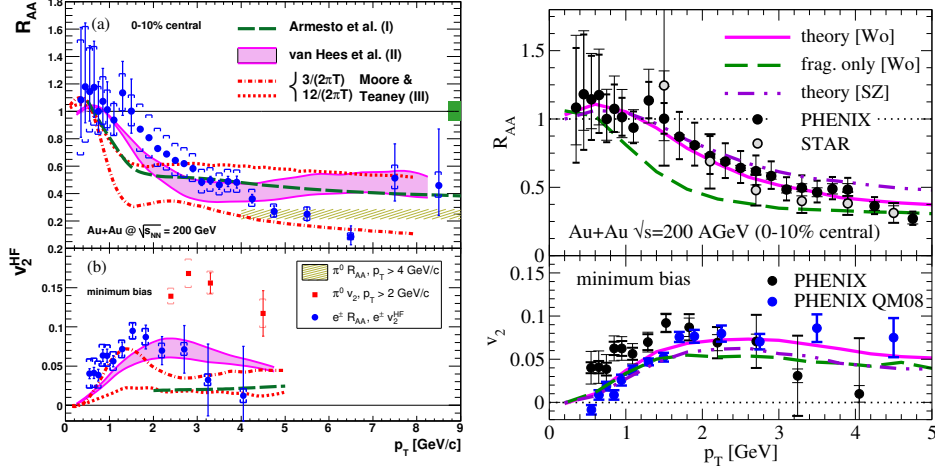


Fig. 27. (Color online) Left panel: Comparison of PHENIX  $e^\pm$  data<sup>22</sup> to theoretical predictions based on (i) Langevin simulations with the resonance+LO-pQCD interactions plus quark coalescence (bands)<sup>28</sup>, (ii) Langevin simulations with (upscaled) HTL-improved LO-pQCD interactions (dash-dotted and dotted lines)<sup>26</sup>, and (iii) radiative E-loss calculations (dashed lines)<sup>36</sup>. For further illustration, PHENIX data for  $\pi^0$  suppression and elliptic flow are shown<sup>170</sup>. Right panel: Comparison of PHENIX<sup>22,35</sup> and STAR<sup>34</sup>  $e^\pm$  data to Langevin-fireball simulations for HQ transport using  $T$ -matrices with lQCD-based heavy-quark potentials<sup>44</sup>; an uncertainty due to different lQCD internal energies is indicated by the solid and dash-dotted curve; the dashed lines are obtained without the effects of heavy-light quark coalescence at  $T_c$ .

(i) the missing drag in (radiative) E-loss calculations entails a substantial underprediction of the  $v_2$ ; (ii) Langevin calculations using elastic scattering require rather small HQ diffusion coefficients,  $D_s(2\pi T) \simeq 4-6$ , to be compatible with the observed level of suppression and elliptic flow, and, (iii) quark coalescence improves the simultaneous description of these two observables.

The heavy-light quark  $T$ -matrix approach, based on input potentials estimated from thermal lattice-QCD, has been applied within the same Langevin-fireball + coalescence/fragmentation scheme as the effective resonance model<sup>44</sup>. The pertinent  $e^\pm$  spectra (cf. right panel of Fig 27) exhibit a comparable level of agreement with current RHIC data<sup>22,34,35</sup> as in the resonance model, with a similar uncertainty due to different extractions of the HQ internal energy. Although the  $T$ -matrix calculations involve, in principle, no tunable parameters, the inherent theoretical uncertainties are appreciable (e.g., in the definition of the in-medium potential in terms of internal or free energy). Let us, however, recall a rather general feature of the  $T$ -matrix approach which was visible already at the level of the HQ spectra in Fig. 21: the weak temperature dependence of, e.g., the friction coefficient implies that the HQ coupling to the medium remains rather strong in the later QGP and mixed phase stages of the evolution. Since the bulk  $v_2$  is largest in these later stages, while the suppression largely occurs in the first 1-2 fm/ $c$ <sup>39</sup>, the  $T$ -matrix interactions generate relatively more  $v_2$  than suppression compared to, e.g., the resonance

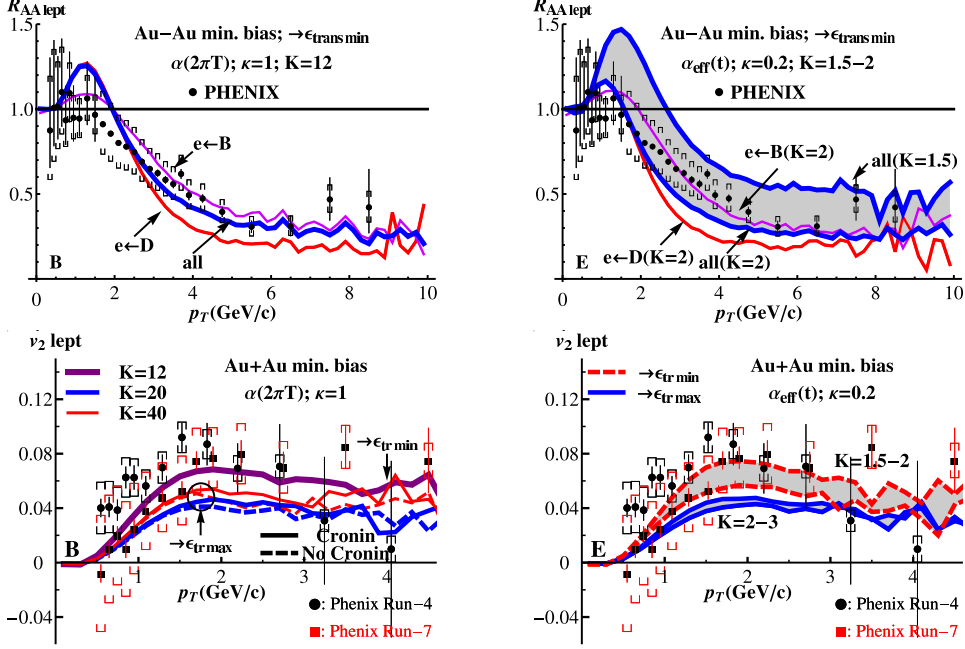


Fig. 28. (Color online) Boltzmann-transport model results for electron  $R_{AA}$  (upper panels) and  $v_2$  (lower panels)<sup>67</sup> in a hydrodynamic evolution using different versions of LO-pQCD HQ interactions, compared to PHENIX data<sup>22,35</sup> in 200 AGeV Au-Au collisions at RHIC. The curves in the left panels are computed with fixed  $\alpha_s(2\pi T)$  at given temperature, conventional infrared regulator ( $\tilde{\mu}_D^2 = r\mu_D^2$  with  $r \equiv \kappa = 1$ ) and large  $K$ -factors; the curves in the right panels are computed with a running  $\alpha_s$ , reduced IR regulator ( $r=0.2$ ) and reduced  $K$  factors of 1.5-2 (or 2-3), as represented by the bands.  $\epsilon_{trmax}$  or  $\epsilon_{trmin}$  indicate freezeout at the beginning or end of the mixed phase, respectively.

model (or, alternatively: for the same  $v_2$ , the suppression in the  $T$ -matrix approach is smaller). This traces back to the increasing color-Debye screening with increasing temperature, which leads to a gradual melting of the resonance correlations and a marked increase of the spatial diffusion constant,  $D_s/(2\pi T)$ , with temperature (recall Fig. 14). Such a temperature dependence appears to improve the consistency in the simultaneous description of the  $e^\pm R_{AA}$  and  $v_2$ , but more precise data are needed to scrutinize this feature (including  $d$ -A collisions to quantify the Cronin effect, which could increase the  $R_{AA}$  without noticeably affecting  $v_2$ ).

Finally, we reproduce in Fig. 28 selected results of the Boltzmann-transport approach of HQ diffusion<sup>67</sup> with the background medium described by the hydrodynamical model of Ref.<sup>13</sup>; hadronization is treated in a combined coalescence+fragmentation approach similar to the one in Refs.<sup>28,44</sup>. The HQ interactions in the QGP are implemented via the elastic pQCD scattering amplitudes described in Sec. 2.2.3. The left panels in Fig. 28 refer to a model with fixed coupling con-

stant,  $\alpha_s(2\pi T)$ , at given temperature and standard screening mass ( $r=1$ ). A large  $K$  factor of  $K = 12$  is needed to simultaneously reproduce the electron  $R_{AA}$  and  $v_2$  data. The final elliptic flow is found to be rather sensitive to the late QGP stages of the evolution, favoring hadronization at the end of the mixed phase (i.e., at a small transition energy-density,  $\epsilon_{\text{trans}}$ ); this is consistent with the findings of Ref.<sup>39</sup> and the above discussion of the  $T$ -matrix interaction. It thus corroborates that anisotropic matter-flow can only be transferred to the heavy quarks if the latter is sufficiently large, while E-loss (reflected in high- $p_T$  suppression) is mostly effective when the fireball density is high. The simulations find little impact of the initial-state Cronin effect on the final heavy-quark  $v_2$ , but the suppression is somewhat reduced primarily for  $e^\pm$  momenta of  $p_T \simeq 1\text{-}3$  GeV. The right panel of Fig. 28 illustrates that similar results can be achieved with smaller  $K$ -factors,  $K=1.5\text{-}2$ , if the pQCD cross sections are augmented by a running coupling,  $\alpha_s(t)$  ( $t$ : 4-momentum transfer in the elastic scattering process), and a small infrared regulator,  $\tilde{\mu}_D^2 = r\mu_D^2$  with  $r=0.2$ , in  $t$ -channel gluon-exchange scattering.

### 3.6. Viscosity?

In this section we utilize the quantitative estimates for the HQ diffusion coefficient as extracted from current RHIC data to obtain a rough estimate of the ratio of shear viscosity to entropy density,  $\eta/s$ , in the QGP. This quantity has received considerable attention recently since (a) it allows to quantify deviations from the predictions of ideal fluid dynamics for observables like the elliptic flow, and (b) conformal field theories in the strong coupling limit are conjectured to set a universal lower bound for any liquid, given by  $\eta/s = 1/(4\pi)^{17}$ , referred to as KSS bound. In the following we will bracket the estimates derived from HQ observables by using relations of  $D_s$  and  $\eta/s$  in the weak- and strong-coupling limit (the latter assumed to be given by the AdS/CFT correspondence).

Following the discussion in Sec. 2.4, the strong coupling limit in the AdS/CFT framework results in a (spatial) HQ diffusion constant of  $D_s \simeq 1/(2\pi T)$ . Combining this with the lower bound of the viscosity-to-entropy-density quoted above, one obtains

$$\frac{\eta}{s} = \frac{1}{2} T D_s . \quad (85)$$

For a weakly coupled dilute gas, an estimate for a relation between  $D_s$  and  $\eta$  can be inferred starting from the calculation of the shear viscosity from kinetic theory for an ultrarelativistic gas<sup>172,173</sup>,

$$\eta \approx \frac{4}{15} n \langle p \rangle \lambda_{\text{tr}} , \quad (86)$$

where  $n$  denotes the particle density,  $\langle p \rangle$  the average momentum of the gas particles and  $\lambda_{\text{tr}}$  its transport-mean free path. With the estimate,  $n \langle p \rangle \simeq \epsilon$ , for the energy

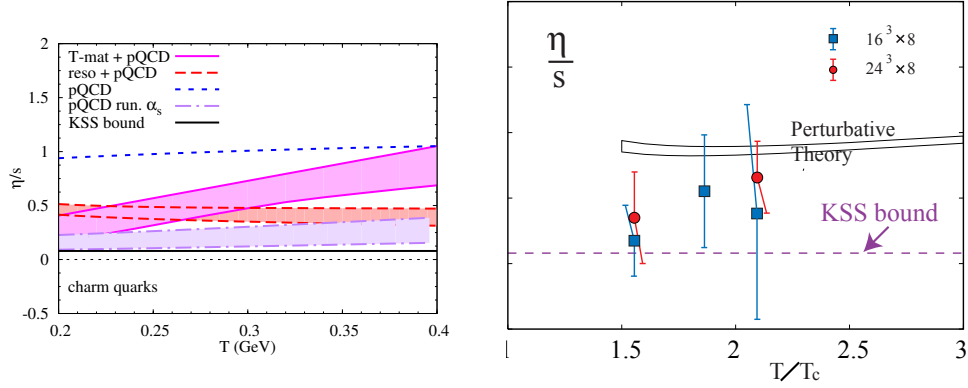


Fig. 29. (Color online) The ratio of shear viscosity to entropy density,  $\eta/s$ . Left panel: schematic estimates using charm-quark diffusion constants based on (a) schematic LO pQCD elastic scattering ( $\alpha_s=0.4$ ) in the weakly interacting limit, Eq. (88) (dashed line), (b) pQCD elastic scattering with running coupling constant and small IR regulator (band enclosed by dash-dotted lines using the weak- and strong-coupling limits), (c) the effective resonance + pQCD model in the strong-coupling limit, Eq. (86) (band enclosed by long-dashed lines for  $\Gamma=0.4-0.75$  GeV), and (d) the lattice-QCD potential based  $T$ -matrix approach augmented by pQCD scattering off gluons (band enclosed by solid lines constructed from the weak- and strong-coupling limits). Right panel: lattice QCD computations in a gluon plasma<sup>174</sup> compared to results inferred from perturbation theory<sup>175,176</sup>.

density and the corresponding equation of state,  $Ts = \epsilon + P = 4/3\epsilon$ , one arrives at

$$\frac{\eta}{s} \simeq \frac{1}{5} T \lambda_{\text{tr}} . \quad (87)$$

Finally, equating the transport mean-free path  $\lambda_{\text{tr}}$  to the mean-free time  $\tau_{\text{tr}}$  and taking into account the delay due to the mass effect of the heavy quark on the thermalization time,  $\tau_Q \approx \tau_{\text{tr}} T/m_Q$ , one finds

$$\frac{\eta}{s} \approx \frac{1}{5} T D_s . \quad (88)$$

In comparison to the “strong-coupling” estimate within AdS/CFT, Eq. (86), the shear viscosity appears to be underestimated when the kinetic theory for a dilute gas is applied to liquids. These estimates are now applied to several of the HQ diffusion calculations discussed above, see the left panel of Fig. 29. Since  $\eta/s \propto D_s(2\pi T)$ , the main features of Fig. 14 are transmitted to  $\eta/s$ , in particular the weak temperature dependence of the LO-pQCD calculations and the effective resonance model. Of course, the absolute values of these calculations differ considerably. A different behavior is only found for the  $T$ -matrix+pQCD model, which suggests a transition from a strongly coupled regime close to  $T_c$  to relatively weak coupling above  $\sim 2T_c$ . In fact, the uncertainty band has been constructed as follows: for the lower limit, the weak-coupling estimate Eq. (88) is used; for the upper limit, the strong-coupling limit estimate, Eq. (86), at  $T=0.2$  GeV is linearly interpolated with the LO-pQCD weak-coupling limit at  $T=0.4$  GeV (the strong-coupling estimate for

$T$ -matrix+pQCD overshoots the LO-pQCD result at this temperature). As for the spatial diffusion constant, the increase of  $\eta/s$  with temperature is related to color-Debye screening of the lQCD-based potentials which entails a gradual melting of the dynamically generated resonances in the heavy-light quark  $T$ -matrix. It is tempting to interpret the decrease of  $\eta/s$  when approaching  $T_c$  from above as a precursor-phenomenon of hadronization and thus connected to the phase transition itself. It remains to be seen whether a similar mechanism is operative in the light-quark and/or gluon sector (three-body interactions are unlikely to produce this due to the decrease in particle density when approaching  $T_c$  from above). Such a behavior is rather general in that it has been observed around phase-transition points for a large variety of substances, see, e.g., the discussion in Refs.<sup>177,178</sup>.

Finally we show in the right panel of Fig. 29 a quenched lQCD computation of  $\eta/s$ <sup>174</sup>. The error bars are appreciable but the results tend to favor  $\eta/s$  values which are below LO-pQCD calculations. The specific pQCD result included in this plot employs a next-to-leading logarithm calculation for the shear viscosity<sup>176</sup> and a self-consistent hard-thermal-loop calculation for the entropy density<sup>175</sup>. It is rather close to the schematic LO calculation (using  $\alpha_s=0.4$ ) in the left panel of Fig. 29.

#### 4. Heavy Quarkonia in Medium

In recent years it has become increasingly evident that observables in the heavy-quarkonium and open heavy-flavor sectors are intimately connected. In the original picture of charmonium suppression as a probe of color-screening in hot and dense QCD matter<sup>179</sup> there are no obvious such connections. Several recent developments have changed this situation. Thermal lattice QCD calculations find that charmonium correlation functions are remarkably stable up to temperatures of  $\sim 2T_c$  or higher, suggestive for the survival of the ground state ( $\eta_c, J/\psi$ ) well into the QGP. This interpretation is supported by probabilistic extractions of the pertinent quarkonium spectral functions. It implies that quarkonia can not only dissociate but also regenerate in the QGP<sup>i</sup>. It immediately follows that the yield and spectra of regenerated quarkonia are, in principle, sensitive to the abundance and momentum spectra of open-charm states in the system. E.g., for a fixed total charm number in the system, a softening of the heavy-quark spectra is expected to increase  $c\bar{c}$  overlap in phase space and thus enhance the probability for charmonium formation. At the same time, elliptic flow of charm quarks will imprint itself on regenerated charmonia. Furthermore, HQ interactions with light quarks (and possibly gluons) may be closely related to the interaction (or potential) between two heavy quarks. E.g., the  $T$ -matrix approach discussed in the previous section is directly based on potentials which are extracted from the HQ free energy computed in lattice QCD. As we argued there, this approach to evaluate HQ diffusion has several attractive features, both theoretically (it may provide maximal inter-

<sup>i</sup>Note that higher dissociation rates also imply higher formation rates.

action strength in the vicinity of  $T_c$ ) and phenomenologically (it describes current HQ observables at RHIC fairly well).

In the remainder of this section we address several aspects of quarkonia in medium and in heavy-ion collisions with a focus on connections to the open heavy-flavor sector. More extensive reviews on quarkonia in medium have recently been given in Refs.<sup>8,9,10</sup>, which we do not attempt to reproduce here. In Sec. 4.1 we give a brief review of theoretical issues in the understanding of in-medium quarkonium spectral properties, in terms of thermal lattice QCD results for correlation and spectral functions and their interpretation using effective potential models (Sec. 4.1.1). The latter are employing input potentials extracted from heavy-quark free energies computed in lattice QCD, thus enabling, in principle, an internal consistency check, provided a suitable potential can be defined. While color screening is a key medium effect in the potentials (governing the binding energy of the bound states), a quantitative assessment of spectral functions requires the inclusion of finite-width effects induced by dissociation reactions and possibly elastic scattering (Sec. 4.1.2). In Sec. 4.2 we elaborate on recent developments in describing heavy-quarkonium production in heavy-ion collisions. The main focus is on transport models which track the dissociation and regeneration of charmonia (and bottomonia) through the QGP, mixed and hadronic phases (Sec. 4.2.1), complemented by a brief discussion of initial conditions as affected by cold-nuclear-matter (CNM) effects (shadowing, Cronin effect and nuclear absorption). This is followed by an assessment of the current status of charmonium phenomenology at SPS and RHIC.

#### 4.1. *Spectral Properties of Quarkonia in the QGP*

##### 4.1.1. *Lattice QCD and Potential Models*

The phenomenological Cornell potential<sup>85</sup> for the interaction between two heavy-quark (color-) charges in the color-singlet channel,

$$V_{\bar{Q}Q}(r; T = 0) = -\frac{4}{3} \frac{\alpha_s}{r} + \sigma r, \quad (89)$$

has been very successful in reproducing the vacuum spectroscopy of charmonium and bottomonium bound states. It consists of a (color-) Coulomb plus a (linear) confining part with a very limited number of parameters, i.e., a strong coupling constant,  $\alpha_s$ , and string tension,  $\sigma$  (in addition, an effective HQ mass,  $m_Q$ , needs to be specified). Subsequent developments have put this framework on a more rigorous footing by showing that (a) the potential description can be recovered as a low-energy effective theory of QCD with heavy quarks<sup>83,84</sup>, and (b) lattice QCD computations of the color-singlet heavy-quark free energy,  $F_1$ , have found excellent agreement with the functional form (and parameters) of the Cornell potential<sup>180</sup>.

Early calculations<sup>181</sup> of  $Q\bar{Q}$  bound-state properties in the QGP have supplemented the Cornell potential by a phenomenological ansatz for color screening of

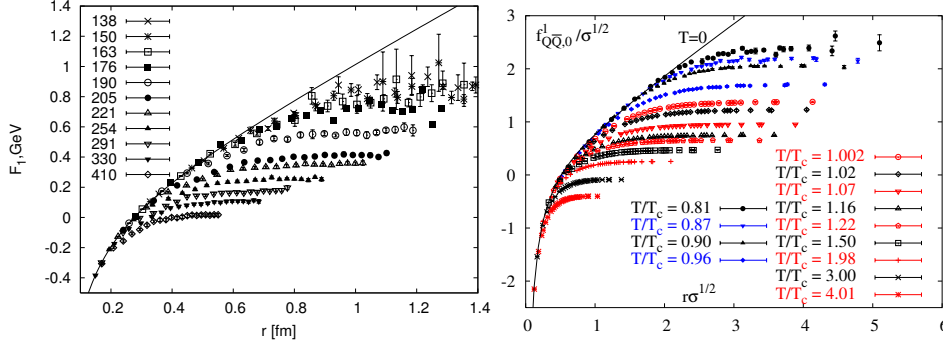


Fig. 30. (Color online) Free energy of a static color-singlet HQ pair as computed in lattice QCD for  $N_f = 3^{93}$  (left) and  $N_f=2^{182}$  flavors (right). The critical temperature is  $T_c = 193(170)$  MeV for the  $N_f = 3(2)$  calculation, and the string tension typically amounts to  $\sigma^{1/2} \simeq 420$  MeV =  $1/(0.45 \text{ fm})$ .

both the Coulomb and confining parts,

$$V_{\bar{Q}Q}(r; T) = \frac{\sigma}{\mu_D(T)} \left(1 - e^{-\mu_D(T)r}\right) - \frac{4\alpha_s}{3r} e^{-\mu_D(T)r}. \quad (90)$$

The key quantity carrying the temperature dependence is the Debye screening mass,  $\mu_D$  ( $\propto gT$  in thermal pQCD). Already at that time the possibility was established that ground-state charmonia (and even more so bottomonia) can survive until temperatures (well) above  $T_c$ . More recently, quantitative lQCD computations of the finite-temperature color-singlet free energy of a HQ pair,  $F_1(r; T)$ , have become available, see, e.g., Fig. 30. The results nicely illustrate the color-screening effect and its gradual penetration to smaller distances. When inserting the in-medium free energy as an improved estimate of the finite-temperature HQ potential into a Schrödinger equation, the “melting” temperature of the  $J/\psi$  ( $\psi'$ ,  $\chi_c$ ) was found to be just above (below)  $T_c$ <sup>183</sup>.

Further progress in thermal lQCD came with the computation of heavy quarkonium correlation functions,

$$G_\alpha(\tau, \mathbf{r}) = \langle\langle j_\alpha(\tau, \mathbf{r}) j_\alpha^\dagger(0, \mathbf{0}) \rangle\rangle \quad (91)$$

(also referred to as temporal correlators), as a function of Euclidean time,  $\tau$ .  $j_\alpha$  represent the creation/annihilation operators of a hadronic current of given quantum numbers,  $\alpha$ . In the pseudoscalar and vector charmonium channels (corresponding to  $c\bar{c}$   $S$ -waves with  $\eta_c$  and  $J/\psi$  states, respectively), the Euclidean correlators were found to exhibit a surprisingly weak temperature dependence up to  $\sim 2T_c$ , even at large  $\tau$ , suggestive for rather stable bound states. The temporal correlators are related to the physical spectral function,  $\sigma_\alpha(E, p; T)$ , via

$$G_\alpha(\tau, p; T) = \int_0^\infty dE \sigma_\alpha(E, p; T) K(E, \tau; T) \quad (92)$$

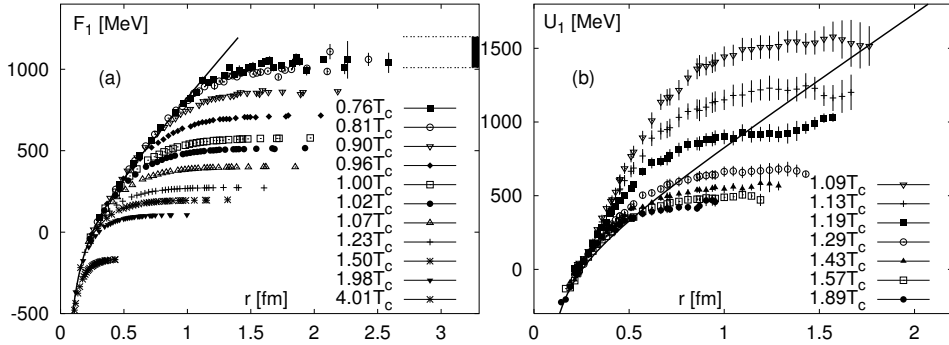


Fig. 31. HQ free energy in the color-singlet channel computed in thermal  $N_f = 2$  lattice QCD (left)<sup>180</sup> and corresponding numerically extracted internal energy (right)<sup>94</sup>.

with a thermal integral kernel

$$K(E, \tau; T) = \frac{\cosh[E(\tau - 1/2T)]}{\sinh[E/2T]} . \quad (93)$$

Eq. (92) implies that the extraction of the spectral function from the Euclidean correlator requires a nontrivial integral inversion. Especially at finite  $T$ , where periodic boundary conditions limit the information on  $G_\alpha(\tau, p; T)$  to a finite interval,  $0 \leq \tau \leq 1/T$ , and for a finite number of  $\tau$  points, the unambiguous inversion to obtain  $\sigma_\alpha(E, p; T)$  becomes an ill-defined problem. However, using probabilistic methods (in particular the so-called maximum entropy method (MEM)), a statistical reconstruction of  $\sigma_\alpha(E, p; T)$  is possible and has been applied<sup>41,42</sup>. The approximate constancy of the temporal correlators lead to spectral functions with rather stable ground-state peaks corroborating the notion of surviving ground states well above  $T_c$ .

To resolve the apparent discrepancy with the low dissociation temperature found in the potential model discussed above, it has been suggested to employ as potential the internal rather than the free energy, which are related via

$$F(r; T) = U(r; T) - TS(r; T) . \quad (94)$$

Especially in the color-singlet channel, the (positive) entropy contribution rises significantly with  $Q\bar{Q}$  separation,  $r$ , thus producing “deeper” potentials (cf. Fig. 31) entailing stronger binding. Consequently, pertinent evaluations of quarkonium spectra lead to larger dissociation temperatures, which seemingly agree better with the IQCD spectral functions. These assertions have been made more quantitative<sup>56,57,58,59,60,61,62,63</sup> by employing potential models to calculate in-medium spectral functions, perform the straightforward integral in Eq. (92) and compare to the rather precise temporal correlators from IQCD. It is important to realize that the Euclidean correlators involve the pertinent spectral function at *all* energies. In Ref.<sup>56</sup> the in-medium bound-state spectrum obtained from a Schrödinger equation (using either a screened Cornell potential or IQCD internal

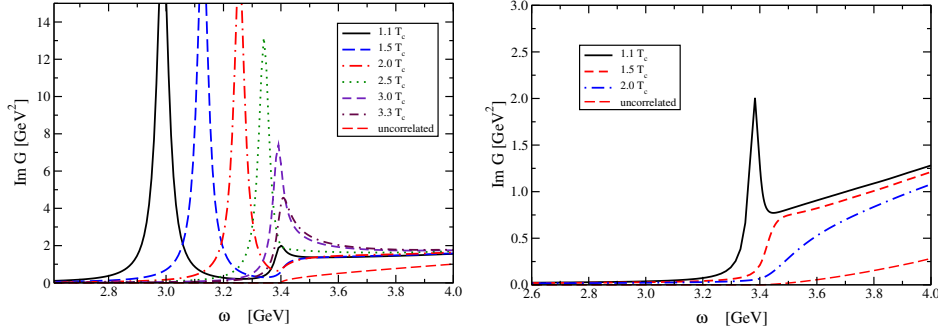


Fig. 32. (Color online) Charmonium spectral functions computed in a  $T$ -matrix approach<sup>58</sup> using internal HQ free energies extracted from  $N_f = 3$  thermal lattice QCD<sup>93</sup>. For numerical purposes, a small charm-quark width of  $\gamma_c = 20$  MeV has been implemented into the intermediate  $Q\bar{Q}$  propagator in the scattering equation (46).

energies) has been combined with a perturbative ansatz for the  $Q\text{-}\bar{Q}$  continuum above threshold. No agreement with lQCD correlators could be established. In Refs.<sup>57,58</sup> the importance of rescattering effects for the interacting  $Q\text{-}\bar{Q}$  continuum was emphasized and implemented into the calculations of the  $Q\text{-}\bar{Q}$  spectral functions. In Ref.<sup>57</sup> continuum correlations were implemented via Gamov resonance states in Breit-Wigner approximation, while in Ref.<sup>58</sup> a thermodynamic  $T$ -matrix approach was employed,

$$T_\alpha(E) = V_\alpha + \int \frac{d^3\mathbf{k}}{(2\pi)^3} V_\alpha G_{Q\bar{Q}}(E; k) T_\alpha(E) [1 - f_Q(\omega_k^Q) - f_{\bar{Q}}(\omega_k^{\bar{Q}})], \quad (95)$$

exactly as introduced in the context of HQ diffusion in Sec. 2.3.2, recall Eq. (46). The  $T$ -matrix approach enables a consistent treatment of bound and continuum states on equal footing, as well as the implementation of medium effects (selfenergies) into the intermediate two-particle propagator,  $G_{Q\bar{Q}}$ , recall Eq. (48). Pertinent results for  $S$ - and  $P$ -wave charmonium spectral functions, using the internal energy extracted from the  $N_f = 3$  free energy<sup>93</sup> (left panel of Fig. 30), are shown in Fig. 32 for a constant ( $T$ -independent) charm-quark mass of  $m_c = 1.7$  GeV. One clearly recognizes the reduction in binding energy as a result of color screening by the upward moving bound-state peak position with increasing temperature (the  $c\bar{c}$  threshold is fixed at  $2m_c = 3.4$  GeV). Also note that nonperturbative rescattering effects close to and above threshold induce a substantial enhancement in the  $Q\text{-}\bar{Q}$  spectral function over the non-interacting continuum (indicated by the red long-dashed lines), an effect which is of prime importance in the calculation of HQ diffusion in  $q\text{-}Q$  scattering as well. When applied to the calculation of Euclidean correlators<sup>58</sup> in Eq. (92), the upward shift of low-energy strength due to the moving bound states in the  $S$ -wave spectral function shown in the left panel of Fig. 32 entails a suppression of  $G(\tau)$  with temperature which disagrees with the weak temperature dependence found in lQCD.

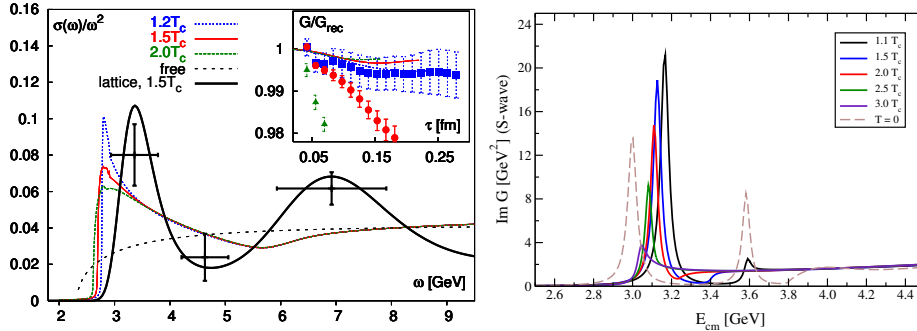


Fig. 33. (Color online)  $S$ -wave charmonium spectral functions ( $\eta_c$  or  $J/\psi$ ) computed employing: (i) a screened Cornell potential within nonrelativistic Green’s function approach (left)<sup>61,62</sup>, and (ii) an IQCD-based  $N_f = 3$  internal energy<sup>93</sup> within a  $T$ -matrix approach<sup>58</sup>. Both calculations account for in-medium charm-quark masses, and approximately reproduce the weak temperature dependence of the temporal correlators computed in IQCD up to temperatures of at least  $2T_c$  (see, e.g., inset in the left panel). However, in calculation (i) the bound-state has disappeared at temperatures below  $1.5T_c$ , while in calculation (ii) it is visible up to  $\sim 2.5T_c$ .

Another important ingredient to understand the behavior of the correlators is the temperature dependence of the HQ mass. Schematically, the, say,  $J/\psi$  bound-state mass may be written as

$$m_{J/\psi} = 2m_c^* - \epsilon_B . \quad (96)$$

This illustrates that a small (large) binding energy,  $\epsilon_B$ , can be compensated by a small (large) effective quark mass in a way that the ground-state mass stays approximately constant. Indeed, when interpreting the asymptotic value of the in-medium potential as an effective HQ mass correction,

$$m_c^* = m_c^0 + \Delta m_c \quad , \quad \Delta m_c \equiv X(r = \infty; T)/2 , \quad (97)$$

with  $X = U$  or  $F$  (or an appropriate combination thereof), the use of  $U$  implies strong binding with large effective quark masses while the use of  $F$  leads to weak binding with small  $m_c^*$  (recall from Fig. 31 that the “ $U$ -potential” is deeper than the “ $F$ -potential” but features a larger asymptotic value for  $r \rightarrow \infty$ ). Consequently, it has been found that reasonable agreement with IQCD correlators can be achieved with different spectral functions, covering a rather large range of dissociation temperatures, e.g., slightly above  $T_c$  using screened Cornell potentials similar to the free energy ( $F_1$ )<sup>61,62</sup>,  $\sim 1.5T_c$  using a linear combination of free and internal energy<sup>57,63</sup>, or up to  $\sim 2.5T_c$  when using internal energies<sup>58j</sup>, cf. Fig. 33.

<sup>j</sup>We do not address here the issue of so-called zero-mode contributions to quarkonium correlators, which arise on the lattice due to the periodic boundary conditions in temporal direction<sup>184</sup>. These contributions are essential to obtain quantitative agreement with the IQCD correlators in all mesonic quantum-number channels except the pseudoscalar one ( $\eta_c$ ); they are rather straightforward to implement in quasi-particle approximation.

To resolve this redundancy, it will be necessary to develop independent means of determining the in-medium quark mass and the appropriate quantity to be identified with the HQ potential. First estimates of the HQ mass from thermal lQCD have been obtained by approximating the HQ number susceptibility within a quasi-particle model with effective quark mass<sup>46</sup>. The results suggest a rather moderate temperature variation of the latter, which deviates significantly from the perturbative predictions up to  $T \simeq 3T_c$ . In Refs.<sup>80,81,82</sup> hard-thermal-loop and HQ effective theory techniques have been applied to derive the leading terms in a perturbative and HQ mass expansion of a finite temperature potential. An interesting finding of these investigations is that the potential develops an imaginary part in the medium which arises from the Landau damping of the exchanged gluons, representing a decay channel of the HQ bound state. A more general discussion of the in-medium decay width of heavy quarkonia, which plays a central role for phenomenology in heavy-ion collisions, is the subject of the following section.

The impact of finite-width effects on charmonium correlators has been studied within the  $T$ -matrix approach in Ref.<sup>58</sup>, by implementing an imaginary part into the charm-quark propagators. A broadening of charmonium spectral functions leads to an enhancement of the temporal correlators (due to additional strength at lower energies), which, however, is only a few percent for a charmonium width on the order of  $\Gamma_\Psi \simeq 100$  MeV. On the one hand, such a value for the width is phenomenologically significant, as it implies that about 60% of the charmonia decay within a time of 2 fm/ $c$ . On the other hand, for larger widths, their impact on the correlators should be accounted for in quantitative comparisons to lQCD “data”.

#### 4.1.2. Dissociation Widths

The spectral width of a quarkonium state propagating through matter can, in principle, receive contributions from elastic and inelastic reactions with the medium particles. Elastic scattering affects the momentum distribution of the quarkonium while inelastic interactions change its abundance (via dissociation or formation). More formally, the quarkonium acquires a complex selfenergy which can be expressed via the in-medium scattering amplitude,  $\mathcal{M}_{\Psi i}$ , folded over the (thermal) distribution,  $f_i$ , of the medium particles,

$$\Sigma_\Psi(p) = \sum_i \int \frac{d^3k}{(2\pi)^3 2\omega_i(k)} f_i(\omega_i(k); T) \mathcal{M}_{\Psi i}(p, k). \quad (98)$$

The real part of  $\Sigma_\Psi$  characterizes in-medium changes of the quarkonium mass while the imaginary part determines its width,  $\Gamma_\Psi(E) = -2 \text{Im} \Sigma_\Psi(E)$ <sup>k</sup>. Most of the attention thus far has been directed to the inelastic reactions (rather than elastic

<sup>k</sup>In addition, mass and width changes are induced at the  $Q\bar{Q}$  level via in-medium effects on the  $Q\bar{Q}$  potential and direct  $\Psi \rightarrow Q + \bar{Q}$  decays, respectively. These effects can be accounted for, e.g., in the underlying  $Q\bar{Q}$   $T$ -matrix, Eq. (95).

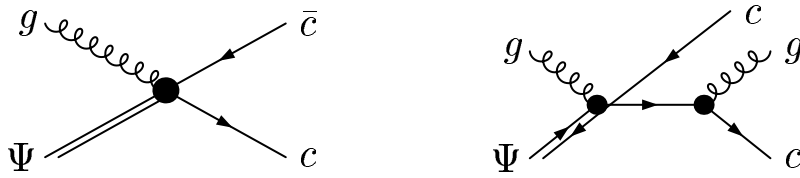


Fig. 34. Diagrams for quarkonium-dissociation reactions via parton impact; left panel: gluodissociation<sup>186,185</sup>; right panel: quasifree dissociation<sup>47</sup>.

scattering). Using the optical theorem to relate the imaginary part of the forward scattering amplitude to the cross section, one arrives at the well-known expression

$$\Gamma_{\Psi} = \sum_i \int \frac{d^3k}{(2\pi)^3} f_i(\omega_k, T) v_{\text{rel}} \sigma_{\Psi i}^{\text{diss}}(s), \quad (99)$$

where  $v_{\text{rel}}$  denotes the relative velocity of the incoming particles and  $s=(p+k)^2$  the squared center-of-mass energy of the  $\Psi$ - $i$  collision. The first evaluation of the inelastic quarkonium reaction cross section with gluons was conducted in Refs.<sup>185,186</sup>. Employing Coulomb wave functions for the quarkonium bound state, the leading-order process,  $\Psi + g \rightarrow Q + \bar{Q}$ , is the analog of photo-dissociation of hydrogen, see left panel of Fig. 34. For an  $S$ -wave  $\Psi$  bound state with binding energy  $\varepsilon_B$ , the cross section is given as a function of incoming gluon energy,  $k_0$ , by

$$\sigma_{g\Psi}(k_0) = \frac{2\pi}{3} \left(\frac{32}{3}\right)^2 \left(\frac{m_Q}{\varepsilon_B}\right)^{1/2} \frac{1}{m_Q^2} \frac{(k_0/\varepsilon_B - 1)^{3/2}}{(k_0/\varepsilon_B)^5}. \quad (100)$$

This expression has a rather pronounced maximum structure with the peak cross section reached for a gluon energy,  $k_0^{\text{max}} = \frac{7}{5}\varepsilon_B$ . The applicability of the gluodissociation formula should be reasonable for the free bottomonium ground state ( $\varepsilon_{\Upsilon} \simeq 1$  GeV), but borderline for  $J/\psi$  ( $\varepsilon_{J/\psi} \simeq 0.6$  GeV). Taken at face value for QGP temperatures of  $T = 300$ - $400$  MeV, where the typical thermal energy of (massless) gluons is around  $k_0 = 1$  GeV, the convolution of the gluodissociation cross section with a thermal gluon distribution function in Eq. (99) results in an inelastic  $J/\psi$  width (lifetime) of  $\Gamma_{J/\psi} \simeq 150$ - $400$  MeV ( $\tau_{J/\psi} \simeq 0.5$ - $1.3$  fm/ $c$ ), see the dashed line in the right panel of Fig. 35.

The situation changes if the quarkonium binding energy decreases due to color-screening as discussed in the previous section (or for excited charmonia which are weakly bound even in vacuum). In this case, the peak of the gluodissociation cross section moves to smaller energies and becomes rather narrow; the loss of phase space can be basically understood by the fact that for a loosely bound  $\Psi$  state, the absorption of an on-shell gluon on an (almost) on-shell quark is kinematically impossible (suppressed). Consequently, with decreasing binding energy, the cross section has less overlap with the thermal gluon spectrum<sup>47,187</sup>, leading to a decreasing width with temperature (cf. dotted line in the left panel of Fig. 35). This unphysical be-

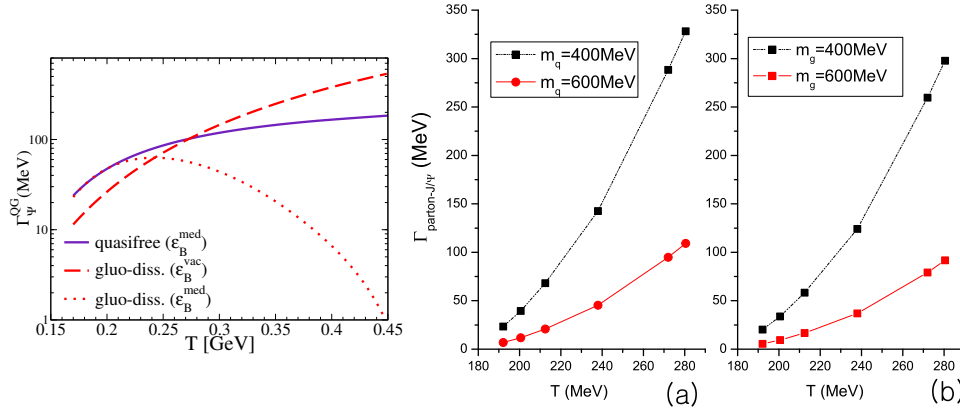


Fig. 35. (Color online) Parton-induced dissociation widths for  $J/\psi$  at rest in a QGP as a function of temperature. Left panel: gluo-dissociation width based on the cross section, Eq. (100), with free (dashed line) and in-medium decreasing binding energy (dotted line), as well as “quasifree dissociation” width ( $J/\psi + p \rightarrow c + \bar{c} + p$ ) with in-medium decreasing  $\varepsilon_B$ <sup>47,187</sup>. Right panel: full NLO calculation for (a) quark- and (b) gluon-induced dissociation for different thermal parton masses<sup>188</sup>.

havior signals the presence of other inelastic processes taking over. In Ref.<sup>47</sup> the so-called “quasifree” dissociation mechanism has been suggested,  $J/\psi + p \rightarrow c + \bar{c} + p$ , where a thermal parton ( $p = g, q, \bar{q}$ ) scatters “quasi-elastically” off an individual heavy quark in the bound state (see right panel of Fig. 34). The  $p$ - $Q$  scattering amplitude has been evaluated in leading-order (LO) perturbation theory<sup>65</sup>, including thermal parton and Debye masses and slightly modified kinematics due to the small but finite binding energy. While naively of next-to-leading order (NLO) in  $\alpha_s$  compared to gluo-dissociation, the additional outgoing parton opens a large phase space rendering the quasifree process significantly more efficient for weakly bound states. Therefore, it readily applies to excited states as well, thus enabling a treatment of all charmonia on an equal footing (which is essential even for  $J/\psi$  observables, since the latter receive significant feed-down contributions from  $\chi_c$  and  $\psi'$  states, see Sec. 4.2.1 below). For a coupling constant of  $\alpha_s \simeq 0.25$ , the quasifree dissociation rate reaches  $\Gamma_{J/\psi} = 100$ - $200$  MeV for temperatures,  $T = 300$ - $400$  MeV (cf. solid line in the left panel of Fig. 35). These values could be substantially enhanced if non-perturbative  $p$ - $Q$  scattering mechanisms are operative, much like the ones discussed in Sec. 2.3. A complete NLO calculation for parton-induced charmonium destruction has recently been carried out in Ref.<sup>188</sup>, including the effects of in-medium reduced binding energies. The right panels of Fig. 35 show the results for quark- and gluon-induced breakup of the  $J/\psi$  for  $\alpha_s = 0.5$  and different (fixed) thermal parton masses. For temperatures around 250 MeV, the sum of both contributions ( $\Gamma_{\text{parton-}J/\psi} \simeq 350$  MeV) is about a factor  $\sim 4$  larger than the quasifree results ( $\Gamma_{J/\psi} \simeq 80$  MeV) in the left panel, calculated for  $\alpha_s = 0.25$ <sup>47</sup>. Thus, there is good agreement between these two calculations, since the rate is basically  $\propto \alpha_s^2$

(for  $T = 250\text{MeV}$  the  $T$ -dependent Debye-mass in Ref.<sup>47</sup>,  $\mu_D = gT$ , amounts to  $\mu_D \simeq 440\text{ MeV}$ ).

The three-momentum dependence of the dissociation rate of a moving quarkonium,  $\Gamma_\Psi(p)$ , has been calculated for full NLO and the quasifree rates in Refs.<sup>189,190</sup>, respectively. In both calculations a weak increase of the rate with increasing three-momentum is found. Since the quasifree cross section is essentially constant, this increase is caused by the increasing flux of thermal partons encountered by the moving bound state. A similar result has been obtained in a calculation employing the AdS/CFT correspondence<sup>191</sup> (recall Sec. 2.4 for more details on this framework and its caveats). On the other hand, gluo-dissociation leads to a rather pronounced decrease of the dissociation rate with increasing three-momentum, since the pertinent cross section is peaked at relatively low energies and falls off rapidly at large center-of-mass energies,  $s = (p + k)^2$ . Of course, if gluo-dissociation becomes ineffective, its three-momentum dependence becomes immaterial. A decreasing  $p$ -dependence should also be expected in quasifree dissociation if non-perturbative (resonance-like)  $q$ - $Q$  interactions are operative (recall Sec. 2.3), since the pertinent cross sections are concentrated at small  $\sqrt{s}$  as well.

To utilize quarkonium observables as a probe of QGP formation in URHICs, it is mandatory to have good control over the modifications of quarkonia in hadronic matter, in particular their inelastic reaction rates. From current lattice QCD calculations it is very difficult to extract information on excited states (say,  $\psi'$ ). In addition, the results in the  $P$ -wave (scalar and axialvector) channels (corresponding to  $\chi_{c,0}$  and  $\chi_{c,1}$ , respectively) are sensitive to the so-called zero-mode contributions which are not directly related to the bound-state properties (as briefly mentioned in a previous footnote). Potential models find that  $\psi'$ ,  $\chi_{c,0}$  and  $\chi_{c,1}$  “melt” close to or even below  $T_c$ , suggesting substantial modifications in the hadronic phase. Even for the  $J/\psi$ , hadronic dissociation may lead to significant suppression (in addition to suppressed feed down from  $\psi'$  and  $\chi_c$  states). One main obstacle in a reliable assessment of these reactions is that low-energy reactions of the type  $h + J/\psi \rightarrow D + \bar{D} + X$  constitute a nonperturbative problem with little experimental information available to constrain effective models.

An initial estimate of quarkonium dissociation by light hadrons has been obtained by using the gluo-dissociation cross section, Eq. (100), convoluted over the gluon distribution inside hadrons<sup>192</sup>. Since the latter is rather soft ( $k_0 \simeq 0.1\text{ GeV}$ ), the gluon energy is in general not sufficient to break up the  $J/\psi$ , leading to a (low-energy) cross section of order  $\sigma_{h,J/\psi}^{\text{inel}} \simeq 0.1\text{ mb}$ . Quark-exchange reactions<sup>193</sup>, e.g., in meson-induced breakup,  $h + J/\psi \rightarrow D + \bar{D}$  (including excited  $D$  mesons in the final-state), are presumably more relevant. Effective quark models predict dissociation cross sections of order 1-2mb, see, e.g., Refs.<sup>194,195</sup>. An alternative approach is to construct effective hadronic models, pioneered in Ref.<sup>196</sup>. Guiding principles are basic symmetries including gauge invariance for vector mesons ( $J/\psi$ ,  $\rho$ ) as well as flavor symmetries, most notably SU(4) (albeit explicitly broken by

the charm-quark mass) and chiral symmetry which is operative in interactions with (pseudo-) Goldstone bosons ( $\pi$  and  $K$ )<sup>197,198,199,200,201,202</sup>. The main uncertainty in these models remains a reliable determination of the cutoff scales figuring into the hadronic vertex form factors. With cutoff values of around 1 GeV, the agreement with quark models is quite reasonable; dissociation reactions induced by  $\rho$  mesons appear to be the most important channel. Their thermal density in hadronic matter (i.e., for temperatures of  $\sim 180$  MeV) is not very large, so that the total  $J/\psi$  width does not exceed a few MeV, and therefore is substantially smaller than in the QGP. E.g., for a total hadron density of  $\varrho_h = 3\varrho_0$  and a thermally averaged cross section of  $\langle \sigma_{hJ/\psi}^{\text{diss}} \rangle = 1$  mb (corresponding to significantly larger peak cross sections), a rough estimate for the dissociation rate gives  $\Gamma_{hJ/\psi}^{\text{diss}} = \langle \sigma_{hJ/\psi}^{\text{diss}} v_{\text{rel}} \rangle \varrho_h \simeq 5$  MeV. An interesting possibility to constrain effective hadronic vertices in a rather model-independent way is to use QCD sum rules<sup>203,200</sup>. Pertinent estimates yield, e.g., a thermally averaged  $\pi J/\psi$  dissociation cross section of  $\langle \sigma_{\pi J/\psi}^{\text{diss}} v_{\text{rel}} \rangle = 0.3$  mb at  $T = 150$  MeV, in the same range as the above estimate. We finally remark that in-medium effects, e.g., modified spectral distributions of  $D$ -mesons, can increase the final-state phase space and lead to an appreciable increase of the dissociation rate<sup>204</sup>. This is especially pertinent to excited charmonia like the  $\psi'$ , whose mass is close to the free  $D\bar{D}$  threshold, so that a slight reduction (or broadening) in the  $D$ -meson mass can open the direct decay channel,  $\psi' \rightarrow D\bar{D}$ <sup>205</sup>.

## 4.2. Quarkonium Production in Heavy-Ion Collisions

Similar to the open heavy-flavor sector, a key objective (and challenge) in the quarkonium sector is to connect their equilibrium properties to observables in heavy-ion collisions, and eventually deduce more general insights about basic properties of QCD matter, e.g., color de-/confinement and Debye screening. Since quarkonium states in heavy-ion collisions are even more rare than individual heavy quarks, it is suitable to adopt a transport treatment for their distribution functions in a realistic “background medium” whose evolution is not affected by the heavy quarks or quarkonia. The connection between observables extracted from the distribution function (after its “transport” through the medium) and the equilibrium properties discussed in the previous section is given by the coefficients and equilibrium limit of the transport equation, as elaborated in the following section, 4.2.1. The current status in comparing various model implementations to charmonium data at SPS and RHIC will be assessed in Sec. 4.2.2.

### 4.2.1. Quarkonium Transport in Heavy-Ion Collisions

The (classical) Boltzmann equation describing the time-evolution of the phase-space distribution function,  $f_{\Psi}(\mathbf{r}, \tau; \mathbf{p})$ , of an (on-shell) quarkonium state,  $\Psi$  (with energy  $p_0 = \omega_p = (\mathbf{p}^2 + m_{\Psi}^2)^{1/2}$ ), may be written as

$$p^{\mu} \partial_{\mu} f_{\Psi}(\mathbf{r}, \tau; \mathbf{p}) = -\omega_p \Gamma_{\Psi}(\mathbf{r}, \tau; \mathbf{p}) f_{\Psi}(\mathbf{r}, \tau; \mathbf{p}) + \omega_p \beta_{\Psi}(\mathbf{r}, \tau; \mathbf{p}) \quad (101)$$

(a mean-field term has been neglected assuming that the real part of the  $\Psi$  self-energy is small). When focusing on inelastic reactions,  $\Gamma_\Psi(\mathbf{r}, \tau; \mathbf{p})$  represents the dissociation rate discussed in Sec. 4.1.2 above, which governs the loss term, i.e., the first term on the right-hand-side (*rhs*) of Eq. (101). The  $(\mathbf{r}, \tau)$  dependence of  $\Gamma_\Psi$  typically converts into a temperature dependence via the fireball evolution of a heavy-ion reaction for given projectile/target ( $A/B$ ), collision energy ( $\sqrt{s}$ ) and impact parameter ( $b$ ). The second term on the *rhs* of Eq. (101) is the gain term accounting for the formation of quarkonia. For a  $2 \rightarrow 2$  process (as, e.g., realized via the inverse of gluo-dissociation,  $Q + \bar{Q} \rightarrow g + \Psi$ ), it takes the form<sup>206</sup>

$$\begin{aligned} \beta_\Psi(\mathbf{p}; \mathbf{r}, \tau) &= \frac{1}{2p_0} \int \frac{d^3k}{(2\pi)^3 2\omega_k} \frac{d^3p_Q}{(2\pi)^3 2\omega_{p_Q}} \frac{d^3p_{\bar{Q}}}{(2\pi)^3 2\omega_{p_{\bar{Q}}}} f^Q(\mathbf{p}_Q; \mathbf{r}, \tau) f^{\bar{Q}}(\mathbf{p}_{\bar{Q}}; \mathbf{r}, \tau) \\ &\quad \times W_{Q\bar{Q}}^{g\Psi}(s) \Theta[T_{\text{diss}} - T(\mathbf{r}, \tau)] (2\pi)^4 \delta^{(4)}(p + k - p_Q - p_{\bar{Q}}). \end{aligned} \quad (102)$$

To ensure detailed balance, the cross section figuring into the formation probability,  $W_{Q\bar{Q}}^{g\Psi}(s) = \sigma_{Q\bar{Q} \rightarrow g\Psi}^{\text{form}} v_{\text{rel}} 4\omega_{p_Q} \omega_{p_{\bar{Q}}}$ , has to be the same (up to a kinematic and statistical factor) as the one used in the dissociation rate, Eq. (99). For reactions beyond  $2 \leftrightarrow 2$  (such as the quasifree process,  $p + Q + \bar{Q} \rightarrow p + \Psi$ ), the microscopic evaluation of the gain term becomes more involved. Note the explicit dependence on the HQ phase-space distribution functions,  $f^{Q, \bar{Q}}$ , in Eq. (102), whose modifications in heavy-ion reactions are the central theme in Sec. 3 of this review. The temperature-dependent step function in Eq. (102) signifies the limit set by the dissociation temperature,  $T_{\text{diss}}$ , above which a well-defined  $\Psi$  state no longer exists and thus formation reactions are not meaningful.

It is both instructive and useful for practical applications to simplify the gain term by integrating out its spatial and three-momentum dependence. This is possible under the assumption of a homogeneous medium and thermally equilibrated HQ distribution functions; one obtains<sup>207</sup>

$$\frac{dN_\Psi}{d\tau} = -\Gamma_\Psi(N_\Psi - N_\Psi^{\text{eq}}), \quad (103)$$

which now clearly exhibits detailed balance in terms of the approach to the equilibrium limit,  $N_\Psi^{\text{eq}}$ , of the state  $\Psi$ . The latter quantity is given by

$$N_\Psi^{\text{eq}} = V_{\text{FB}} n_\Psi^{\text{eq}}(m_\Psi; T, \gamma_Q) = d_\Psi \gamma_Q^2 \int \frac{d^3p}{(2\pi)^3} f_\Psi(\omega_p; T), \quad (104)$$

carrying the explicit dependence on the (in-medium) quarkonium mass,  $m_\Psi$  (which, in turn, depends on a combination of  $Q$ - $\bar{Q}$  binding energy and in-medium HQ mass, cf. Eq. (96));  $d_\Psi$  denotes the spin degeneracy of the  $\Psi$  state and  $V_{\text{FB}}$  the (time-dependent) fireball volume. The appearance of a HQ fugacity,  $\gamma_Q = \gamma_{\bar{Q}}$ , owes its origin to the (theoretically and experimentally supported) postulate that  $Q\bar{Q}$  production is restricted to hard  $N$ - $N$  collisions upon initial nuclear impact. The number  $N_{Q\bar{Q}} = N_Q = N_{\bar{Q}}$  of heavy anti-/quarks is then conserved in the subsequent fireball evolution (separately for charm and bottom), which is achieved by introducing  $\gamma_Q$

at given fireball volume and temperature into the thermal densities of open and hidden HQ states, i.e.,

$$N_{Q\bar{Q}} = \frac{1}{2} N_{\text{op}} \frac{I_1(N_{\text{op}})}{I_0(N_{\text{op}})} + V_{\text{FB}} \gamma_Q^2 \sum_{\Psi} n_{\Psi}^{\text{eq}}(T), \quad (105)$$

for either charm ( $Q=c$ ) or bottom ( $Q=b$ ). The thermal open-charm (and -bottom) number,  $N_{\text{op}}$ , depends on whether one is evaluating it in terms of individual quark states,  $N_{\text{op}} = V_{\text{FB}} \gamma_Q 2n_Q^{\text{eq}}(m_Q^*, T)$  (appropriate for a (weakly interacting) QGP), or in terms of hadronic states,  $N_{\text{op}} = V_{\text{FB}} \gamma_Q \sum_{\alpha} n_{\alpha}^{\text{eq}}(T, \mu_B)$ . This is, in principle, a nontrivial issue, since both hadronic and partonic evaluations of  $N_{\text{op}}$  can be subject to corrections, see, e.g., Refs.<sup>207,53,208</sup>. In the hadronic phase one expects the spectral functions of  $D$ -mesons,  $\Lambda_c$  baryons, etc. to undergo significant medium effects, e.g., reduced masses and/or increased widths. In the partonic phase, especially close to  $T_c$ , it is not inconceivable that hadronic bound states are still present and thus an approximation with weakly interacting quasi-quarks may not be an accurate one. Even within a quasi-quark description, significant uncertainty is associated with the value of the HQ mass adopted in the calculation of  $N_{\text{op}}$  and thus in the quantitative determination of  $\gamma_Q$ . The general trend is that for a given temperature, volume and  $N_{Q\bar{Q}}$ , a smaller value for  $m_Q^*$  results in a larger value for  $n_Q^{\text{eq}}$  and thus in a smaller value for  $\gamma_Q$ , which, in turn, reduces  $N_{\Psi}^{\text{eq}}$  quadratically. The underlying physics is that of relative chemical equilibrium: for a given number of heavy anti-/quarks, the latter preferentially occupy the states of the lowest energy. In the simplest case, where a quasi-quark description applies and the  $\Psi$  mass is given by the expression (96), the  $\Psi$  number is essentially determined by its binding energy (larger  $\varepsilon_B$  implying larger  $N_{\Psi}^{\text{eq}}$ ). The gain term as written in Eq. (102) is, strictly speaking, only applicable in the quasi-quark approximation. If additional resonances are present in the medium (e.g.,  $D$ -meson resonances or  $cq$  diquark states), additional reaction channels would have to be included in a coupled rate-equation framework to account for the competition of these resonances to harbor  $c$  quarks. In the simplified treatment given by Eq. (103), this competition is included via the  $c$ -quark fugacity figuring into  $N_{\Psi}^{\text{eq}}$ .

A slightly different view on regeneration and suppression processes in the QGP is advocated in Ref.<sup>209</sup>, based on the strongly coupled nature of the QGP (sQGP) as produced at SPS and RHIC (i.e., at not too high temperatures). It is argued that a small charm-quark diffusion constant (cf. Secs. 2 and 3) inhibits the separation of the produced  $c$  and  $\bar{c}$  pair in the sQGP. In connection with the survival of  $J/\psi$  bound states well above  $T_c$  (as, e.g., in the right panel of Fig. 33), this enhances the probability for a produced  $c\bar{c}$  pair to bind into a charmonium state (relative to  $p$ - $p$  collisions). In particular, this approach accounts for the possibility that the pairwise produced  $c$  and  $\bar{c}$  quarks do not explore the entire fireball volume as usually assumed in equilibrium models. Such an effect has also been implemented in a more simplified manner in the thermal-rate equation approach of Refs.<sup>207,190</sup> in terms of a time dependent correlation volume.

Let us briefly discuss the initial conditions for the quarkonium distribution functions. Starting point are measured quarkonium spectra in  $p$ - $p$  collisions. In a heavy-ion collision, these are subject to modifications before the medium can be approximated with a thermal evolution. “Pre-equilibrium” effects may be distinguished according to whether they occur before or after the hard  $Q\bar{Q}$ -production process takes place. The former include nuclear modifications of the parton distribution functions generically denoted as “shadowing”, as well as  $p_t$  broadening (Cronin effect) attributed to a scattering of the projectile/target partons on their way through the target/projectile nucleus prior to the fusion reaction into  $Q\bar{Q}$ . In a random-walk picture, the accumulated transverse momentum is approximated by  $\Delta p_t^2 = a_{gN}\langle l \rangle$ , where  $\langle l \rangle$  is an average nuclear path length of both gluons before the hard scattering, and  $a_{gN}$  parameterizes the transverse-momentum kick per path length in gluon-nucleon scattering. Both “pre-fusion” effects are in principle universal, i.e., not directly linked to the  $Q\bar{Q}$ -production process. In  $p$ - $p$  collisions, a fraction of 1-2% of  $c\bar{c}$  pairs ( $\sim 0.1\%$  of  $b\bar{b}$  pairs) develop a correlation that leads to the formation of a charmonium (bottomonium) state<sup>210</sup>. In nuclear collisions inelastic collisions of the produced  $Q\bar{Q}$  pair with passing-by nucleons can destroy this correlation. This so-called nuclear absorption may be parameterized by an effective absorption-cross section,  $\sigma_{\text{abs}}^{\Psi N}$ .<sup>1</sup> As is well-known, the finite (and different) formation times of quarkonia imply that the  $Q\bar{Q}$  pair interacting with a nucleon does, in general, not represent a fully formed quarkonium, but rather a pre-resonance state. A microscopic description of nuclear absorption is therefore a rather challenging task<sup>211,212</sup>. At a minimal level, finite formation times imply that the values for effective nuclear absorption cross sections should be expected to depend on collision energy ( $\sqrt{s}$ ), rapidity ( $y$ ) and bound-state quantum numbers (since different binding energies imply different formation times). A careful measurement and systematic interpretation of quarkonium suppression in  $p$ - $A$  collisions, where the formation of a thermal medium is not expected (at least at SPS and RHIC), is therefore an inevitable prerequisite for quantitative interpretations of heavy-ion data, see, e.g., Refs.<sup>213,214,215</sup> for recent work. Pre-equilibrium effects not only modify the momentum dependence of the quarkonium distribution functions but also their spatial dependence.

#### 4.2.2. *Quarkonium Phenomenology in Heavy-Ion Collisions*

As discussed in the Introduction, there is ample evidence for both chemical and thermal equilibration in the low- $p_t$  regime of (bulk) particle production in ultrarelativistic heavy-ion collisions. A well defined set of thermodynamic variables characterizing the temperature evolution and flow fields of the fireball greatly facilitates

<sup>1</sup>Nuclear absorption typically occurs at a rather large  $\Psi$ - $N$  center-of-mass energy (comparable to the  $\sqrt{s}$  of primordial  $N$ - $N$  collisions) and is therefore in a very different energy regime than the low-energy hadronic absorption cross section relevant for the later hadron-gas stage of the fireball evolution.

the comparison of independent calculations for quarkonium production and maintains direct contact to their in-medium properties in equilibrated QCD matter. In this section we therefore focus on rate-equation approaches implemented into thermal background media.

We recall that the experimental quarkonium yields usually include feed down contributions due to decays of higher resonances. E.g., for  $J/\psi$  production in  $p$ - $p$  collisions about 30% (10%) of the observed number arises from decays of  $\chi_c$  ( $\psi'$ ) states<sup>216,217</sup>. The standard assumption in heavy-ion collisions is that primordial production fractions of excited states scale as in  $p$ - $p$  collisions, but subsequent suppression (and/or regeneration) will change these ratios (due to different inelastic cross sections at all stages). This needs to be taken into account for realistic comparisons to heavy-ion data (unless otherwise stated, it is included in the theoretical models discussed below). After thermal freezeout, the decay branchings are assumed to be as in vacuum (since the  $J/\psi$  lifetime after freezeout (ca. 2000 fm/ $c$ ) is about a factor of  $\sim 200$  larger than the fireball lifetime, in-medium dilepton decays contribute a small fraction to the spectrum observed in the detectors).

Let us start by analyzing  $J/\psi$  production in Pb-Pb ( $\sqrt{s} = 17.3$  AGeV) collisions at SPS in the context of NA50 data<sup>218,219,220,48</sup>, cf. Fig. 36. The left panels display the outcome of thermal-rate equation calculations<sup>207,190</sup>, where quasifree dissociation rates in the QGP (cf. left panel of Fig. 35) and hadronic SU(4) cross sections for meson-induced dissociation in the HG are evolved over an expanding fireball model (adjusted to empirical information on hadron production and flow velocities). The prevalent effect is identified as suppression in the QGP, controlled by an effective strong coupling constant,  $\alpha_s \simeq 0.25$ , in the quasifree rate. This value is adjusted to reproduce the suppression level in central collisions (where the average initial temperature amounts to about  $T_0 \simeq 210$  MeV). Regeneration is a rather small effect, based on a  $p$ - $p$  open-charm cross section of  $\sigma_{\bar{c}c} = 5.5 \mu\text{b}$  distributed over two fireballs (the covered rapidity window amounts to  $\Delta y = 3.6$ , resulting in a rapidity density of  $d\sigma_{\bar{c}c}/dy \simeq 1.53 \mu\text{b}$ ). A recent compilation<sup>222</sup> of charm production at fixed-target energies finds a total cross section of  $\sigma_{\bar{c}c} \simeq 3.6$ - $5.2 \mu\text{b}$ ; with an experimental rapidity width of around  $\Delta y = 2$ <sup>223</sup>, the resulting rapidity density is approximately  $d\sigma_{\bar{c}c}/dy = (2.2 \pm 0.5) \mu\text{b}$ ). In addition, a correction for incomplete charm-quark thermalization has been implemented<sup>207</sup> via a kinetic relaxation time ( $\tau_c^{\text{eq}}$ ) reducing the equilibrium  $J/\psi$  number. The lower left panel of Fig. 36 suggests that the centrality dependence of the average  $J/\psi$ 's transverse-momentum squared,  $\langle p_t^2 \rangle$ , is largely governed by the Cronin effect as extracted from experimental  $p$ - $A$  data<sup>219</sup>. The quasifree charmonium dissociation rates, which increase with three-momentum<sup>190</sup>, lead to a slight suppression of  $\langle p_t^2 \rangle$  for central collisions.

The right panels in Fig. 36 are calculated within the statistical hadronization model<sup>221</sup>, assuming that all primordial charmonia are suppressed and production entirely occurs at the critical temperature for hadronization based on relative chemical equilibrium of open- and hidden-charm hadrons (with  $N_{\bar{c}c}$  fixed as in Eq. (105)). This also implies that the charm-quark momentum distributions are

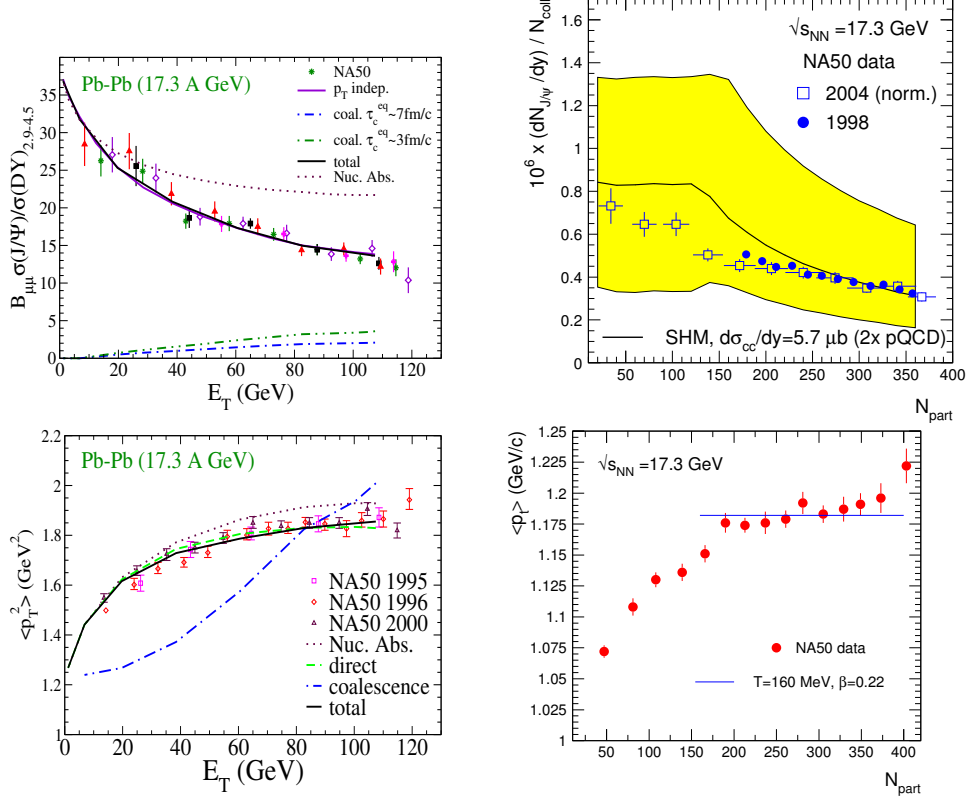


Fig. 36. (Color online)  $J/\psi$  production at SPS in the thermal rate-equation approach<sup>207,190</sup> (left panels) and the statistical hadronization model<sup>221</sup> (right panels). Upper panels display the centrality dependence of the inclusive  $J/\psi$  yield (normalized to Drell-Yan production or the number of binary  $N-N$  collisions), lower panels the average squared  $J/\psi$  transverse momentum.

kinetically equilibrated. With a rapidity density for the  $p-p$  charm cross section of  $d\sigma_{c\bar{c}}/dy = 5.7 \mu\text{b}$  the NA50 data can be reproduced reasonably well. This input  $c\bar{c}$  number is larger by a factor of  $\sim 4$  compared to the input in the left panels, which accounts for most of the difference to the regeneration yield in the rate-equation calculation for central collisions (remaining discrepancies are largely due to the  $c$ -quark relaxation correction which becomes more pronounced toward more peripheral collisions)<sup>m</sup>. The interpretation of the  $J/\psi$ 's average  $p_t$  is also rather different, in that it entirely stems from a thermal source (with moderate collective flow) in the vicinity of  $T_c$  (the resulting  $\langle p_t^2 \rangle$  is quite consistent with the regeneration component in the lower left panel of Fig. 36).

NA50 has also measured  $\psi'$  production<sup>224,225,227</sup>. Using  $p-A$  collisions, the ex-

<sup>m</sup>The charm ensemble at SPS is in the canonical limit,  $N_{\text{op}} \ll 1$ , for which  $I_1(N_{\text{op}})/I_0(N_{\text{op}}) \simeq 0.5N_{\text{op}}$  in Eq. (105), and thus  $N_{\psi} \propto N_{c\bar{c}}$ .

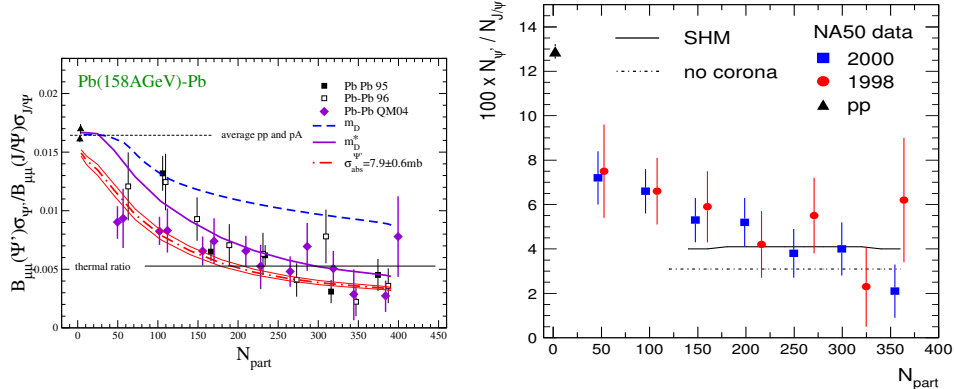


Fig. 37. (Color online) NA50 data for the  $\psi'/(J/\psi)$  ratio in Pb-Pb( $\sqrt{s} = 17.3$  AGeV) collisions<sup>224,225</sup> compared to calculations within the thermal rate-equation approach<sup>207,226</sup> (left panel) and the statistical hadronization model<sup>221</sup> (right panel). In the left panel, the dashed (solid) curve is obtained without (with) the inclusion of hadronic medium effects (modeled by reduced  $D$ -meson masses); both calculations utilize a  $\psi'$  nuclear absorption-cross section of  $\sigma_{\text{nuc}}^{\psi'} = \sigma_{\text{nuc}}^{J/\psi} = 4.4$  mb, while in the third calculation (dash-dotted line) the value has been updated to 7.9 mb (with the associated band indicating a  $\pm 0.6$  mb uncertainty). In the right panel, the statistical model yield involves either the full hadronization volume (dash-dotted line) or excludes a dilute nuclear surface (“corona”), where neither suppression nor regeneration is operative.

tracted nuclear absorption cross section has been updated<sup>227</sup> to  $\sigma_{\text{nuc}}^{\psi'} = (7.7 \pm 0.9)$  mb, which is significantly larger than for  $J/\psi$ ,  $\sigma_{\text{nuc}}^{J/\psi} = (4.2 \pm 0.5)$  mb. In Pb-Pb collisions ( $\sqrt{s} = 17.3$  AGeV), the ratio  $\psi'/(J/\psi)$  is suppressed substantially already in rather peripheral collisions, cf. Fig. 37<sup>224,225</sup>. Within the thermal rate-equation approach<sup>207</sup>, this behavior cannot be explained by inelastic reactions in the QGP alone, since very little (if any) QGP is formed in peripheral Pb-Pb collisions at SPS. However, hadronic dissociation of the  $\psi'$  can account for the suppression pattern, but only if in-medium effects are included (cf. left panel of Fig. 37)<sup>207,226</sup>, specifically a reduction of the  $D\bar{D}$  threshold which accelerates  $\psi'$  suppression due to the opening of the direct decay mode,  $\psi' \rightarrow D\bar{D}$  (a similar effect can result from a broadening of the  $D$ -meson spectral functions as discussed in Sec. 2.7). The updated (larger)  $\psi'$  nuclear absorption cross section<sup>227</sup> also plays a significant role in the quantitative description of the low-centrality data. The statistical hadronization model predicts a flat  $\psi'/(J/\psi)$  ratio, basically given by the ratio of thermal densities at the hadronization temperature. The shape and magnitude of the calculated ratio is rather consistent with the NA50 data for central and semicentral collisions where hadronization from a QGP can be expected to be applicable; deviations occur for more peripheral centralities. Thus, the  $\psi'/(J/\psi)$  ratio does not provide a clear discrimination of regeneration- and suppression-dominated scenarios at SPS.

One of the controversies in the interpretation of the NA50 data has been whether they feature any “sharp” drop in their centrality dependence, e.g., around  $E_T \simeq 35$  GeV (or  $N_{\text{part}} \simeq 120$ ) in the upper left (right) panel of Fig. 36. Such a

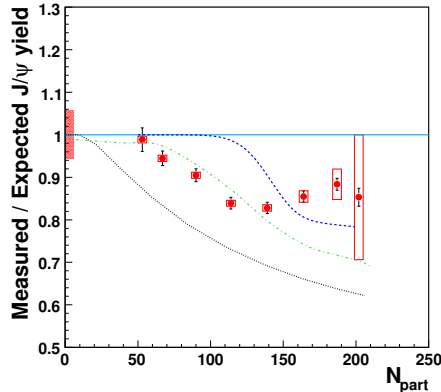


Fig. 38. (Color online) NA60 data for the centrality dependence of  $J/\psi$  production in In-In ( $\sqrt{s} = 17.3$  AGeV) collisions<sup>228</sup>, compared to theoretical predictions based on (from top to bottom): (a) the threshold-melting scenario<sup>229</sup> (dashed line), (b) the thermal rate-equation approach<sup>187</sup> (dash-dotted line) and (c) the comover suppression approach<sup>230</sup> (dotted line). Nuclear absorption effects have been divided out of the data and calculations based on measured suppression in  $p$ -A collisions.

drop has been associated with a threshold behavior for QGP formation resulting in an abrupt “melting” of the  $\chi_c$  states due to color screening<sup>229</sup> (recall that  $\chi_c$  feed down presumably makes up  $\sim 30\%$  of the inclusive  $J/\psi$  yield). The investigation of this question was one of the main objectives of the successor experiment of NA50, NA60, where  $J/\psi$  production in a medium size nuclear system (In-In) has been measured<sup>228</sup>. Fig. 38 compares the NA60  $J/\psi$  data as a function of centrality to three theoretical predictions<sup>229,187,230</sup>, all of which reproduce the NA50 data reasonably well. The predictions of the thermal rate-equation approach<sup>207,187</sup> roughly reproduce the onset and magnitude of the suppression (except for the most central data points); the threshold-melting scenario<sup>229</sup> misplaces the onset of the suppression (which in the data is below  $N_{\text{part}} = 100$ , contrary to the Pb-Pb system) and the comover calculation<sup>230</sup> overpredicts the suppression. The leveling-off (or even increasing trend) of the data for  $N_{\text{part}} \geq 150$  is somewhat unexpected and deserves further study.

The thermal rate-equation framework has been used to predict  $J/\psi$  production at RHIC<sup>207n</sup>. With updates<sup>190</sup> for the experimental input (a smaller nuclear absorption cross section<sup>232</sup> and a larger  $J/\psi$  number in  $p$ - $p$  collisions<sup>49</sup> which figures into the denominator of the nuclear modification factor and leads to a relative reduction of the regeneration yield), an approximate agreement with current PHENIX data on the centrality dependence of inclusive  $J/\psi$  production and  $p_t$  spectra emerges,

<sup>n</sup>The underlying fireball model is the same as used in the open heavy-flavor sector in connection with Figs. 19, 21, etc., with average initial temperatures of  $T_0 \simeq 340$ -370 MeV for semi-/central Au-Au collisions.

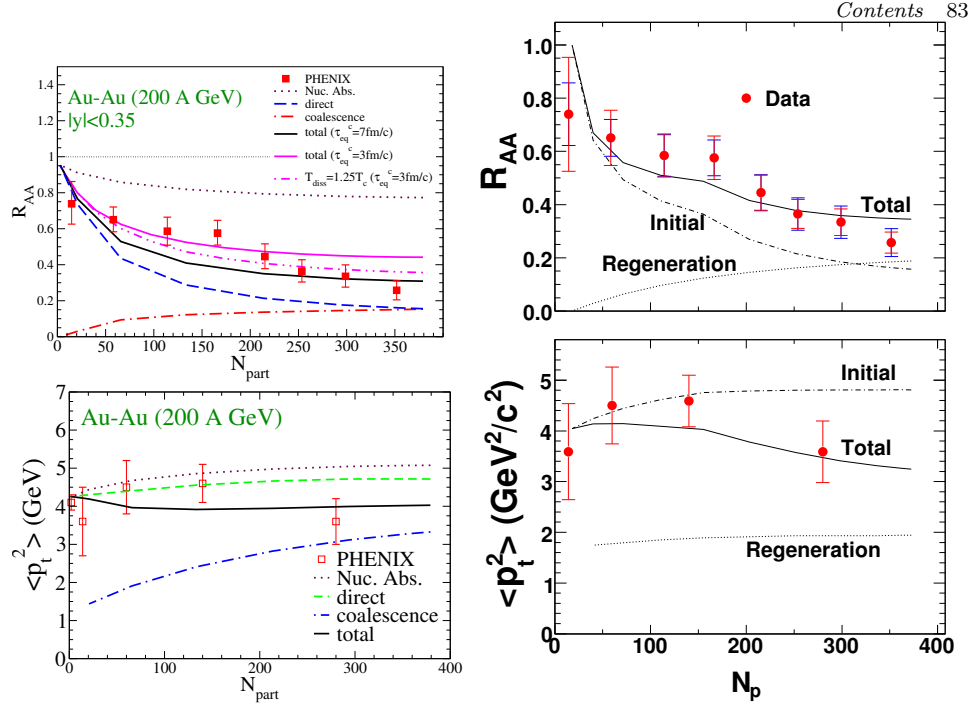


Fig. 39. (Color online)  $J/\psi$  production in 200 AGeV Au-Au collisions at RHIC in the transport approach of Ref.<sup>190</sup> (left panels, using an expanding thermal fireball with reaction rates based on the quasifree dissociation process) and Ref.<sup>231</sup> (right panels, using a hydrodynamic evolution with reaction rates based on the gluo-dissociation process). The upper (lower) panels display the inclusive  $J/\psi$   $R_{AA}$  (average  $p_t^2$ ) as a function of nucleon-participant number. The data are from the PHENIX collaboration<sup>49</sup>.

see left panels of Fig. 39 (the underlying charm cross section in  $p$ - $p$ ,  $\sigma_{c\bar{c}} = 570 \mu\text{b}$ , translates into  $d\sigma_{c\bar{c}}/dy \simeq 100 \mu\text{b}$ , consistent with PHENIX measurements<sup>233,234</sup>). The main features of this interpretation are an about equal share of (suppressed) primordial and regenerated  $J/\psi$ 's in central Au-Au collisions (where the average initial temperature is about  $T_0 = 370 \text{ MeV}$ ), as well as a significant reduction of the average  $p_t^2$  due to secondary production, as compared to primordial production with an estimated Cronin effect (the latter is not yet accurately determined from  $p$ - $A$  data). Consequently, the regeneration component is concentrated in the low- $p_t$  regime of the spectra. The dependence on the kinetic relaxation time for  $c$  quarks is rather moderate while the inclusion of the momentum dependence in the quasifree dissociation rate<sup>190</sup> has little effect.

The right panels of Fig. 39 show the results of the rate-equation approach of Refs.<sup>206,231</sup>, where gluo-dissociation rates in the QGP are convoluted over a 2+1-dimensional hydrodynamic evolution (employing a charm cross section of  $d\sigma_{c\bar{c}}/dy = 120 \mu\text{b}$ , in line with PHENIX data<sup>233</sup>); reactions in the hadronic phase are neglected. It is very encouraging that the results are in good agreement with the ones in the left panels<sup>190</sup> which are obtained with similar physics input but

in a different realization (e.g., fireball vs. hydro but with comparable initial temperatures ( $T_0 \simeq 350$  MeV in central collisions) and charm cross section, etc.). The centrality dependence of the inclusive  $J/\psi$  yield shows a slight step-structure in the upper right panel<sup>231</sup>, induced by different dissociation temperatures for  $J/\psi$  ( $T_{\text{diss}} = 320$  MeV) and  $\chi_c, \psi'$  ( $T_{\text{diss}} = T_c = 165$  MeV) above which the suppression is assumed to be practically instantaneous (similar findings have been reported in Ref.<sup>235</sup>). The  $\langle p_t^2 \rangle$  of the regenerated component is somewhat smaller in Ref.<sup>231</sup> compared to Ref.<sup>190</sup>, since in the former it is computed via continuous regeneration based on Eq. (102), while in the latter the  $p_t$  spectra of the regenerated component are approximated with a thermal blast wave.

Recent experimental data on  $J/\psi$  production in Cu-Cu collisions indicate that the nuclear modification factor tends to increase at high  $p_t > 5$  GeV<sup>236,237</sup>. Such a trend is not present in QGP suppression calculations based on the quasifree dissociation rate which increases with the three-momentum of the  $J/\psi$ <sup>190</sup>. However, the inclusion of charmonium-formation time effects<sup>238,239,240</sup> (which reduce the dissociation rate due to time dilation in the development of the hadronic wave packet) and the contributions from bottom feed-down<sup>241</sup> can lead to an increase of  $R_{AA}^{J/\psi}$  at high  $p_t$ <sup>242</sup>.

An initially promising signature to discriminate suppression and  $c\bar{c}$  coalescence mechanisms is the elliptic flow of charmonia (which also provides a close connection to, and thus consistency check with, the collective flow of open charm). If only suppression mechanisms are operative, the azimuthal asymmetry of the charmonium momentum distributions entirely develops from the path length differences caused by the long vs. the short axis of the almond shaped nuclear overlap zone. As for open-charm (recall middle panel of Fig. 24), this effect is rather small, generating a maximal  $v_2(p_t)$  of up to 2-3%<sup>243</sup>. On the other hand, for  $c\bar{c}$  coalescence, the charmonium bound state inherits up to twice the  $c$ -quark  $v_2$ <sup>155,157</sup> at the time of formation, especially if the  $c\bar{c}$  binding energy is small (in that case little  $v_2$  is carried away by an outgoing light parton). This effect is further maximized if the coalescence occurs late in the evolution, e.g., at the hadronization transition (where most of the elliptic flow is believed to have built up). However, according to the above discussion, the charmonium regeneration yield is mostly concentrated at rather low  $p_t < 3$  GeV, where the magnitude of the  $c$ -quark  $v_2(p_t/2)$  is not very large (this is a consequence of the mass ordering of  $v_2$ , whose rise in  $p_t$  is shifted to larger values for heavier particles), recall, e.g., the right panel of Fig. 19. Consequently, within the transport models displayed in Fig. 39, the net  $v_2(p_t)$  of regenerated and primordial  $J/\psi$ 's combined does not exceed 2-3%<sup>206,242,244</sup> and would therefore be difficult to discriminate from primordial production only. An interesting question, which thus far has received little attention, concerns elastic interactions of charmonia in the medium and whether they could contribute to their  $v_2$  in heavy-ion collisions. Elastic interactions should become more relevant as the binding energy of the charmonium increases, rendering them more compact objects which are less

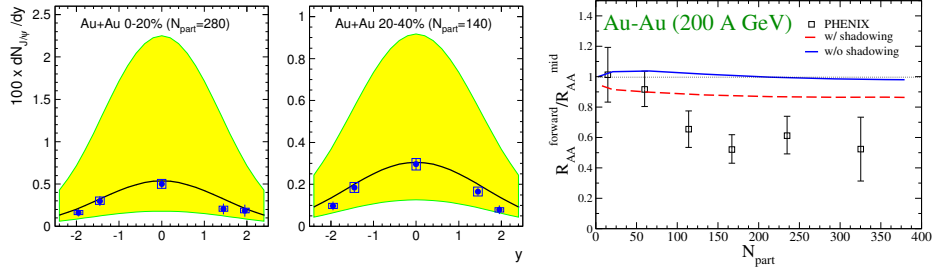


Fig. 40. (Color online) Rapidity dependence of  $J/\psi$  production in Au-Au ( $\sqrt{s} = 200$  AGeV) collisions at RHIC. Left and middle panel: results of the statistical hadronization model<sup>221</sup> for the  $J/\psi$  rapidity density in central (left) and semicentral (middle) collisions, compared to PHENIX data<sup>49</sup>. The central lines (shaded error bands) correspond to (the uncertainty in) pQCD charm cross sections,  $\sigma_{pp}^{c\bar{c}} = 256_{-146}^{+400} \mu\text{b}^{145}$ . Right panel: the ratio of  $R_{AA}(N_{\text{part}})$  for forward to mid-rapidity  $J/\psi$  yields in the thermal rate-equation approach<sup>246</sup>, compared to PHENIX data<sup>49</sup>.

likely to break up. Interestingly, the NA60 collaboration has reported a rather large inclusive ( $p_t > 0.5$  GeV) elliptic flow of  $v_2 = (6.8 \pm 4)\%$  for  $J/\psi$ 's in semicentral In-In ( $\sqrt{s} = 17.3$  AGeV) collisions at the SPS<sup>245</sup>. This observation will be difficult to explain based on dissociation reactions alone.

Next, we address the rapidity dependence of  $J/\psi$  production at RHIC, where PHENIX measurements in the dielectron channel at central rapidity,  $|y| < 0.35$ , and in the dimuon channel, at  $|y| = 1.2-2.2$ , indicate a maximum in  $R_{AA}(y)$  around  $y = 0$  for central and semicentral collisions. This trend can be nicely reproduced by the statistical hadronization model as a consequence of the underlying  $c$ -quark distributions (cf. left and middle panel in Fig. 40) which are expected to be narrower than for bulk particle production, implying higher  $c$ -quark densities and thus larger charmonium yields at central rapidity. This dependence is more difficult to explain in the thermal rate-equation approaches<sup>246</sup> where only about 50% (or less) of the  $J/\psi$ 's originate from  $c\bar{c}$  regeneration. In addition, the charm ensemble at RHIC is not yet fully in the grand canonical limit<sup>o</sup> for which  $I_1/I_0 \rightarrow 1$  in Eq. (105), and thus the sensitivity on the  $c$ -quark density (fugacity) is less pronounced. Furthermore, the thermal suppression of the primordial component exhibits an opposite trend, being slightly less suppressed at forward  $y$  due to reduced light-particle production. It is quite conceivable that cold-nuclear-matter effects imprint significant rapidity dependencies on the primordial component (e.g., stronger shadowing and/or nuclear absorption at forward  $|y|$ )<sup>214,213</sup>. In Ref.<sup>213</sup>, e.g., stronger nuclear absorption of  $J/\psi$ 's at RHIC has been found as a consequence of different production mechanisms which probe different kinematics in the nuclear parton distribution functions.

Recent calculations of charmonium production within microscopic transport models for the bulk-medium evolution can be found, e.g., in Refs.<sup>247,248</sup>. The results

<sup>o</sup>In part, this is due to a finite correlation volume introduced for  $c\bar{c}$  quarks in the approach of Refs.<sup>207,190</sup>.

are generally quite reminiscent of the rate-equation calculations discussed above. In particular, the description of RHIC data requires the inclusion of regeneration interactions. This is also true for the so-called comover approach, which has been extended to include charmonium formation reactions in Ref.<sup>249</sup>.

The interplay of suppression and regeneration should lead to interesting consequences for the excitation function of charmonium production. The approximate degeneracy of  $J/\psi$  suppression by about a factor of  $\sim 3$  in central  $A$ - $A$  collisions at both SPS and RHIC has been anticipated in the two-component model of Ref.<sup>47</sup>, with a rather flat behavior for  $\sqrt{s} = 17$ -200 AGeV. This degeneracy is expected to be lifted at higher (LHC,  $\sqrt{s} = 5500$  AGeV) and lower (FAIR,  $\sqrt{s} = 8$  AGeV) collision energies. At LHC, the statistical hadronization model predicts the inclusive  $J/\psi$   $R_{AA}$  in central Pb-Pb collisions to recover the level in  $p$ - $p$  collisions, i.e.,  $R_{AA}(N_{\text{part}} = 350) \rightarrow 1$ , based on a  $p$ - $p$  open-charm cross section of  $d\sigma_{c\bar{c}}/dy = 640 \mu\text{b}$ . At FAIR energies, on the other hand, statistical production is small<sup>208</sup>, while transport<sup>250</sup> and rate-equation approaches predict about a factor of two suppression, mostly dominated by nuclear absorption. The effective nuclear absorption cross section will thus be an essential quantity to be determined in  $p$ - $A$  reactions at FAIR.

Finally, let us turn to bottomonium production, which adds several new aspects compared to charmonium production: (i) the binding energies of bottomonium states are larger by about a factor of  $\sim 2$  which opens a wider window to study their dependence on color screening (due to larger dissociation temperatures) and makes them more robust in the hadronic phase; (ii) at given collision energy, the number of  $b\bar{b}$  pairs is substantially smaller than the number of  $c\bar{c}$  ones (e.g., by about a factor of  $\sim 200$  at RHIC<sup>145,28</sup>) (iii) bottom-quarks are less susceptible to changes in their momentum distributions due to their factor  $\sim 3$  larger mass (as discussed in Secs. 2 and 3 of this review). The latter 2 points suggest that regeneration processes play less of a role<sup>P</sup>. Early analyses of  $\Upsilon$  production in heavy-ion collisions have focused on the  $p_t$ -dependence of suppression scenarios where instantaneous dissociation above a critical energy density has been combined with formation-time effects, both at LHC<sup>54,251,252</sup> and RHIC<sup>252</sup>. The opposite limit of secondary production alone has been evaluated in the statistical hadronization model<sup>221</sup>. The thermal rate-equation approach, Eq. (103), has been applied to  $\Upsilon$  production in Ref.<sup>53</sup>, in analogy to the charmonium sector as displayed in the left panels of Figs. 36 and 39. The time evolution of the  $\Upsilon(1S)$  yield in central Au-Au collisions at RHIC has been calculated for the following two scenarios (as shown in Fig. 41): in the first one (left panel), reduced in-medium binding energies (according to solutions of a Schrödinger equation with a color-screened Cornell potential<sup>181</sup>)

<sup>P</sup>However, care has to be taken in deducing that this renders  $\Upsilon$  regeneration irrelevant at RHIC, since (a) the bottom ensemble is in the canonical limit, and (b) the regeneration yield needs to be compared to the primordial yield: in  $p$ - $p$  collisions the ratio  $\Upsilon/(b\bar{b}) \simeq 0.1\%$  is about a factor of 10 smaller than in the charm sector where  $J/\psi/(c\bar{c}) \simeq 1\%$ .

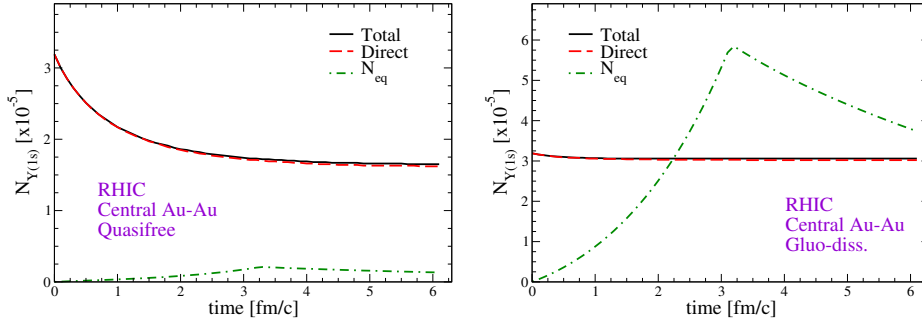


Fig. 41. (Color online) Time dependence of  $\Upsilon(1S)$  production in central Au-Au( $\sqrt{s} = 200$  AGeV) collisions at RHIC<sup>53</sup> using the quasifree dissociation-cross section with in-medium reduced binding energies (left panel) and the gluo-dissociation cross section with the free binding energy (assumed to be  $\varepsilon_B^\Upsilon = 1.1$  GeV; left panel). The time evolution of the background medium is based on an expanding fireball as in the left panels of Fig. 39.

are combined with quasifree dissociation (and formation) reactions; in the second one, the gluo-dissociation process is applied to the  $\Upsilon(1S)$  with vacuum binding energy (assuming  $m_b = 5.28$  GeV in connection with  $\varepsilon_B = 1.1$  GeV). One finds that color-screening enables a  $\sim 40\%$  suppression of the  $\Upsilon(1S)$  within the first 1-2 fm/c (where the average medium temperature is above 200 MeV), with insignificant contributions from regeneration since  $N_\Upsilon^{\text{eq}}$  is too small. On the other hand, with its vacuum binding energy, the  $\Upsilon(1S)$  is basically unaffected at RHIC. This suggests a very promising sensitivity of  $\Upsilon(1S)$  production to color-screening at RHIC (of course, the observed  $\Upsilon(1S)$  yield contains feed down contributions, amounting to ca. 50% in  $p$ - $p$  collisions; this underlines again the importance of measuring the excited  $\Upsilon'$  and  $\chi_b$  states). Note that  $N_\Upsilon^{\text{eq}}$  is quite different in the two scenarios even though  $m_\Upsilon = 2m_b - \varepsilon_B^\Upsilon$  is assumed to be constant in both cases. The reason is the difference in *relative* chemical equilibrium: a larger binding energy implies a larger  $m_b$ , which leads to a larger  $\gamma_b$  via Eq. (105), i.e., it is thermodynamically more favorable to allocate  $b$  and  $\bar{b}$  quarks in an  $\Upsilon$  (relative to a smaller  $\varepsilon_B^\Upsilon$  with smaller  $m_b$  and thus smaller  $\gamma_b$ ).

## 5. Conclusions

Heavy-quark physics is an increasingly useful and adopted tool in the theoretical analysis of hot and dense QCD matter and its study in ultrarelativistic collisions of heavy nuclei. Key reasons for this development lie in a combination of exciting new data becoming available not only for quarkonia but also for open heavy-flavor observables, together with attractive features of charm and bottom quarks from a theoretical point of view. These features are, of course, rooted in the large scale introduced by the heavy-quark (HQ) mass, which enables the use of expansion techniques, most notably HQ effective theories and Brownian motion for HQ diffusion in a QGP fluid. Furthermore, the production of heavy quarks in nuclear reactions

is presumably restricted to primary  $N$ - $N$  collisions which renders HQ spectra a calibrated probe of the medium over the *entire range of transverse momentum*. The latter provides a unique opportunity for a comprehensive investigation of the QCD medium at all scales, ranging from diffusion physics in the low- $p_t$  limit to a “standard” hard probe at  $p_t \gg m_Q$ . Heavy quarks thus connect transport coefficients in the QGP and observables in ultrarelativistic heavy-ion collisions in the arguably most direct way. Finally, relations between the open and hidden heavy-flavor sectors promise valuable mutual constraints, both theoretically and phenomenologically. In this review we have largely focused on aspects of soft physics for HQ propagation and binding in the QGP.

Interactions of slowly moving heavy quarks in a QGP are dominated by elastic scattering off thermal partons. A perturbative expansion of these interactions, specifically for the HQ diffusion coefficient, shows poor convergence for coupling constants believed to be relevant for a QGP as formed in heavy-ion collisions. Several options of amending the perturbative treatment have been suggested, e.g., a reduced screening mass or running coupling constant at low momentum transfer. While increasing the interaction strength, they inevitably face the problem of little control over higher order “corrections”. Nonperturbative approaches have been put forward which can, in principle, overcome this problem by a (partial) resummation of large contributions. E.g., a potential-based  $T$ -matrix approach characterized by a scattering equation becomes particularly promising if the input interaction can be specified in a model-independent way, i.e., from thermal lattice QCD. Currently, open questions remain as to the validity of the potential approach at finite temperature, and a suitable definition of the potential from the HQ free energy. Here, a close connection between the open and hidden heavy-flavor sectors emerges via the same low-energy interaction operative for HQ diffusion and quarkonium bound states. Qualitatively, one finds that, if ground-state quarkonia survive until temperatures well above  $T_c$ , potential scattering of heavy quarks in the QGP builds up resonance-like correlations which are instrumental in obtaining a small HQ diffusion coefficient close to  $T_c$ . As an alternative nonperturbative approach, HQ diffusion has been estimated in the strong-coupling limit of conformal field theory (CFT) using a conjectured correspondence to string theory in Anti-de-Sitter (AdS) space. With CFT parameters adapted to resemble QCD, the resulting HQ diffusion constant is comparable to the  $T$ -matrix approach close to  $T_c$ , but is approximately constant with increasing temperature while the  $T$ -matrix interaction and ultimately approaches pQCD estimates.

Quantitative applications of the Brownian-motion framework to HQ observables at RHIC critically hinge on a reliable description of the background medium evolution. The latter specifies the ambient conditions in the (approximately) thermal bath including its temperature and collectivity, whose magnitudes directly impact the nuclear modification and elliptic flow of HQ spectra. A survey of available calculations indicates that the translation of a given HQ diffusion coefficient into suppression and elliptic flow of HQ spectra is currently at the  $\sim 50\%$  accuracy level.

This needs to be further scrutinized and improved. In line with the theoretical expectations for HQ diffusion in a QGP at  $T=1-2T_c$ , the current data call for significantly stronger interactions than provided by LO pQCD. A simultaneous and consistent evaluation of spectra ( $R_{AA}(p_t)$ ) and elliptic flow ( $v_2(p_t)$ ) is pivotal to this conclusion. A non-negligible role is played by the hadronization process: heavy-light quark coalescence processes seem to improve the experimentally observed correlation of a rather large  $v_2$  and a moderately suppressed  $R_{AA}$  in the electron spectra at moderate  $p_T^e \leq 3$  GeV. More robust conclusions will require a better knowledge of the Cronin effect figuring into the initial conditions for the HQ spectra. A theoretically appealing aspect of quark coalescence is its close relation to resonance correlations in the QGP, which could be at the origin of the nonperturbative interaction strength in HQ diffusion. From the experimental side, important discrimination power will come with an explicit measurement of  $D$ -mesons, to explicitly separate the bottom contribution (present in the electron spectra). Theoretical investigations should take advantage of the opportunity to predict angular correlation measurements which will become feasible soon. We believe that charm data at SPS energy would constitute a valuable complement to RHIC data, which could help in deciding how much of the bulk flow (and suppression) can be imparted on charm quarks in a medium at smaller temperatures.

In the heavy-quarkonium sector we have started with a brief synopsis of current applications of potential models in medium. At this stage, the comparison of calculated spectral functions to Euclidean correlation functions computed in lattice QCD suggests that scenarios with either strong binding and rather large in-medium HQ mass, or weak binding and smaller HQ mass, are both viable. On the contrary, inelastic reaction rates are rather sensitive to the binding energy and thus to the strength of color-Debye screening, especially for bottomonia. This translates into a promising discrimination power of bottomonium suppression measurements at RHIC and LHC. The phenomenology of charmonia is presumably more involved; e.g., kinetic rate-equation calculations for  $J/\psi$  production in central Au-Au collisions at RHIC indicate that the number of surviving primordial  $J/\psi$ 's is comparable to the number of secondary produced ones via  $c\bar{c}$  coalescence in the QGP (and/or at hadronization). Such an interpretation is consistent with  $J/\psi$   $p_T$  spectra where the coalescence yield is concentrated at low  $p_T$ , thus reducing the average  $p_T^2$  compared to primordial production. Kinetic approaches furthermore suggest that regeneration is subleading at the SPS, and that the observed suppression occurs at energy densities above the critical one. Deeper insights will follow when advanced theoretical models meet future precision data, including rapidity dependencies, elliptic flow, excited charmonia and much needed constraints from d-Au collisions at RHIC (to pin down cold-nuclear matter effects). An extended excitation function via a RHIC energy scan, LHC and FAIR will further disentangle suppression and regeneration effects. We emphasize again that the presence of regeneration mechanisms would imply valuable connections to the open heavy-flavor sector, as coalescing heavy quarks necessarily imprint their kinematics on HQ bound states.

In summary, we believe that in-medium HQ physics will continue as a challenging but rewarding forefront research field for many years to come, with ample opportunities for surprises, insights and progress.

### Acknowledgments

We are indebted to D. Cabrera, V. Greco, C.M. Ko, M. Mannarelli, I. Vitev and X. Zhao for productive and enjoyable collaboration on various aspects of the topics discussed in this review. We furthermore thank J. Aichelin, P. Gossiaux, W. Horowitz and P. Petreczky for illuminating discussions. This work has been supported by a U.S. National Science Foundation CAREER award under grant no. PHY-0449489 and by the A.-v.-Humboldt foundation through a Bessel award (RR) and Feodor-Lynen fellowship (HvH).

### References

1. H. Fritzsch, M. Gell-Mann and H. Leutwyler, *Phys. Lett. B* **47** (1973) 365.
2. D. J. Gross and F. Wilczek, *Phys. Rev. Lett.* **30** (1973) 1343.
3. H. D. Politzer, *Phys. Rev. Lett.* **30** (1973) 1346.
4. M. Cheng *et al.*, *Phys. Rev. D* **77** (2008) 014511.
5. U. W. Heinz and M. Jacob (2000), [arXiv:nuc1-th/0002042](#).
6. I. Arsene *et al.* (BRAHMS Collaboration), *Nucl. Phys. A* **757** (2005) 1,  
B.B. Back *et al.* (PHOBOS Collaboration), *ibid.* 28,  
J. Adams *et al.* (STAR Collaboration), *ibid.* 102,  
K. Adcox *et al.* (PHENIX Collaboration), *ibid.* 184.
7. M. Gyulassy, I. Vitev, X.-N. Wang and B.-W. Zhang (2003), published in R. C. Hwa, X. N. Wang (editors), *Quark-gluon plasma* vol. 3 (World Scientific, 2004) p123, [arXiv:nuc1-th/0302077](#).
8. R. Rapp, D. Blaschke and P. Crochet (2008), [arXiv:0807.2470\[hep-ph\]](#).
9. P. Braun-Munzinger and J. Stachel (2009), accepted for publ. in Landolt-Börnstein vol. **1-23A** (2009), [arXiv:0901.2500\[nuc1-th\]](#).
10. L. Kluberg and H. Satz (2009), accepted for publ. in Landolt-Börnstein vol. **1-23A** (2009), [arXiv:0901.4014\[hep-ph\]](#).
11. C. Gale and K. L. Haglin (2003), published in R. C. Hwa, X. N. Wang (editors), *Quark-gluon plasma* vol. 3 (World Scientific, 2004) p364, [arXiv:hep-ph/0306098](#).
12. R. Rapp, J. Wambach and H. van Hees, *Landolt-Börnstein* **I/23** (2010) "4, [arXiv:0901.3289\[hep-ph\]](#).
13. P. F. Kolb and U. W. Heinz (2003), published in R. C. Hwa, X. N. Wang (editors), *Quark-gluon plasma* vol. 3 (World Scientific, 2004) p634, [arXiv:nuc1-th/0305084](#).
14. E. V. Shuryak, *Nucl. Phys. A* **750** (2005) 64.
15. P. Huovinen and P. V. Ruuskanen, *Ann. Rev. Nucl. Part. Sci.* **56** (2006) 163.
16. T. Hirano (2008), [arXiv:0812.4651\[nuc1-th\]](#).
17. P. Kovtun, D. T. Son and A. O. Starinets, *Phys. Rev. Lett.* **94** (2005) 111601.
18. A. D. Frawley, T. Ullrich and R. Vogt, *Phys. Rept.* **462** (2008) 125.
19. B. Müller (2008), [arXiv:0812.4638\[nuc1-th\]](#).
20. P. Levai, B. Müller and X.-N. Wang, *Phys. Rev. C* **51** (1995) 3326.
21. J. C. Collins, D. E. Soper and G. Sterman, *Nucl. Phys. B* **263** (1986) 37.
22. A. Adare *et al.* (PHENIX Collaboration), *Phys. Rev. Lett.* **98** (2007) 172301.
23. B. Svetitsky, *Phys. Rev. D* **37** (1988) 2484.

24. M. Golam Mustafa, D. Pal and D. Kumar Srivastava, *Phys. Rev. C* **57** (1998) 889, erratum: *Phys. Rev. C* **57** 3499 (1998).
25. H. van Hees and R. Rapp, *Phys. Rev. C* **71** (2005) 034907.
26. G. D. Moore and D. Teaney, *Phys. Rev. C* **71** (2005) 064904.
27. M. G. Mustafa, *Phys. Rev. C* **72** (2005) 014905.
28. H. van Hees, V. Greco and R. Rapp, *Phys. Rev. C* **73** (2006) 034913.
29. K. J. Eskola, H. Honkanen, C. A. Salgado and U. A. Wiedemann, *Nucl. Phys. A* **747** (2005) 511.
30. G.-Y. Qin, J. Ruppert, C. Gale, S. Jeon and G. D. Moore, *Phys. Rev. Lett.* **100** (2008) 072301.
31. Z. Xu, C. Greiner and H. Stöcker, *Phys. Rev. Lett.* **101** (2008) 082302.
32. Y. L. Dokshitzer and D. E. Kharzeev, *Phys. Lett. B* **519** (2001) 199.
33. S. S. Adler *et al.* (PHENIX), *Phys. Rev. Lett.* **96** (2006) 032301.
34. B. I. Abelev *et al.* (STAR Collaboration), *Phys. Rev. Lett.* **98** (2007) 192301.
35. T. C. Awes (PHENIX Collaboration) (2008), [arXiv:0805.1636\[nuc1-ex\]](https://arxiv.org/abs/0805.1636).
36. N. Armesto, M. Cacciari, A. Dainese, C. A. Salgado and U. A. Wiedemann, *Phys. Lett. B* **637** (2006) 362.
37. Y. Akiba (PHENIX), *Nucl. Phys. A* **774** (2006) 403.
38. S. Wicks, W. Horowitz, M. Djordjevic and M. Gyulassy, *Nucl. Phys. A* **784** (2007) 426.
39. R. Rapp and H. van Hees (2008), published in *The Physics of Quarks: New Research*, Nova Publishers 2009, [arXiv:0803.0901\[hep-ph\]](https://arxiv.org/abs/0803.0901).
40. O. Linnyk, E. L. Bratkovskaya and W. Cassing, *Int. J. Mod. Phys. E* **17** (2008) 1367.
41. M. Asakawa and T. Hatsuda, *Phys. Rev. Lett.* **92** (2004) 012001.
42. F. Karsch and E. Laermann (2003), published in R. C. Hwa, X. N. Wang (editors), *Quark-gluon plasma* vol. 3 (World Scientific, 2004) p1, [arXiv:hep-lat/0305025](https://arxiv.org/abs/hep-lat/0305025).
43. O. Kaczmarek, F. Karsch, F. Zantow and P. Petreczky, *Phys. Rev. D* **70** (2004) 074505.
44. H. van Hees, M. Mannarelli, V. Greco and R. Rapp, *Phys. Rev. Lett.* **100** (2008) 192301.
45. E. V. Shuryak and I. Zahed, *Phys. Rev. D* **70** (2004) 054507.
46. P. Petreczky, *Eur. Phys. J. C* **62** (2009) 85.
47. L. Grandchamp and R. Rapp, *Phys. Lett. B* **523** (2001) 60.
48. B. Alessandro *et al.*, *Eur. Phys. J. C* **39** (2005) 335.
49. A. Adare *et al.* (PHENIX Collaboration), *Phys. Rev. Lett.* **98** (2007) 232301.
50. R. L. Thews, M. Schroedter and J. Rafelski, *Phys. Rev. C* **63** (2001) 054905.
51. P. Braun-Munzinger and J. Stachel, *Phys. Lett. B* **490** (2000) 196.
52. M. I. Gorenstein, A. P. Kostyuk, H. Stoecker and W. Greiner, *Phys. Lett. B* **509** (2001) 277.
53. L. Grandchamp, S. Lumpkins, D. Sun, H. van Hees and R. Rapp, *Phys. Rev. C* **73** (2006) 064906.
54. F. Karsch and H. Satz, *Z. Phys. C* **51** (1991) 209.
55. S. Caron-Huot and G. D. Moore, *Phys. Rev. Lett.* **100** (2008) 052301.
56. A. Mocsy and P. Petreczky, *Phys. Rev. D* **73** (2006) 074007.
57. C.-Y. Wong and H. W. Crater, *Phys. Rev. D* **75** (2007) 034505.
58. D. Cabrera and R. Rapp, *Phys. Rev. D* **76** (2007) 114506.
59. W. M. Alberico, A. Beraudo, A. De Pace and A. Molinari, *Phys. Rev. D* **75** (2007) 074009.
60. M. Laine, *JHEP* **05** (2007) 028.

61. A. Mocsy and P. Petreczky, *Phys. Rev. Lett.* **99** (2007) 211602.
62. A. Mocsy and P. Petreczky, *Phys. Rev. D* **77** (2008) 014501.
63. W. M. Alberico, A. Beraudo, A. De Pace and A. Molinari, *Phys. Rev. D* **77** (2008) 017502.
64. R. Pawula, *Phys. Rev.* **162** (1967) 186.
65. B. L. Combridge, *Nucl. Phys. B* **151** (1979) 429.
66. A. Peshier (2008), [arXiv:0801.0595](https://arxiv.org/abs/0801.0595)[hep-ph].
67. P. B. Gossiaux and J. Aichelin, *Phys. Rev. C* **78** (2008) 014904.
68. E. Braaten and M. H. Thoma, *Phys. Rev. D* **44** (1991) 1298.
69. E. Braaten and M. H. Thoma, *Phys. Rev. D* **44** (1991) 2625.
70. Y. L. Dokshitzer, G. Marchesini and B. R. Webber, *Nucl. Phys. B* **469** (1996) 93.
71. A. C. Mattingly and P. M. Stevenson, *Phys. Rev. D* **49** (1994) 437.
72. S. Caron-Huot and G. D. Moore, *JHEP* **02** (2008) 081.
73. W. Liu and C. M. Ko (2006), [arXiv:nuc1-th/0603004](https://arxiv.org/abs/nuc1-th/0603004).
74. E. Shuryak, *Prog. Part. Nucl. Phys.* **62** (2009) 48.
75. M. Asakawa and T. Hatsuda, *Nucl. Phys. A* **721** (2003) 869.
76. G. Aarts, C. Allton, M. B. Oktay, M. Peardon and J.-I. Skullerud, *Phys. Rev. D* **76** (2007) 094513.
77. A. Adil and I. Vitev, *Phys. Lett. B* **649** (2007) 139.
78. D. Blaschke, G. Burau, T. Barnes, Y. Kalinovsky and E. Swanson, *Heavy Ion Phys.* **18** (2003) 49.
79. D. Blaschke, G. Burau, Y. L. Kalinovsky and V. L. Yudinchev, *Prog. Theor. Phys. Suppl.* **149** (2003) 182.
80. M. Laine, O. Philipsen, P. Romatschke and M. Tassler, *JHEP* **03** (2007) 054.
81. M. Laine, O. Philipsen and M. Tassler, *JHEP* **09** (2007) 066.
82. N. Brambilla, J. Ghiglieri, A. Vairo and P. Petreczky, *Phys. Rev. D* **78** (2008).
83. G. S. Bali, *Phys. Rept.* **343** (2001) 1.
84. N. Brambilla *et al.* (2004), [arXiv:hep-ph/0412158](https://arxiv.org/abs/hep-ph/0412158).
85. E. Eichten, K. Gottfried, T. Kinoshita, K. D. Lane and T.-M. Yan, *Phys. Rev. D* **21** (1980) 203.
86. S. Godfrey and N. Isgur, *Phys. Rev. D* **32** (1985) 189.
87. M. Avila, *Phys. Rev. D* **49** (1994) 309.
88. O. Kaczmarek, F. Karsch, P. Petreczky and F. Zantow, *Nucl. Phys. Proc. Suppl.* **129** (2004) 560.
89. O. Kaczmarek, S. Ejiri, F. Karsch, E. Laermann and F. Zantow, *Prog. Theor. Phys. Suppl.* **153** (2004) 287.
90. C.-Y. Wong, *Phys. Rev. C* **72** (2005) 034906.
91. M. Mannarelli and R. Rapp, *Phys. Rev. C* **72** (2005) 064905.
92. C. Amsler *et al.*, *Phys. Lett. B* **667** (2008) 1.
93. P. Petreczky and K. Petrov, *Phys. Rev. D* **70** (2004) 054503.
94. O. Kaczmarek and F. Zantow (2005), [arXiv:hep-lat/0506019](https://arxiv.org/abs/hep-lat/0506019).
95. A. Nakamura and T. Saito, *Phys. Lett. B* **621** (2005) 171.
96. M. Döring, K. Hübner, O. Kaczmarek and F. Karsch, *Phys. Rev. D* **75** (2007) 054504.
97. G. E. Brown, C.-H. Lee, M. Rho and E. Shuryak, *Nucl. Phys. A* **740** (2004) 171.
98. G. Brown, *Philos. Mag.* **43** (1952) 467.
99. R. H. Thompson, *Phys. Rev. D* **1** (1970) 110.
100. R. Blankenbecler and R. Sugar, *Phys. Rev.* **142** (1966) 1051.
101. M. I. Haftel and F. Tabakin, *Nucl. Phys. A* **158** (1970) 1.
102. S. Caron-Huot, M. Laine and G. D. Moore, *JHEP* **0904** (2009) 053.

103. P. Petreczky and D. Teaney, *Phys. Rev. D* **D73** (2006) 014508.
104. M. Laine, G. D. Moore, O. Philipsen and M. Tassler, *JHEP* **0905** (2009) 014.
105. C. P. Herzog, A. Karch, P. Kovtun, C. Kozcaz and L. G. Yaffe, *JHEP* **07** (2006) 013.
106. S. S. Gubser, *Phys. Rev. D* **74** (2006) 126005.
107. J. Casalderrey-Solana and D. Teaney, *Phys. Rev. D* **74** (2006) 085012.
108. S. S. Gubser, *Phys. Rev. D* **76** (2007) 126003.
109. J. M. Maldacena, *Phys. Rev. Lett.* **80** (1998) 4859.
110. S. S. Gubser, *Nucl. Phys. B* **790** (2008) 175.
111. J. Casalderrey-Solana and D. Teaney, *JHEP* **04** (2007) 039.
112. S.-J. Rey, S. Theisen and J.-T. Yee, *Nucl. Phys. B* **527** (1998) 171.
113. A. Brandhuber, N. Itzhaki, J. Sonnenschein and S. Yankielowicz, *Phys. Lett. B* **434** (1998) 36.
114. R. Rapp (2008), [arXiv:0812.3850](https://arxiv.org/abs/0812.3850)[hep-ph].
115. Y. Akamatsu, T. Hatsuda and T. Hirano (2008), [arXiv:0809.1499](https://arxiv.org/abs/0809.1499)[hep-ph].
116. R. Baier, Y. L. Dokshitzer, S. Peigne and D. Schiff, *Phys. Lett. B* **345** (1995) 277.
117. R. Baier, Y. L. Dokshitzer, A. H. Mueller, S. Peigne and D. Schiff, *Nucl. Phys. B* **483** (1997) 291.
118. R. Baier, *Nucl. Phys. A* **715** (2003) 209.
119. M. G. Mustafa, D. Pal, D. K. Srivastava and M. Thoma, *Phys. Lett.* **B428** (1998) 234, [nucl-th/9711059](https://arxiv.org/abs/nuc1-th/9711059).
120. N. Armesto, C. A. Salgado and U. A. Wiedemann, *Phys. Rev. D* **69** (2004) 114003.
121. M. Gyulassy, P. Levai and I. Vitev, *Nucl. Phys. B* **594** (2001) 371.
122. M. Djordjevic and M. Gyulassy, *Nucl. Phys. A* **733** (2004) 265.
123. J. D. Bjorken (1982), FERMILAB-PUB-82-059-THY.
124. M. H. Thoma and M. Gyulassy, *Nucl. Phys. B* **351** (1991) 491.
125. M. Gyulassy, P. Levai and I. Vitev, *Phys. Lett. B* **538** (2002) 282.
126. A. Sibirtsev, K. Tsushima and A. W. Thomas, *Eur. Phys. J. A* **6** (1999) 351.
127. A. Hayashigaki, *Phys. Lett. B* **487** (2000) 96.
128. L. Tolos, J. Schaffner-Bielich and A. Mishra, *Phys. Rev. C* **70** (2004) 025203.
129. M. F. M. Lutz and C. L. Korpa, *Phys. Lett. B* **633** (2006) 43.
130. L. Tolos, A. Ramos and T. Mizutani, *Phys. Rev. C* **77** (2008) 015207.
131. C. Fuchs, B. V. Martemyanov, A. Faessler and M. I. Krivoruchenko, *Phys. Rev. C* **73** (2006) 035204.
132. E. L. Bratkovskaya, W. Cassing, H. Stoecker and N. Xu, *Phys. Rev. C* **71** (2005) 044901.
133. B. Zhang, L.-W. Chen and C.-M. Ko, *Phys. Rev. C* **72** (2005) 024906.
134. D. Molnar, *Eur. Phys. J. C* **49** (2007) 181.
135. J. Dunkel and P. Hänggi, *Phys. Rept.* **471** (2009) 1.
136. J. Dunkel and P. Hänggi, *Phys. Rev. E* **71** (2005) 016124.
137. P. Arnold, *Phys. Rev. E* **61** (2000) 6091.
138. P. Arnold, *Phys. Rev. E* **61** (2000) 6099.
139. H. van Hees (2009), in preparation.
140. D. Teaney, J. Lauret and E. V. Shuryak, *Phys. Rev. Lett.* **86** (2001) 4783.
141. P. F. Kolb, J. Sollfrank and U. W. Heinz, *Phys. Rev. C* **62** (2000) 054909.
142. T. Hirano, U. W. Heinz, D. Kharzeev, R. Lacey and Y. Nara, *Phys. Lett. B* **636** (2006) 299.
143. A. Pukhov *et al.* (1999), [hep-ph/9908288](https://arxiv.org/abs/hep-ph/9908288).
144. R. Rapp, V. Greco and H. van Hees, *Nucl. Phys. A* **774** (2006) 685.
145. M. Cacciari, P. Nason and R. Vogt, *Phys. Rev. Lett.* **95** (2005) 122001.

146. K. P. Das and R. C. Hwa, *Phys. Lett. B* **68** (1977) 459, erratum *ibid.* **73**, 504 (1978).
147. E. Braaten, Y. Jia and T. Mehen, *Phys. Rev. Lett.* **89** (2002) 122002.
148. R. Rapp and E. V. Shuryak, *Phys. Rev. D* **67** (2003) 074036.
149. A. Adare *et al.* (PHENIX Collaboration), *Phys. Rev. Lett.* **98** (2007) 162301.
150. B. I. Abelev *et al.* (STAR Collaboration), *Phys. Rev. C* **75** (2007) 054906.
151. R. C. Hwa and C. B. Yang, *Phys. Rev. C* **67** (2003) 034902.
152. V. Greco, C. M. Ko and P. Levai, *Phys. Rev. C* **68** (2003) 034904.
153. R. J. Fries, B. Müller, C. Nonaka and S. A. Bass, *Phys. Rev. C* **68** (2003) 044902.
154. D. Molnar and S. A. Voloshin, *Phys. Rev. Lett.* **91** (2003) 092301.
155. V. Greco, C. M. Ko and R. Rapp, *Phys. Lett. B* **595** (2004) 202.
156. Z. wei Lin and D. Molnar, *Phys. Rev. C* **68** (2003) 044901.
157. L. Ravagli and R. Rapp, *Phys. Lett. B* **655** (2007) 126.
158. L. Ravagli, H. van Hees and R. Rapp, *Phys. Rev. C* **79** (2009) 064902.
159. G. Martinez-Garcia, S. Gadrat and P. Crochet, *Phys. Lett. B* **663** (2008) 55.
160. P. R. Sorensen and X. Dong, *Phys. Rev. C* **74** (2006) 024902.
161. X. Dong, S. Esumi, P. Sorensen, N. Xu and Z. Xu, *Phys. Lett. B* **597** (2004) 328.
162. Y. Akamatsu (2008), private communication.
163. I. Vitev, A. Adil and H. van Hees, *J. Phys. G* **34** (2007) S769.
164. I. Vitev, *Phys. Lett. B* **639** (2006) 38.
165. M. Djordjevic, M. Gyulassy, R. Vogt and S. Wicks, *Phys. Lett. B* **632** (2006) 81.
166. S. A. Butsyk, *Nucl. Phys. A* **774** (2006) 669.
167. M. Djordjevic and U. W. Heinz, *Phys. Rev. Lett.* **101** (2008) 022302.
168. R. Rapp and H. van Hees, *J. Phys. G* **32** (2006) S351.
169. J. Bielcik, *Nucl. Phys. A* **A774** (2006) 697.
170. S. S. Adler *et al.*, *Phys. Rev. Lett.* **96** (2006) 202301.
171. D. Teaney (2006), private communication based on Ref.<sup>26</sup>.
172. W. Israel and J. N. Vandalas, *Lett. Nuovo Cim.* **19** (1970) 887.
173. P. Danielewicz and M. Gyulassy, *Phys. Rev. D* **31** (1985) 53.
174. A. Nakamura and S. Sakai, *Phys. Rev. Lett.* **94** (2005) 072305.
175. J.-P. Blaizot and E. Iancu, *Nucl. Phys. B* **557** (1999) 183.
176. P. Arnold, G. D. Moore and L. G. Yaffe, *JHEP* **05** (2003) 051.
177. R. A. Lacey and A. Taranenko, *PoS C FRNC2006* (2006) 021.
178. L. P. Csernai, J. I. Kapusta and L. D. McLerran, *Phys. Rev. Lett.* **97** (2006) 152303.
179. T. Matsui and H. Satz, *Phys. Lett. B* **178** (1986) 416.
180. O. Kaczmarek and F. Zantow, *Phys. Rev. D* **71** (2005) 114510.
181. F. Karsch, M. T. Mehr and H. Satz, *Z. Phys. C* **37** (1988) 617.
182. M. Döring, S. Ejiri, O. Kaczmarek, F. Karsch and E. Laermann, *Eur. Phys. J. C* **46** (2006) 179.
183. S. Digal, P. Petreczky and H. Satz, *Phys. Rev. D* **64** (2001) 094015.
184. T. Umeda, *Phys. Rev. D* **75** (2007) 094502.
185. M. E. Peskin, *Nucl. Phys. B* **156** (1979) 365.
186. G. Bhanot and M. E. Peskin, *Nucl. Phys. B* **156** (1979) 391.
187. R. Rapp, *Eur. Phys. J. C* **43** (2005) 91.
188. Y. Park, K.-I. Kim, T. Song, S. H. Lee and C.-Y. Wong, *Phys. Rev. C* **76** (2007) 044907.
189. T. Song, Y. Park, S. H. Lee and C.-Y. Wong, *Phys. Lett. B* **659** (2008) 621.
190. X. Zhao and R. Rapp, *Phys. Lett. B* **664** (2008) 253.
191. H. Liu, K. Rajagopal and U. A. Wiedemann, *Phys. Rev. Lett.* **98** (2007) 182301.

192. D. Kharzeev and H. Satz, *Phys. Lett. B* **334** (1994) 155.
193. K. Martins, D. Blaschke and E. Quack, *Phys. Rev. C* **51** (1995) 2723.
194. T. Barnes, E. S. Swanson, C. Y. Wong and X. M. Xu, *Phys. Rev. C* **68** (2003) 014903.
195. M. A. Ivanov, J. G. Korner and P. Santorelli, *Phys. Rev. D* **70** (2004) 014005.
196. S. G. Matinyan and B. Muller, *Phys. Rev. C* **58** (1998) 2994.
197. Z. wei Lin and C. M. Ko, *Nucl. Phys. A* **715** (2003) 533.
198. K. L. Haglin and C. Gale, *Phys. Rev. C* **63** (2001) 065201.
199. Y. seok Oh, T. soo Song, S. H. Lee and C.-Y. Wong, *J. Korean Phys. Soc.* **43** (2003) 1003.
200. F. Carvalho, F. O. Duraes, F. S. Navarra and M. Nielsen, *Phys. Rev. C* **72** (2005) 024902.
201. A. Bourque and C. Gale, *Phys. Rev. C* **78** (2008) 035206.
202. D. B. Blaschke, H. Grigorian and Y. L. Kalinovsky (2008), [arXiv:0808.1705\[hep-ph\]](#).
203. F. O. Duraes, H. chong Kim, S. H. Lee, F. S. Navarra and M. Nielsen, *Phys. Rev. C* **68** (2003) 035208.
204. D. Blaschke, G. Bureau, Y. Kalinovsky and T. Barnes, *Eur. Phys. J. A* **18** (2003) 547.
205. B. Friman, S. H. Lee and T. Song, *Phys. Lett. B* **548** (2002) 153.
206. L. Yan, P. Zhuang and N. Xu, *Phys. Rev. Lett.* **97** (2006) 232301.
207. L. Grandchamp, R. Rapp and G. E. Brown, *Phys. Rev. Lett.* **92** (2004) 212301.
208. A. Andronic, P. Braun-Munzinger, K. Redlich and J. Stachel, *Phys. Lett. B* **659** (2008) 149.
209. C. Young and E. Shuryak (2008), [arXiv:0803.2866\[nucl-th\]](#).
210. M. Bedjidian *et al.* (2004), [arXiv:hep-ph/0311048](#).
211. J. Cugnon and P. B. Gossiaux, *Z. Phys. C* **58** (1993) 95.
212. Y. B. He, J. Hufner and B. Z. Kopeliovich, *Phys. Lett. B* **477** (2000) 93.
213. E. G. Ferreira, F. Fleuret, J. P. Lansberg and A. Rakotozafindrabe (2008), [arXiv:0809.4684\[hep-ph\]](#).
214. D. Kharzeev, E. Levin, M. Nardi and K. Tuchin (2008), [arXiv:0809.2933\[hep-ph\]](#).
215. C. Lourenco, R. Vogt and H. K. Woehri, *JHEP* **02** (2009) 014.
216. I. Abt *et al.* (HERA-B Collaboration), *Phys. Lett. B* **561** (2003) 61.
217. I. Abt *et al.* (HERA-B Collaboration), *Eur. Phys. J. C* **49** (2007) 545.
218. M. C. Abreu *et al.* (NA50 Collaboration), *Phys. Lett. B* **410** (1997) 327.
219. M. C. Abreu *et al.* (NA50 Collaboration), *Phys. Lett. B* **499** (2001) 85.
220. L. Ramello *et al.* (NA50 Collaboration), *Nucl. Phys. A* **715** (2003) 243.
221. A. Andronic, P. Braun-Munzinger, K. Redlich and J. Stachel, *Nucl. Phys. A* **789** (2007) 334.
222. C. Lourenco and H. K. Woehri, *Phys. Rept.* **433** (2006) 127.
223. P. Braun-Munzinger, D. Miskowiec, A. Drees and C. Lourenco, *Eur. Phys. J. C* **1** (1998) 123.
224. M. C. Abreu *et al.* (NA50 Collaboration), *Nucl. Phys. A* **638** (1998) 261.
225. B. Alessandro *et al.* (NA50 Collaboration), *Eur. Phys. J. C* **49** (2007) 559.
226. L. Grandchamp, R. Rapp and G. E. Brown, *J. Phys. G* **30** (2004) S1355.
227. B. Alessandro *et al.* (NA50 Collaboration), *Eur. Phys. J. C* **48** (2006) 329.
228. R. Arnaldi *et al.* (NA60 Collaboration), *Phys. Rev. Lett.* **99** (2007) 132302.
229. S. Digal, S. Fortunato and H. Satz, *Eur. Phys. J. C* **32** (2004) 547.
230. A. Capella and E. G. Ferreira, *Eur. Phys. J. C* **42** (2005) 419.
231. Y. Liu, Z. Qu, N. Xu and P. Zhuang (2009), [arXiv:0901.2757\[nucl-th\]](#).

232. A. Adare *et al.* (PHENIX Collaboration), *Phys. Rev. C* **77** (2008) 024912.
233. A. Adare *et al.* (PHENIX Collaboration), *Phys. Rev. Lett.* **97** (2006) 252002.
234. D. Hornback (PHENIX Collaboration), *J. Phys. B* **35** (2008) 104113.
235. T. Gunji, H. Hamagaki, T. Hatsuda and T. Hirano, *Phys. Rev. C* **76** (2007) 051901.
236. A. Adare *et al.* (PHENIX Collaboration), *Phys. Rev. Lett.* **101** (2008) 122301.
237. Z. Tang (STAR Collaboration), *J. Phys. G* **35** (2008) 104135.
238. F. Karsch and R. Petronzio, *Phys. Lett. B* **193** (1987) 105.
239. J. P. Blaizot and J.-Y. Ollitrault, *Phys. Lett. B* **199** (1987) 499.
240. S. Gavin and R. Vogt, *Nucl. Phys. B* **345** (1990) 104.
241. Z. Xu and Z. Tang (2008), private communication.
242. X. Zhao and R. Rapp (2008), [arXiv:0806.1239\[nucl-th\]](https://arxiv.org/abs/0806.1239).
243. X.-N. Wang and F. Yuan, *Phys. Lett. B* **540** (2002) 62.
244. D. Krieg and M. Bleicher, *Eur. Phys. J. A* **39** (2009) 1.
245. R. Arnaldi *et al.* (NA60 Collaboration), *J. Phys. G* **32** (2006) S51.
246. X. Zhao and R. Rapp (2008), [arXiv:0810.4566\[nucl-th\]](https://arxiv.org/abs/0810.4566).
247. B. Zhang, C. M. Ko, B.-A. Li, Z.-W. Lin and S. Pal, *Phys. Rev. C* **65** (2002) 054909.
248. O. Linnyk, E. L. Bratkovskaya and W. Cassing, *Nucl. Phys. A* **807** (2008) 79.
249. A. Capella *et al.*, *Eur. Phys. J. C* **58** (2008) 437.
250. O. Linnyk, E. L. Bratkovskaya, W. Cassing and H. Stoecker, *Nucl. Phys. A* **786** (2007) 183.
251. J. F. Gunion and R. Vogt, *Nucl. Phys. B* **492** (1997) 301.
252. D. Pal, B. K. Patra and D. K. Srivastava, *Eur. Phys. J. C* **17** (2000) 179.